ANALYSIS OF LAMINAR FLOW, THERMAL STABILITY, AND ENTROPY GENERATION IN POROUS CHANNEL

By

EEGUNJOBI ADETAYO SAMUEL

(Student Number 211281425)

B.Tech(Hons)(FUTA), M.Sc(U.I Ibadan)

Thesis submitted in fulfillment of the requirements for the degree

Doctor of Technology: Mechanical Engineering

Cape Peninsula University of Technology

Supervisor: Professor O. D. Makinde

Senior Professor & Director, Institute for Advanced Research in Mathematical Modelling & Computations,

Cape Peninsula University of Technology, South Africa.

YEAR: 2013

DECLARATION

I, **Adetayo Samuel EEGUNJOBI** hereby declare that, this thesis represents my own work and has not been submitted previously for examination towards any degree or diploma qualification at any other University. Furthermore, it represents my own opinion and not necessarily those of the Cape Peninsula University of Technology.

Signed **Date**

Acknowledgements

There is a saying that when kindness cannot be returned, it has to be appreciated. I thank Almighty God for helping me through the course of this programme. I acknowledge wholeheartedly the intellectual tutelage and fatherly understanding of my supervisor, Professor O. D. Makinde. I remain highly indebted to his valuable advice, encouragement and gaining a lot from his wealth of knowledge, which were of help for the successful completion of the thesis.

My deep appreciation goes to my loving and wonderful wife -Ruth and my son - Victor, who supported me each step of the way. Thank you dear. I equally extend my appreciation to my In-laws Prof and Dr(Mrs) Oyedokun for their parental advice. Similarly, my appreciation goes to Prof. S. A. Reju, Dr. I.K.O. Ajibola, Dr. M. Gabere, Mr Temitope Carter Ajayi, my mother Racheal Eegunjobi, Mr Idowu Adetomokun, my friends and my colleagues at work. I say thank you all.

Dedication

This work is dedicated to the Lord of Lords. The Almighty God.

And to my beloved wife - Ruth who has been a great source of motivation and inspiration.

And to my mother, the vehicle that conveyed my existence.

Abstract

Fluid flow through a porous channel and cylindrical pipe walls are important area of research due to its wide applications in transpiration cooling, gaseous diffusion technology, cooling of rocket, mechanized irrigation and filtration processes. It is therefore necessary to examine the effect of Navier slip, combined effects of buoyancy forces and variable viscosity on the entire flow structure. Analyzing the magneto-hydrodynamics (MHD) of unsteady flow with buoyancy effect and also investigate numerically the entropy generation in an unsteady flow through porous pipe. We have also examined the thermal stability and entropy generation in the system. The problems were investigated theoretically using appropriate mathematical models for both transient and steady state scenario. Both analytical techniques and numerical methods are employed to tackle the model nonlinear equations derived from the law of conservation of mass, momentum and energy balance.

Some definitions of terms to come across and introduction to fluid flow are given in chapter 1, together with literature reviews, statement of problem and objectives of the study.

Chapter 2 lays the foundation for basic fundamental equations governing fluid flow.

In chapter 3, the combined effect of suction/injection and asymmetric Navier slip on the entropy generation rate for steady flow of an incompressible viscous fluid through

a porous channel subjected to different temperature at the walls are investigated. Chapter 4 analyze combined effects of buoyancy forces together with Navier slip on the entropy generation in a vertical porous channel wall with suction/injection wall. Analysis of MHD unsteady flow through a porous pipe with buoyancy effects are carried out in chapter 5, while chapter 6 investigates numerically entropy generation of unsteady flow through a porous pipe with suction and chapter 7 gives concluding remarks.

Nomenclature

c_p	Specific heat at a constant pressure.
k	Thermal Conductivity.
CV	Control Volume.
CS	Control Surface.
h	Channel width.
u	Velocity of the fluid.
P	Fluid pressure.
V	Uniform Suction/Injection.
E_G	Volumetric Entropy Generation.
g	Aceleration due to gravity.
Re	Reynolds Number.
Pe	Peclet Number.
Pr	Prandtl Number.
Br	Brinkmann Number.
q_w	Heat Transfer Rate at the Channel.
Be	Bejan Number.
C_f	Dimensionless Wall Shear Stress.
N_u	Dimensionless Heat Transfer.
R	Pipe Radius.
T_0	Fluid Initial Temperature.
T_w	Channel Wall Temperature.
Gr	Grashof Number.
M	Magnetic Field Parameter.
N_s	Dimensionless Entropy Generation.
$\bar{u}$	Axial Velocity.
$\bar{r}, \bar{z}$	Distance measured in the radial and axial directions.

Greek letters

ρ	Density.
μ	Coefficient of dynamic viscosity.
θ	Dimensionless Temperature.
$\bar{\tau_w}$	Shear stress.
σ	Thermal Diffusivity
β_1, β_2	Dimensionless Slip Parameters.
ν	Fluid Viscosity.
γ_1, γ_2	Slip Coefficient.
ϕ	Irreversibility Ratio.
Ω	Temperature Difference.
σ	Electrical Conductivity.
τ	Time.

Contents

List of Figures

List of Tables

Chapter 1

Introduction

A fluid is any substance that deforms continuously when subjected to a shear stress (tangential force per unit area), no matter how small according to McDonough [85]. The work of Leonardo Da Vinci gave rapid advancement to the study of fluids mechanics more than 500 years ago, but earlier than this time; fluid behavior were much more available by the time of ancient Egyptian. Enough practical information had been gathered during the Roman Empire to allow fluid dynamics application. Several centuries ago both father and son began more modern understanding of fluids motion known as Bernoulli's equation. Since then, many researchers have done numerous work on fluid mechanics. A porous channel walls is a channel with permeable walls. The walls are made up of a solid matrix with its void space filled with fluids. The walls are interconnected such that fluids can flow through the medium. The study of fluids convection processes in porous channel fascinated mankind for many centuries due to its applications in many areas of life. Such areas are: agriculture (e.g. irrigation, land drainage), geothermal system, microelectric heat transfer equipment, coal and grain storage, nuclear waste disposal, hydraulic engineering (e.g. storage reservoirs, seepage, channel hydraulics), atmospheric sciences (e.g. global circulation, mesoscale

weather patterns), oceanography (e.g. ocean circulation pattern, effects of pollution on living organisms), geophysics (e.g. convection in the earth's mantle, convection in earth's molten core). So also in astrophysics (e.g. galactic structure and clustering, stellar evolution), chemical and petroleum engineering (e.g. industrial filtration, fluidization, sedimentation, metallurgy, ceramics, powders, drying and wetting of textiles and wood), building engineering (e.g. aeration insulation against moisture) and biological area (e.g. flow of blood and water in the system, action of kidney and rise of juices in plant). Another applications of fluids flow in a porous channel is found in heat pumps and thermoacoustic prime mover (Rott[100],Swift [107]). Fig. (1.1) shows some of the above mentioned applications. Universality of modern science arises through the investigation of fluids convection and thus, the diversity of background has caused the investigations to be many-faced, even to the thinking of the applied Mathematician. In this thesis, analysis of laminar flow, thermal stability and entropy generation in porous channel and cylindrical pipes are studied.

1.1 Definitions of Terms

Some of the terms that are relevant to this study are defined as follows:

1.1.1 Porous channel

This consists of a channel with permeable walls. The walls are made up of a solid matrix with its void space filled with fluids. The walls are interconnected such that fluids can flow through the medium.

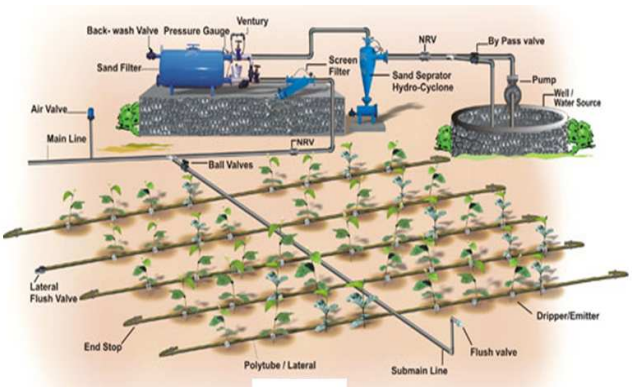

(a) Irrigation

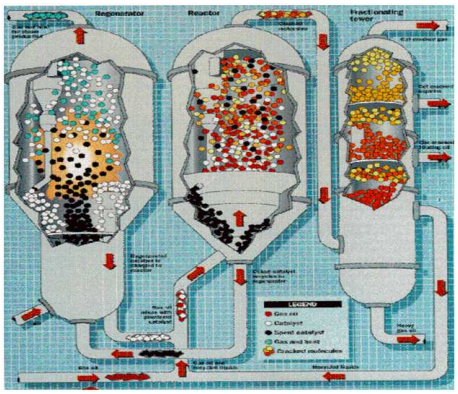

(b) Fluid catalytic cracking

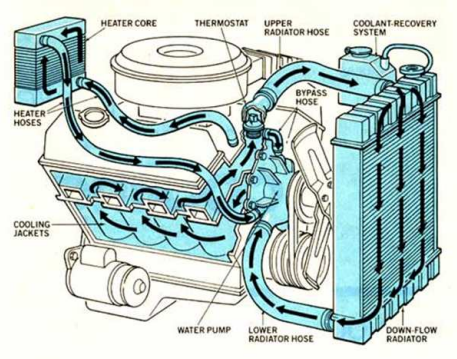

(c) Engine cooling system

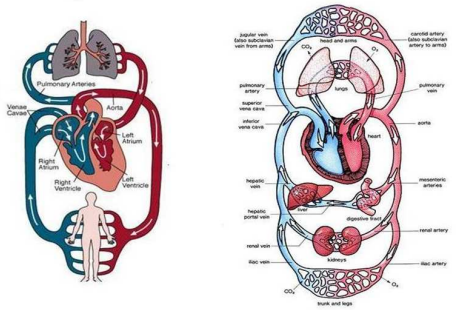

(d) Circulatory System

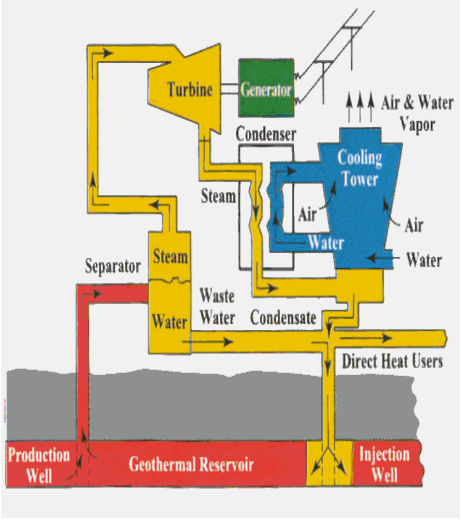

(e) Sketch of Heat pump

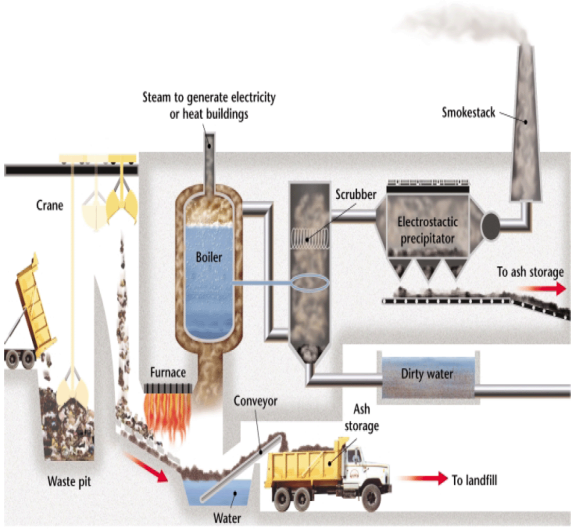

(f) Incinerator

Figure 1.1: Applications of fluids flow

1.1.2 Streamline

This is an imaginary curve in the fluid across which, at a given instant, there is no flow. The velocity of every particles of the fluid along the streamline is tangential to it at that moment. Since at the boundaries, there can be no flow, then this can be referred to as streamline.

1.1.3 The control volume

A control volume (CV) is a volume in space through which fluid may flow; in some cases, the volume may move or deform. It has a boundary which separates it from the surrounding and defines as control surfaces.

1.1.4 Material Derivative

Given a velocity of the fluid by $\vec{V} = (u(t, x(t)), v(t, y(t)), w(t, z(t)))$ where $u = \frac{\partial x}{\partial t}, \quad v = \frac{\partial y}{\partial t}, \quad w = \frac{\partial z}{\partial t}$ and function $f(t, \vec{V})$ describing some properties of a fluid particles. Then,

$$\begin{aligned} \frac{df}{dt} &= \frac{\partial f}{\partial t} + \frac{\partial x}{\partial t}\frac{\partial f}{\partial x} + \frac{\partial y}{\partial t}\frac{\partial f}{\partial y} + \frac{\partial z}{\partial t}\frac{\partial f}{\partial z} \\ &= \frac{\partial f}{\partial t} + u\frac{\partial f}{\partial x} + v\frac{\partial f}{\partial y} + w\frac{\partial f}{\partial z} \\ &= \frac{\partial f}{\partial t} + \vec{V} \cdot \nabla f \end{aligned}$$

This implies:

$$\frac{D}{Dt} = \frac{\partial}{\partial t} + \vec{V} \cdot \nabla$$

$\frac{\partial}{\partial t}$ is the local derivative, $\vec{V} \cdot \nabla$ is the convective derivative and $\frac{D}{Dt}$ is the material derivative.

1.1.5 The Reynolds Transport Theorem

The extensive quantity B, a scalar or vector or tensor, is defined as a property of a fluid and b (as the corresponding value per unit mass) the intensive value. The Reynold transport theorem for moving and arbitrarily deforming control volume (CV), with boundary control surface (CS) states that:

$$\frac{d}{dt}B_{system} = \frac{d}{dt}\iiint_{CV} \rho b dv + \iint_{CS} (\rho b V \cdot n) dA$$

where B_{system} is the total quantity of B in the system, n is the outward normal to the CS, V is the velocity of the fluid particle and $\frac{d}{dt}$ is the derivative of the fluid mass comprising the system.

Reynolds transport theorem states that the time rate of change of the total B in the system is equal to the rate of change within the CV plus the net flux of B through the CS.

1.1.6 Laminar Flow

When a flow is so slow that no mixing of the fluid takes place, Laminar flow takes place as if the fluid consists of thin layer sliding parallel over each other. Laminar flow represents highly ordered fluid motion characterized by smooth layers of fluid. Newton's law of viscosity is applicable here.

1.1.7 Thermal Stability

This represents the quantitative response of a material to temperature change or variation.

1.1.8 Thermal Diffusivity

When the temperature distribution changes with time, there is occurrence of transient heat transfer. Thermal diffusivity is a fundamental quantity that enters into heat transfer situation not at steady state. Thermal diffusivity measures how quick a body can change its temperature and relates to thermal conductivity through the equation:

$$\alpha = \frac{k}{\rho C_p},$$

where α is the thermal diffusivity, k is the thermal conductivity, C_p is the specific heat at a constant pressure and ρ is the density.

1.1.9 Buoyancy

An object submerged when a fluid exerts a force in it. Such a force due to a fluid in equilibrium is known as the buoyancy or the upthrust. Buoyancy is very important in many engineering application such as in the designing of ships, boats, buoys and so on. The weight of the displace volume of fluid and the buoyance has the same magnitude. Buoyancy acts upwards through the centre of gravity of the displaced

volume of fluid is referring to as centre of buoyancy.

1.1.10 Viscosity

With the viscosity of a fluid, we normally mean the thickness of the fluid. Viscosity of a fluid could be regarded as the resistance that the fluid offer against deforming under the influence of a shear stress. Shearing force does not applicable to fluid at rest. If such forces acts on a fluid which is in contact with solid boundary, the fluid will flow over the boundary in such a way that the particle immediately in contact with the boundary have the same velocity as the boundary while successive layers of fluid parallel to the boundary move with increasing velocity. Shear stresses opposing the relative motion of these layers are set up and their magnitude depending on the velocity gradient from layer to layer. The shear stress of fluid obeying Newton's law of viscosity, taking the direction of motion as the x-direction and u as the velocity of the fluid in the same x-direction at a distance y from the boundary is given by White[128]

$$\tau_x = \nu \frac{du}{dy},$$

where the constant ν is the coefficient of the dynamic viscosity.

Classification of fluids into either Newtonian or non-Newtonian fluids can be done through the help of viscosity property. The unit of dynamic viscosity is $kgm^{-1}s^{-1}$. Viscosity is the most important material property and good knowledge of fluid responses required a basic understanding of viscosity. Its associated with collective currents that carry momentum from one region of the fluid to another. In general, the Newtonian model describes the rheological behavior of fluids. The Newtonian

model is simply a special case with a constant viscosity. However, viscosity is a strong deformation of fluids. It is the key factor in determining the amount of fluid flowing in channels. It also helps to determine whether the flow regime is laminar, transitional or turbulent. Accurate knowledge of viscosity is very useful for computation of the pressure, velocity and temperature within the channels.

Viscosity also helps to describe the flow behaviour of shear stress with respect to the rate of deformation of the fluid. In general the application of viscosity includes reservoir modelling, in which production rates and mobility for water flooding plays a major role.

1.1.11 Temperature-Dependent Viscosity

If the temperature of the fluid increases, the rate of molecular interchange moves faster and further away from each other, so that the cohesive forces decrease rapidly. As the cohesive forces are decreasing, the shear stress will be decreasing as well. Similarly, as the rate of molecular interchange is increasing, there will be increase in shear stress. For instance most lubricants used in automobile had a dynamic viscosity of $0.0095Pas$ at $40°C$ and $0.0097Pas$ at $100°C$, the operating oil viscosity being taken as $0.015Pas$ corresponding to an effective operating temperature of $80°C$. Shear rate in the lubricant will thus be in the range $4 \times 10^{-4}s^{-1}$ to $4 \times 10^{-4}s^{-1}$. Such shear rates would certainly cause shear thinning effects in a multigrade lubricant [121]. Unlike liquids for which different temperature-dependent viscosity equations exist only two main laws describes the response of gas viscosity to temperature, they are: power law and Sutherland law. Table 1.1 shows different viscosity models.

Table 1.1: Viscosity-Temperature Equation as in the literatures ([122-124]),a,b,C are constants, T_0 is a reference temperature, μ_0 is the viscosity at T_0 and ν_0 is the kinematic viscosity at T_0.

Name	Equation
Sutherland	$\mu = \frac{(\frac{T}{T_0})^{\frac{3}{2}}(T_0+C)}{T+C}$
Power Law	$\mu = (\frac{T}{T_0})^n$
Reynolds	$\mu = be^{-aT}$
Slotte	$\mu = \frac{a}{(b+T)^c}$
Walther	$\mu = \mu_0 + bd^{\frac{1}{T^C}}$
Vogel	$\mu = ae^{\frac{b}{T-C}}$
Arrhenius Type	$\mu = \mu_0(\frac{T}{T_0})^n e^{(\frac{E}{RT})}$
Williams, Landel, Ferry	$log(\frac{\mu}{\mu_0}) = -\frac{C_1(T-T_0)}{C_2+T-T_0}$

1.1.12 The First Law of Thermodynamics

The first law of thermodynamic states the conservation of energy. The law states that energy cannot be created nor destroyed; but it can be changed from one form to another. The first law of thermodynamics defines the internal energy as a state function and provides a formal statement of the conservation of energy. However, it provides no information about the direction in which processes can spontaneously occur, that is, the reversibility aspect of thermodynamics processes. For example, it cannot say how cells can perform work while existing in an isothermal environment. It gives no information about the inability of any thermodynamics processes to convert heat into mechanical work with full efficiency, or any insight into why mixtures cannot spontaneously separate themselves. An experimentally derived principle to characterize the availability of energy is required to do this. This is precisely the role

of the second law of thermodynamics that will be explained next.

1.1.13 The Second Law of Thermodynamics

Although a spontaneously process can proceed only in a definite direction, the first law of thermodynamics give no information about direction; it merely states that when one form of energy is converted into another, identical quantities of energy are involved regardless of feasibility of the process. In this regard, events could be envisioned that would not violate the first law of thermodynamics, e.g. transfer of certain quantity of heat from a low-temperature body to a high-temperature body, without doing any work. However, the reality shows that, this is impossible and the first law of thermodynamics becomes inadequate in picturizing the complete energy transfer. Furthermore, experiments indicated that when energy in the form of heat is transferred to a system, only a portion of heat can be converted to work.

The second law of thermodynamics established the differences in quality between different forms of energy and explains why some processes can spontaneously occur, whereas others cannot. It indicated a trend of change and is usually expressed as an inequality. The second law of thermodynamics has been confirmed by experimental evidences like other physical laws of nature.

The second law of thermodynamics defines the fundamental physical quantity entropy as randomized energy state unavailable for direct conversion to work. It also states that all spontaneous processes, both chemical and physical, proceed to maximize entropy, that is, to become more randomized and convert energy into a less available form. A direct consequence of fundamental importance is the implication that, at

thermodynamics equilibrium the entropy of a system is at a relative maximum; that is , no further increase in disorder is possible without changing by some external means (such as adding heat) the thermodynamics state of the system.

A basic corollary of the second law of thermodynamics is the statement that the sum of the entropy change of a system and that of the surroundings must always be positive, that is, the universe (the sum of all the systems and surrounds) is constrained to become forever more disordered and to proceed towards thermodynamics equilibrium with some absolute maximum value of entropy. From a biological standpoint this is certainly a reasonable concept, since unless gradients in concentration and temperature are forcibly maintained by the consumption of energy, organisms proceed spontaneously towards the biological equivalent of equilibrium-death.

The second law of thermodynamics is quite general. However, when intermolecular forces are long range, as in the case of particles interacting through gravitation, there are difficulties because our classification into extensive variables (proportional to volume) and intensive variable (independent of volume) does not apply. The total energy is no longer proportional to the volume. Fortunately gravitation forces are the very weak as compared to the short-range intermolecular forces. It is only on the astrophysical scale that this problem becomes important. The generality of the second law of thermodynamics gives us a powerful means to understand the thermodynamics aspects of real systems through the usage of ideal systems. A classical example is Planck's analysis of radiation in thermodynamics equilibrium with matter (blackbody radiation) in which Plank considered simple harmonic oscillators not merely because they are good approximations of molecules but because the properties of radiation in thermal equilibrium with matter are universal, regardless of the particular nature of

the matter with which the radiation interacts. The conclusion one arrives at using idealized oscillators and the laws of thermodynamics must also be valid for all other forms of matter, however, complex they are. What makes this new statement of the second law of thermodynamics valuable as a guide to energy policy is the relationship between entropy and the usefulness of energy. Energy is most useful to us when we can get it to flow from one substance to another, e.g. to warm a house and we can use it to do work. Useful energy thus must have low entropy so that the second law of thermodynamics will allow transfer or conversions to occur spontaneously.

1.1.14 Entropy

Entropy analysis is a medium to quantified the thermodynamics irreversibility in any fluid flow process. The first law of thermodynamics is simply an expression of the conservation of energy principle. The second law of thermodynamics states that all real processes are irreversible. Entropy generation is a measure of the account of irreversibility associated to the real processes. As entropy generation takes place, the quality of energy (i.e exergy) decreases. In order to preserve the quality of energy in a fluid flow process or at least to reduce the entropy generation, it is important to study the distribution of the entropy generation within the fluid volume. The optimal design for any thermal system can be achieved by minimizing entropy generation in the systems. Entropy generation in thermal engineering systems destroys available work and thus reduces its efficiency. Many studies have been published to assess the sources of irreversibility in components and systems. Bejan [11] studies the entropy generation for forced convective heat transfer due to temperature gradient and viscosity effect

in a fluid. Bejan [7] also presented various reasons behind entropy generation in applied thermal engineering where the generation of entropy destroys the available work, called exergy, of a system. The general equation for the entropy generation per unit volume is given by:

$$S^m = \frac{k}{T_w^2}(\nabla T)^2 + \frac{\mu}{T_w}\Phi,$$

the first term in the equation is the irreversibility due to heat transfer and the second term is the entropy generation due to viscous dissipation.

Within the past 50 years our view of nature has changed drastically. Classical science emphasized equilibrium and stability. Now we see fluctuations, instability, evolutionary processes on all levels from chemistry and biology to cosmology. Everywhere we observe irreversible processes in which time symmetry is broken. The distinction between reversible and irreversible processes was first introduced in thermodynamics through the concept of "entropy". In the modern context the formulation of entropy is for the understanding the thermodynamics aspects of self-organization, evolution of order and life that we see in nature. When a system is isolated, energy increase will be zero. In this case the entropy of the system will continue to increase due to irreversibility processes and reach the maximum possible value, which is the state of thermodynamics equilibrium. In the state of equilibrium, all irreversible processes cease. When the system begins to exchange entropy with the exterior then, in general, it is driven away from equilibrium, and the entropy producing the irreversible processes begins to operate. The exchange of entropy is due to exchange of heat and matter. The entropy flowing out of an adiabatic system is always larger than the entropy flowing into the system, the difference arising due to entropy produced by irreversible processes within the system. The internal energy of the system is ran-

domly distributed as kinetic energy at a the molecular and submolecular levels and as energy associated with attractive or repulsive forces between molecular and submolecular entities, which are moving closer together or further apart in relation to the mean separation. This energy is sometimes describe as being 'disordered' as it is not accessible as work at the macroscopic level in the same way as is the kinetic energy or gravitational potential energy that an entire system possesses owning to its velocity or position in the gravitational field. Although energy is the capability to do work, it is not possible directly to access the minute quantities of disordered energy possessed at a given instant by the various modes of energy possession of the entities so as to yield mechanical shaft work on the macroscopic scale. The term 'disorder' refers to the lack of information about exactly how much energy is associated at any moment with each mode of energy possession of each molecular or submolecular entity within the system.

1.1.15 Channel Flow

Channel flow constitutes a very important class of flows in fluid mechanics due to its numerous applications in biological and engineering systems. As a result, it is important that we study the characteristics of this flow. We are particular interested in how the flow pattern is modified by the effects of changing viscosity. The viscosity of many fluids varies with temperature e.g physiological fluids such as blood, various lubricants used in engineering systems like polymer solutions, mineral oils with polymer additives, etc. This variation in the fluid viscosity due to temperature is certainly going to affect the flow characteristics. In this respect, we shall consider two types of channel flows, namely Poiseuille flow and Couette flow. Poiseuille flow

is flow between two parallel stationary plates due to an imposed constant pressure gradient. Its general characteristics is parabolic axial velocity profile. Couette flow is considered with the effect of viscosity due to temperature changes on the lubrication that occurs between two moving plates or between a fixed plate and a moving plate.

1.1.16 Gauss's Divergence Theorem

Let F be a vector field. The Gauss's divergence theorem relates the volume integral of div F $(\nabla \cdot F)$ with the surface flux integral of F (i.e the surface integral of $F \cdot \hat{n}$). i.e

$$\iiint_V \nabla \cdot F dV = \iint_s F \cdot \hat{n} ds$$

where V is the volume and s is its bounding surface, with unit outwards normal $\hat{n}$.

1.2 Literature Review

The study of fluids convection in porous channel has received considerable attention over few centuries due to its wide applications in physical, biological and applied sciences. Berman [8] studied laminar flow in a two-dimensional rectangular channel with porous wall. He showed that the corresponding Navier-Stoke equations can be reduced to a nonlinear third order ordinary differential equation with two point boundary conditions and Reynolds number Re based on injection-velocity. The perturbation results for extremely small Reynolds number was given by him. Some years later, Sellar [108] obtained a solution for large Reynolds number and Yuan [127] obtained solution for large negative Reynolds number. Jocelyne [52] presented an analytical solution for the axial and transverse flow fields in laminar flow in porous

channels for both a rectangular channel with one porous wall and a porous tubular channel. Various asymptotic results and numerical results were given in years later by [94,101,113,115,116]. Makinde [75] considered the computer extension of perturbation series solution, its analysis and analytic continuation in obtainning valuable information on the solution structure at large Reynolds numbers, including bifurcation study for porous tube flow problem. Munson-McGee [86] presented an approximate solution for fluid dynamics of flow through a porous tube, such as encountered in the cross-flow filtration process. Makinde [76] investigated a new series summation and converging improvement technique to study the steady flow of a viscous incompressible fluid flow both in a porous pipe with moving walls and an exponentially diverging asymmetrical channel. Makinde [77] investigated the problem of laminar flow in channels of slow varying width permeable boundaries. Rashidi et at [95] proposed a reliable algorithms to develop exact and approximate solutions for the problem of laminar viscous flow in a semi-porous channel in the presence of a transverse magnetic field. They used differential transform method (DTM) to compute an approximation to the solution of the system of nonlinear differential equations governing the problem and concluded that DTM was applied successfully to find the analytical solution of the resulting ordinary differential equation. It's also reduces the computational difficuties of the other methods. Awartani and Hamdan [4] studied the effects of the porous matrix and the microscopic inertia on the velocity profiles for different flow-driving mechanisms by considering plane, parallel and fully-developed flow through straight porous channels. They concluded that introducing a porous structure in the flow domain resulted in slowing down the flow and the presence of microscopic inertia in a chosen model further reduces the velocity and slows down the flow. Kamisli

[41] developed a model with which to determine the transient velocity profiles of a non-Newtonia fluid that is disturbed by transverse mass suction/injection from the bottom plate. He examined the power-law fluid flow in rectangular channel with one of its walls porous, in terms of determining velocity profiles as functions of time, non-Newtonian behaviour (power-law index) and mass suction/injection rate at the lower plate. Several work have been carried out on porous channel wall (see, example [16,53,55,78,79,87,110,119]).

Recently there has been an increased interest in thermal stability/ heat transfer through porous media. Various fluids flow and heat transfer arrangement have been dealt with both analytical and numerical. Vafai et al [120] investigated the nature and importance of the boundary and inertial effects on the flow and heat transfer in porous media. They showed that the effect of the boundary on the heat transfer was quite important. The inertial effects increase with permeability and decrease with fluid viscosity. Chawla et al [38] investigated the effect of radiation heat transfer on thermally developing Poiseuille flow. Makinde [80] investigated the thermal stability of a reactive viscous fluid flowing steadily through a porous-saturated channel with convective cooling at the boundaries using a special type of Hermite-Pade approximants. Jou [56] investigated onset of thermal stability of the horizontal superpodes system of fluid and porous layers, in a rotating coordinate by employing Boussinesq's approximation, local volume average technique and Darcy's law and assumed the slipping interface. Terril [117] solved heat transfer problem of a discontinuous change in temperature in porous channel. Calgagni et al [39] performed an experimental and numerical study of free convective heat transfer in a square enclosure characterized by a discrete heating at lower walls and cooled from the vertical walls. Aydin at al [5] investigated

numerically the natural convection of air in a vertical square cavity with localized isothermal heating from below and symmetrical cooling from the side walls. Hossain et al [47] studied the effect of temperature dependent viscosity on natural convection of fluid from heated vertical wavy surface. The unsteady MHD convective heat and mass transfer flow past a semi-infinite vertical porous plate with variable viscosity and thermal conductivity, assuming that viscosity of the fluid varies as an inverse linear function of temperature was studied by Reddy et al [98]. Makinde [81] investigated the combined effects of viscosity variation and energy dissipation on steady flow of an incompressible fluid in a pipe with moving surface. Makinde [82] examined the effect of thermal radiation on inherent irreversible in the flow of a variable viscosity optically thin fluid through a channel with isothermal walls. Yeroshenko [125] considered heat transfer in a developed laminar incompressible flow with constant physical properties in a two-dimensional channel with porous walls having constant temperature. They obtained several asymptotic solutions of the energy equation for small and large wall Peclet numbers and large Prandlt numbers. Many research work have been conducted on thermal stability/heat transfer in a porous channel.

Furthermore, entropy generation which is the measure of the destruction of available energy in a system plays an important role in the design and development of engineering processes such as heat exchangers, pumps, turbine and pipe networks. The energy utilization during the convection in any fluids flow as well as the improvement in thermal system is one of the fundamental problems of the engineering processes. An improvement of thermal system according to Makinde [65] will provide better material processing, energy conservation and environmental effects. Second law analysis method is therefore used for predicting the performance of the engineering processes.

The second law of thermodynamics is applied to investigate the irreversibility in terms of the entropy generation rate. Bejan [10] was the pioneer work on entropy generation. He first presented the second law aspect of heat transfer using different examples of fundamental forced convection problem. He introduced the concept of energy generation number, irreversibility distribution ratio and presented the spatial distribution of irreversibility, entropy generation profiles for the examples. Ever since then, numerous researches have been conducted to determine the entropy generation and irreversibility profiles for different geometric configurations, flow situation and thermal boundary conditions. Bejan [7,11] investigated entropy generation and minimization and showed the fundamental importance of entropy minimization for efficient engineering processes. Mahmud [59] investigated second law analysis in fundamental convective heat transfer and entropy generation for natural convection in a two-dimensional circular section enclose. Tasnism et al [111] performed an analytical work to study the first and second law (of thermodynamics) characteristics of flow and heat transfer inside a vertical channel made of two parallel plates embedded in a porous medium and under the action of transverse magnetic field. They showed that, for positive value of heat generation/absorption parameter, entropy generation rate was higher than the negative value of the same magnitude. Makinde [65] investigated the entropy generation rate in a laminar flow through a channel filled with saturated porous media. Makinde [83] studied the second law analysis of a laminar falling viscous incompressible liquid film along an inclined porous heated plate while the upper surface of the liquid film is considered free and adiabatic. Makinde [84] considered criticality and entropy analysis for variable viscosity Couette flow. Tasnim and Makinde [112] considered entropy generation in a vertical concentric isothermal chan-

nel with temperature-dependent viscosity by indicating that the maximum volumetric entropy generation is largely influenced by the fluid viscosity variation. Haddad et al [43] conducted numerical investigation on the entropy generation due to steady laminar forced convection fluid flow through parallel plates micro-channel. Heat transfer and entropy generation for a gravity-driven, non-Newtonian Ostwald-deWaele power-law, liquid film along an inclined isothermal plate was discussed by Makinde [68]. Makinde [68-69] investigated the effect of variable viscosity on thermodynamics irreversibility that occurs in plane Poiseuille flow with convective cooling at the walls. He reported that a decrease in fluid viscosity enhances the entropy generation rate, while the dominant effect of heat transfer irreversibility near the channel walls decreases with an increase in convective cooling. Several work have been conducted on second law analysis as well as entropy generation profiles such as[18,23,24,26,45,66,93].
The present study sets out to investigate the analysis of laminar flow, thermal stability and entropy generation in a porous channel and cylindrical pipes.

1.3 Statement of the Problem

Fluid flow through a porous channel and cylindrical pipe walls are important area of research due to its wide applications in transpiration cooling, gaseous diffusion technology, cooling of rocket, mechanized irrigation and filtration processes. It is therefore necessary to examine the combined effects of buoyancy forces, Navier slip and variable viscosity on the entire flow structure, thermal stability and entropy generation in the system. The problem will be investigated theoretically using appropriate mathematical models for both transient and steady scenarios.

1.4 Aim of the Study

The aim of this study is to analyze theoretically the laminar flow, thermal stability and entropy generation in porous channel and cylindrical pipe walls.

1.5 Objectives of the Study

The objectives of this study are:

(1) To examine velocity profiles, temperature profiles, skin friction and Nusselt number for both time dependent and steady flow problems.

(2) To examine Navier slip effect, combined effects of buoyancy forces and variable viscosity on the entire flow structure.

(3) To obtain the thermal stability condition for flow in porous channel and porous pipe geometries.

(4) To examine the entropy production rate, irreversibility ratio, Bejan number and some of the embedded parameters for the flow.

1.6 Methodology

We employed both the numerical and analytical methods in solving the models equations i.e. the boundary valued problems (BPV). By numerical method, we used shooting method together with fourth order Runge-Kutta integration method. Shooting method reformulates the boundary value problem (BVP) to initial value problem (IVP) by adding sufficient number of conditions at one end and adjust these conditions until the given conditions are satisfied at the other end while Runge-Kutta

method solve the initial value problems. These methods are based on finite-difference numerical techniques.

NUMERICAL APPROACH: Consider the two-point boundary value problem

$$y'' = f(x, y, y'), \quad y(a) = \alpha, \quad y(b) = \beta, \tag{1.1}$$

where $a < b$ and $x \in [a, b]$.

Making an initial guess ϱ for $y'(a)$ and denote by $y(x; \varrho)$ the solution of the initial value problem is

$$y''(x) = f(x, y, y'), \quad y(a) = \alpha, \quad y'(a) = \varrho. \tag{1.2}$$

Introducing the notation $\Upsilon(x; \varrho) = y(x; \varrho)$ and $\nu(x; \varrho) = \frac{\partial}{\partial x} y(x; \varrho)$, equation (1.2) can be rewritten as

$$\begin{aligned} \frac{\partial}{\partial x}\Upsilon(x; \varrho) &= \nu(x; \varrho), \qquad \Upsilon(a; \varrho), \\ \frac{\partial}{\partial x}\nu(x; \varrho) &= f(x, \Upsilon(x; \varrho), \nu(x; \varrho)), \qquad \nu(a; \varrho). \end{aligned} \tag{1.3}$$

The solution $\Upsilon(x; \varrho)$ of the initial value problem (1.3) will coincide with the solution $y(x)$ of the boundary value problem (1.1) provided we can find a value of ϱ such that

$$\Phi(\varrho) \equiv \Upsilon(b; \varrho) - \beta = 0. \tag{1.4}$$

The basic ideal of the shooting method for the numerical solution of the boundary value problem (1.1) is to find a root to the equation (1.4). Here fourth order Runge-Kutta techniques is used to find the root and the scheme for the fourth order Runge-Kutta is

$$y_{n+1} = y_n + \frac{h}{6}\Big(k_1 + 2k_2 + 2k_3 + k_4\Big),$$

where

$$
\begin{aligned}
k_1 &= f(x_n, y_n), \\
k_2 &= f(x_n + \frac{h}{2}, y_n + \frac{hk_1}{2}), \\
k_3 &= f(x_n + \frac{h}{2}, y_n + \frac{hk_2}{2}), \\
k_3 &= f(x_n + h, y_n + hk_3).
\end{aligned}
$$

We developed a numerical code that incorporate the methods described above, using maple to tackled the problems.

ANALYTICAL APPROACH: Due to the nonlinear nature of our model problem, it is convenient to form a power series expansion

$$w = \sum_{n=0}^{\infty} w_n \varepsilon^n,$$

substitute the power series expansion into the problem and collecting the coefficients of the likes powers of ε. Solve the equations for the coefficients of solution series iteratively to get solution for w.

Chapter 2

Basic equations for the Problem

The basis of computational fluid dynamics is the fundamental governing equations of fluid dynamics which are: the continuity, momentum and energy equations. These are the three fundamental physical principle upon which all the fluid dynamics are based on.

2.1 Continuity Equations

Continuity equation represents the law of mass. The total amount of mass conserved inside any control volume can only be changed by the amount that passes in or out of the control volume through the boundary. This means that the mass conserved cannot be created nor destroyed; it can only be changed from one form to another. Fluid in motion moves in such a way that mass is conserved. We shall consider the differential and integral approaches of deriving continuity equation.

Differential Approach

Consider a small control volume (CV) as shown in Fig. (2.1) below:

The principle of conservation of mass states that, the rate at which mass increase within the control volume is equal to the rate at which mass enters or leaves the

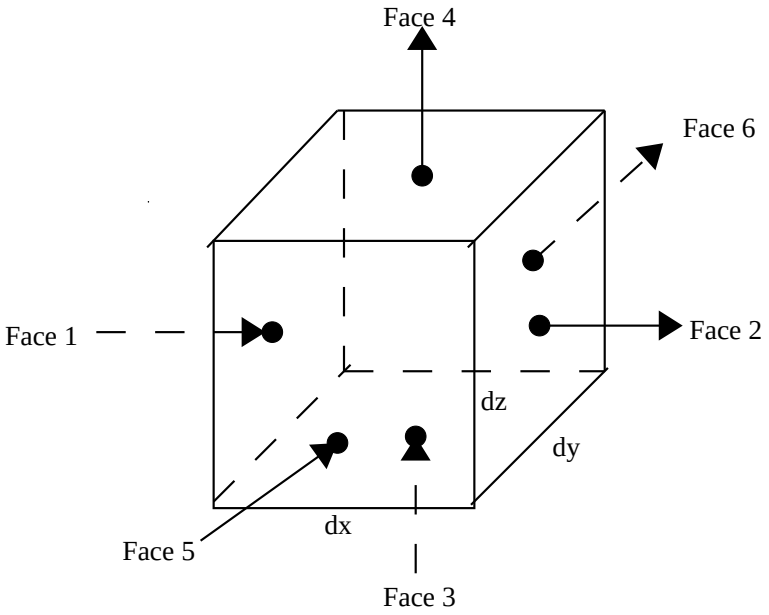

Figure 2.1: Control Volume with six faces

control volume through its six boundaries. Suppose ρ is the average density of the fluid within the control volume with velocity components (u, v, w) and the volume is $dV = dxdydz$. Then,

Mass within the control volume

$$= \rho dV = \rho dxdydz. \tag{2.1}$$

We consider the rate at which mass enters or leaves the control volume through centres of the six faces one by one using Taylor series expansion.

Mass enters through the centre at face 1, we have:

$$\rho u - \frac{dx}{2} = \rho u - \frac{dx}{2}\frac{\partial}{\partial x}(\rho u) + \left(\frac{dx}{2}\right)^2 \frac{\partial^2}{dx^2}(\rho u) - \left(\frac{dx}{2}\right)^3 \frac{\partial^3}{dx^3}(\rho u) + \cdots \tag{2.2}$$

Mass leaves through the centre at face 2, we have

$$\rho u + \frac{dx}{2} = \rho u + \frac{dx}{2}\frac{\partial}{\partial x}(\rho u) + \left(\frac{dx}{2}\right)^2 \frac{\partial^2}{dx^2}(\rho u) + \left(\frac{dx}{2}\right)^3 \frac{\partial^3}{dx^3}(\rho u) + \cdots \tag{2.3}$$

Mass enters through the centre at face 3, we have:

$$\rho v - \frac{dy}{2} = \rho v - \frac{dy}{2}\frac{\partial}{\partial y}(\rho v) + \left(\frac{dy}{2}\right)^2 \frac{\partial^2}{dy^2}(\rho v) - \left(\frac{dy}{2}\right)^3 \frac{\partial^3}{dy^3}(\rho v) + \cdots \tag{2.4}$$

Mass leaves through the centre at face 4, we have:

$$\rho v + \frac{dy}{2} = \rho v + \frac{dy}{2}\frac{\partial}{\partial y}(\rho v) + \left(\frac{dy}{2}\right)^2 \frac{\partial^2}{dy^2}(\rho v) + \left(\frac{dy}{2}\right)^3 \frac{\partial^3}{dy^3}(\rho v) + \cdots \tag{2.5}$$

Mass enters through the centre at face 5, we have:

$$\rho w - \frac{dz}{2} = \rho w - \frac{dz}{2}\frac{\partial}{\partial z}(\rho w) + \left(\frac{dz}{2}\right)^2 \frac{\partial^2}{dz^2}(\rho w) - \left(\frac{dz}{2}\right)^3 \frac{\partial^3}{dz^3}(\rho w) + \cdots \tag{2.6}$$

Mass leaves through the centre at face 6, we have:

$$\rho w + \frac{dz}{2} = \rho w + \frac{dz}{2}\frac{\partial}{\partial z}(\rho w) + \left(\frac{dz}{2}\right)^2 \frac{\partial^2}{dz^2}(\rho w) + \left(\frac{dz}{2}\right)^3 \frac{\partial^3}{dz^3}(\rho w) + \cdots \tag{2.7}$$

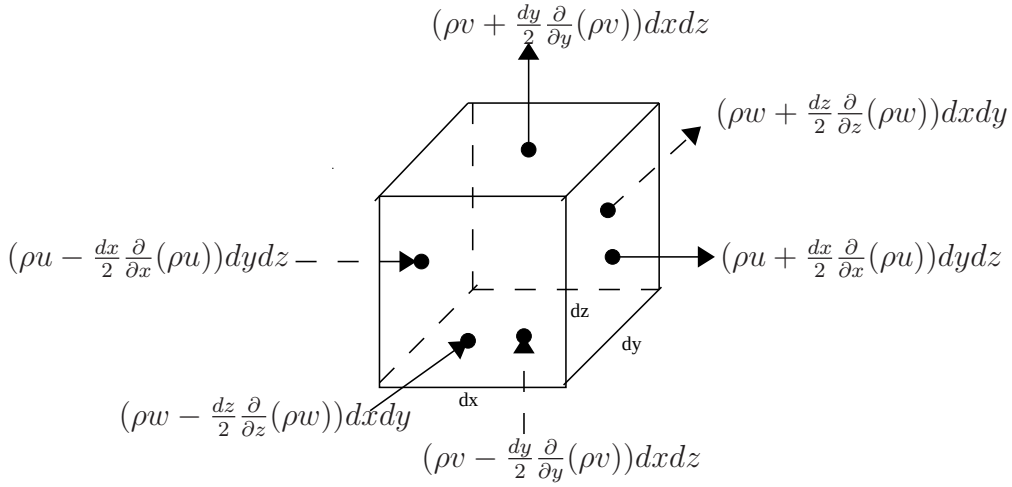

Figure 2.2: Control Volume

Ignoring derivatives of order 2 and higher orders from the above equation, then the mass flow rate into the control volume through faces, $1, 3$ and 5 are

$\Big(\rho u - \frac{dx}{2}\frac{\partial}{\partial x}(\rho u)\Big)dydz$, $\Big(\rho v - \frac{dy}{2}\frac{\partial}{\partial y}(\rho v)\Big)dxdz$, $\Big(\rho w - \frac{dz}{2}\frac{\partial}{\partial z}(\rho w)\Big)dxdy$,

and the mass flow rate out of the control volume through the faces,$2, 4$ and 6 are

$\Big(\rho u + \frac{dx}{2}\frac{\partial}{\partial x}(\rho u)\Big)dydz$, $\Big(\rho v + \frac{dy}{2}\frac{\partial}{\partial y}(\rho v)\Big)dxdz$, $\Big(\rho w + \frac{dz}{2}\frac{\partial}{\partial z}(\rho w)\Big)dxdy$.

The summation of mass flow rate into the control volume is:

$$\begin{aligned}\sum m_{in} &= \Big(\rho u - \frac{dx}{2}\frac{\partial}{\partial x}(\rho u)\Big)dydz + \Big(\rho v - \frac{dy}{2}\frac{\partial}{\partial y}(\rho v)\Big)dxdz + \Big(\rho w - \frac{dz}{2}\frac{\partial}{\partial z}(\rho w)\Big)dxdy \\ &= \Big(\rho u - \frac{1}{2}\frac{\partial}{\partial x}(\rho u) + \rho v - \frac{1}{2}\frac{\partial}{\partial y}(\rho v) + \rho w - \frac{dz}{2}\frac{\partial}{\partial z}(\rho w)\Big)dxdydz.\end{aligned}$$

The summation of mass flow rate out the control volume is:

$$\begin{aligned}\sum m_{out} &= \Big(\rho u + \frac{dx}{2}\frac{\partial}{\partial x}(\rho u)\Big)dydz + \Big(\rho v + \frac{dy}{2}\frac{\partial}{\partial y}(\rho v)\Big)dxdz + \Big(\rho w + \frac{dz}{2}\frac{\partial}{\partial z}(\rho w)\Big)dxdy \\ &= \Big(\rho u + \frac{1}{2}\frac{\partial}{\partial x}(\rho u) + \rho v + \frac{1}{2}\frac{\partial}{\partial y}(\rho v) + \rho w + \frac{dz}{2}\frac{\partial}{\partial z}(\rho w)\Big)dxdydz.\end{aligned}$$

By the conservation of mass equation, the rate of change of mass within the control volume with respect to time is equal to the summation of mass flow rate into the control volume minus summation of the mass flow rate out of the control volume.

$$\begin{aligned}dxdydz\frac{\partial \rho}{\partial t} &= \sum m_{in} - \sum m_{out} \\ &= \Big(\rho u - \frac{1}{2}\frac{\partial}{\partial x}(\rho u) + \rho v - \frac{1}{2}\frac{\partial}{\partial y}(\rho v) + \rho w - \frac{dz}{2}\frac{\partial}{\partial z}(\rho w)\Big)dxdydz \\ &\quad -\left(\Big(\rho u + \frac{1}{2}\frac{\partial}{\partial x}(\rho u) + \rho v + \frac{1}{2}\frac{\partial}{\partial y}(\rho v) + \rho w + \frac{dz}{2}\frac{\partial}{\partial z}(\rho w)\Big)dxdydz\right) \\ &= \left(-\frac{\partial}{\partial x}(\rho u) - \frac{\partial}{\partial y}(\rho v) - \frac{\partial}{\partial z}(\rho w)\right)dxdydz.\end{aligned}$$

This implies:

$$\frac{\partial \rho}{\partial t} + \frac{\partial}{\partial x}(\rho u) + \frac{\partial}{\partial y}(\rho v) + \frac{\partial}{\partial z}(\rho w) = 0 \tag{2.8}$$

Equation (2.8) is called continuity equation. We shall see other ways of written it later.

Integral Approach

Consider a control volume, V, bounded by the control surface S. The net rate of

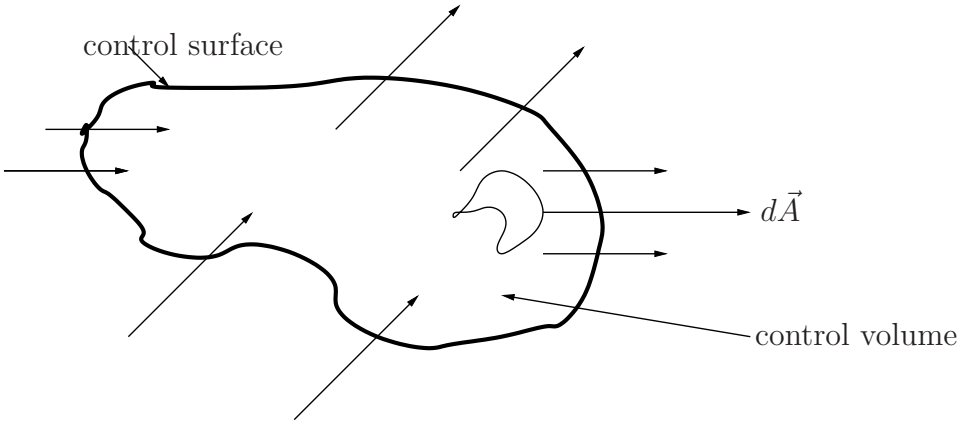

Figure 2.3: Control Volume for derivation of continuity equation (integral form)

mass efflux across the control surface, S, velocity vector $\vec{V}$ at an elemental area $d\vec{A}$ is:

$$\iint_s \rho \vec{V} d\vec{A}.$$

Mass accumulation rate within the control volume is therefore

$$\frac{\partial}{\partial t} \iiint_v \rho dV,$$

where V is the total volume, the principle of conservation of mass states that, the rate of accumulation of mass in the control volume together with the rate of mass efflux from the control volume must be zero. Hence,

$$\frac{\partial}{\partial t} \iiint_v \rho dV + \iint_s \rho \vec{V} d\vec{A} = 0. \tag{2.9}$$

Applying Gauss's divergence theorem on the second expression on the left hand, then

$$\iint_s \rho\vec{V}d\vec{A} = \iiint_v div(\rho\vec{V})dV = \iiint_v \nabla\cdot(\rho\vec{V})dV. \tag{2.10}$$

Subtitute equation (2.10) to (2.9), we have

$$\frac{\partial}{\partial t}\iiint_v \rho dV + \iiint_v \nabla\cdot(\rho\vec{V})dV = 0. \tag{2.11}$$

Since volume does not change with time, then

$$\iiint_v \Big(\frac{\partial\rho}{\partial t} + \nabla\cdot(\rho\vec{V})\Big)dV = 0,$$

therefore,

$$\frac{\partial\rho}{\partial t} + \nabla\cdot(\rho\vec{V}) = 0. \tag{2.12}$$

Since $\nabla = \frac{\partial}{\partial x}i + \frac{\partial}{\partial y}j + \frac{\partial}{\partial z}k$ and $\vec{V} = ui + vj + wk$, therefore equation(2.8) and equation (2.12) are the same and they are called continuity equation for compressible flow.

For a constant density, ρ, then we have continuity equation for incompressible flow

$$\nabla\cdot(\rho\vec{V}) = 0,$$

where $\nabla\cdot(\rho\vec{V})$ is called divergence of the velocity and physically, is the rate of change of volume of a moving fluid element, per unit volume.

The continuity equation in cartesian coordinate is:

$$\frac{\partial\rho}{\partial t} + \frac{\partial}{\partial x}(\rho u) + \frac{\partial}{\partial y}(\rho v) + \frac{\partial}{\partial z}(\rho w) = 0.$$

In spherical polar coordinates:

$$\frac{\partial\rho}{\partial t} + \frac{\partial}{r^2\partial r}(\rho r^2 u_r) + \frac{\partial}{rsin\theta\partial\theta}(\rho u_\theta sin\theta) + \frac{\partial}{rsin\theta\partial\phi}(\rho u\phi) = 0.$$

In cylindrical polar coordinates:

u_r, u_θ and u_z, are the velocity components in their respective direction. The transformation between the cartesian and the polar system is given by the relations,

$$r = \sqrt{x^2 + y^2}, \theta = tan^{-1}\frac{y}{x}, z = z$$

and del operator as $\nabla\rho = \frac{1}{r}\frac{\partial}{\partial r}(r\rho) + \frac{1}{r}\frac{\partial}{\partial\theta}(\rho) + \frac{\partial}{\partial z}(\rho)$, therefore the continuity equation in a cylindrical polar coordinate is given as:

$$\frac{\partial\rho}{\partial t} + \frac{\partial}{r\partial x}(\rho r u_r) + \frac{\partial}{r\partial\theta}(\rho u_\theta) + \frac{\partial}{\partial z}(\rho u_z) = 0.$$

2.2 Navier-Stoke Equations

The central equations for fluid dynamics are the Navier Stoke equations, which are nonlinear partial differential equations with time and space dependency. Its describe the flow of a fluid whose stress depends linearly on velocity and pressure. These equations were originally derived in the 1840s on the basis of conservation laws and first-order approximations. In fact, they are very simple in nature but very difficult to solve. There are very few analytical solutions and the numerical approach is very challenging task. Therefore, many simplification approaches are developed to describe specific fluids. The sets of equations give continuum phenomena in all areas of sciences.

By Newton's second law which state that the net forces on the fluid element equals to its mass times the acceleration of the element.

$$m\vec{a} = m\frac{D\vec{V}}{Dt} = \sum \vec{f}, \tag{2.13}$$

but

$$\rho = \frac{m}{V}, \quad V = dxdydz, \quad m = \rho dxdydz, \tag{2.14}$$

where m is the mass, V is the volume, ρ is the density and $\vec{V}$ is the velocity vector.

By material derivatives

$$\frac{D\vec{V}}{Dt} = \frac{\partial \vec{V}}{\partial t} + (\vec{V} \cdot \nabla)\vec{V}. \tag{2.15}$$

In cartesian coordinates, $\vec{V} = (u, v, w)$ and the material derivatives becomes:

$$\begin{aligned}
\frac{Du}{Dt} &= \frac{\partial u}{\partial t} + u\frac{\partial u}{\partial x} + v\frac{\partial u}{\partial y} + w\frac{\partial u}{\partial z} \\
\frac{Dv}{Dt} &= \frac{\partial v}{\partial t} + u\frac{\partial v}{\partial x} + v\frac{\partial v}{\partial y} + w\frac{\partial v}{\partial z} \\
\frac{Dw}{Dt} &= \frac{\partial w}{\partial t} + u\frac{\partial w}{\partial x} + v\frac{\partial w}{\partial y} + w\frac{\partial w}{\partial z}
\end{aligned}$$

We express the total force as the sum of body forces and surface forces.

$$\sum \vec{f} = \sum \vec{f_b} + \sum \vec{f_s}. \tag{2.16}$$

Body forces consist of gravity force, electromagnetic force, centrifugal force and coriolis force while surface forces consist of pressure forces and viscous forces.

Considering the y-component where $\vec{V} = (u, v, w)$, substitute equations (2.14)-(2.16) and to (2.13), we obtain

$$\rho dxdydz\frac{Dv}{Dt} = \sum \vec{f_{by}} + \sum \vec{f_{sy}}. \tag{2.17}$$

We assume the body force is the gravitational force, then

$$\sum \vec{f_{by}} = mg_y = \rho dxdydzg_y. \tag{2.18}$$

Surface forces act directly on the surface of the fluid element and they are only due to two sources:

(i) The pressure distribution acting on the surfaces, imposed by the outside fluid surrounding the fluid element.

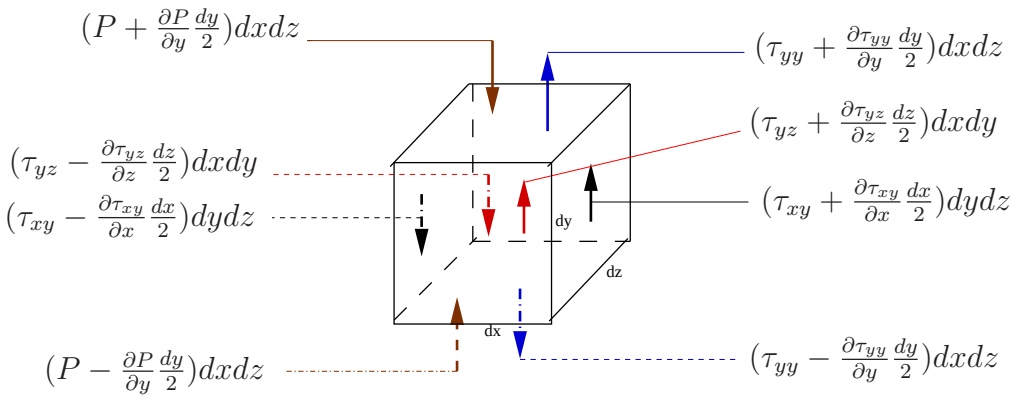

Figure 2.4: Details of forces acting on a three-dimensional control volume

(ii) The shear and normal stress distribution acting as well on the surfaces.

The net y-component of pressure force using Taylor series expansion at the centre of the face neglecting order two and the higher order terms, we obtain

$$\Big(P-\frac{\partial P}{\partial y}\frac{dy}{2}\Big)dxdz-\Bigg[\Big(P+\frac{\partial P}{\partial y}\frac{dy}{2}\Big)dxdz\Bigg]=-\frac{\partial P}{\partial y}dydxdz.$$

The net y-component of the viscous forces using Taylor series expansion at the centre of the faces neglecting order two and the higher order terms:

$$\begin{aligned}
= \quad & -\Big(\tau_{yy}-\frac{\partial \tau_{yy}}{\partial y}\frac{dy}{2}\Big)dxdz+\Big(\tau_{yy}+\frac{\partial \tau_{yy}}{\partial y}\frac{dy}{2}\Big)dxdz \\
& -\Big(\tau_{xy}-\frac{\partial \tau_{xy}}{\partial x}\frac{dx}{2}\Big)dydz+\Big(\tau_{xy}+\frac{\partial \tau_{xy}}{\partial x}\frac{dx}{2}\Big)dydz \\
& -\Big(\tau_{zy}-\frac{\partial \tau_{zy}}{\partial z}\frac{dz}{2}\Big)dxdy+\Big(\tau_{zy}+\frac{\partial \tau_{zy}}{\partial z}\frac{dz}{2}\Big)dxdy \\
= \quad & \Big(\frac{\partial \tau_{yy}}{\partial y}+\frac{\partial \tau_{xy}}{\partial x}+\frac{\partial \tau_{yz}}{\partial z}\Big)dxdydz \qquad (2.19)
\end{aligned}$$

Net surface force in the y-component:

$$\sum \vec{f_{sy}}=\Big(-\frac{\partial P}{\partial y}+\frac{\partial \tau_{yy}}{\partial y}+\frac{\partial \tau_{xy}}{\partial x}+\frac{\partial \tau_{yz}}{\partial z}\Big)dxdydz. \qquad (2.20)$$

The total forces in y-component is the sum of equations (2.18) and (2.20) which is

$$\sum \vec{f} = \Big(- \frac{\partial P}{\partial y} + \frac{\partial \tau_{yy}}{\partial y} + \frac{\partial \tau_{xy}}{\partial x} + \frac{\partial \tau_{yz}}{\partial z} + \rho g_y \Big) dxdydz. \tag{2.21}$$

Combining equations (2.21), (2.13) and (2.14), we obtain,

$$\rho \frac{Dv}{Dt} = -\frac{\partial P}{\partial y} + \frac{\partial \tau_{yy}}{\partial y} + \frac{\partial \tau_{xy}}{\partial x} + \frac{\partial \tau_{yz}}{\partial z} + \rho g_y, \tag{2.22}$$

which is y-component of the momentum for viscous flow. In the same manner, x and z- components can be derived as

$$\rho \frac{Du}{Dt} = -\frac{\partial P}{\partial x} + \frac{\partial \tau_{xx}}{\partial x} + \frac{\partial \tau_{xy}}{\partial y} + \frac{\partial \tau_{xz}}{\partial z} + \rho g_x \tag{2.23}$$

and

$$\rho \frac{Dw}{Dt} = -\frac{\partial P}{\partial z} + \frac{\partial \tau_{xz}}{\partial x} + \frac{\partial \tau_{yz}}{\partial y} + \frac{\partial \tau_{zz}}{\partial z} + \rho g_z. \tag{2.24}$$

These are non-conservative form of Navier-Stoke equations. The Navier-Stoke equations in form of conservative can be obtained by writing $\rho \frac{Dv}{Dt}$ in terms of material derivatives,

$$\begin{aligned} \rho \frac{Dv}{Dt} &= \rho \Big(\frac{\partial v}{\partial t} + u \frac{\partial v}{\partial x} + v \frac{\partial v}{\partial y} + w \frac{\partial v}{\partial z} \Big), \\ &= \rho \frac{\partial v}{\partial t} + \rho \vec{V} \cdot (\nabla v). \end{aligned} \tag{2.25}$$

By product rules,

$$\begin{aligned} \frac{\partial}{\partial t}(\rho v) &= \rho \frac{\partial v}{\partial t} + v \frac{\partial \rho}{\partial t}, \\ \rho \frac{\partial v}{\partial t} &= \frac{\partial}{\partial t}(\rho v) - v \frac{\partial \rho}{\partial t}. \end{aligned} \tag{2.26}$$

Furthermore by divergence product,

$$\begin{aligned} \nabla \cdot (\rho v \vec{V}) &= v \nabla \cdot (\rho \vec{V}) + \rho \vec{V} \cdot (v \nabla) \\ \rho \vec{V} \cdot (v \nabla) &= \nabla \cdot (\rho v \vec{V}) - v \nabla \cdot (\rho \vec{(V)}) \end{aligned} \tag{2.27}$$

Combining equations (2.25),(2.26) and (2.27) we obtain,

$$\rho\frac{Dv}{Dt} = \frac{\partial}{\partial t}(\rho v) - v\Big(\frac{\partial \rho}{\partial t} + \nabla\cdot(\rho\vec{V})\Big) + \nabla\cdot(\rho v\vec{V}). \tag{2.28}$$

The equation in the bracket in equation (2.28) is referred to as continuity equation which is zero. Hence,

$$\rho\frac{Dv}{Dt} = \frac{\partial}{\partial t}(\rho v) + \nabla\cdot(\rho v\vec{V}). \tag{2.29}$$

Combining equations (2.22) and (2.29), we obtain,

$$\frac{\partial}{\partial t}(\rho v) + \nabla\cdot(\rho v\vec{V}) = -\frac{\partial P}{\partial y} + \frac{\partial \tau_{yy}}{\partial y} + \frac{\partial \tau_{xy}}{\partial x} + \frac{\partial \tau_{yz}}{\partial z} + \rho g_y. \tag{2.30}$$

Similarly for x and z-components:

$$\frac{\partial}{\partial t}(\rho u) + \nabla\cdot(\rho u\vec{V}) = -\frac{\partial P}{\partial x} + \frac{\partial \tau_{xx}}{\partial x} + \frac{\partial \tau_{xy}}{\partial y} + \frac{\partial \tau_{xz}}{\partial z} + \rho g_x, \tag{2.31}$$

$$\frac{\partial}{\partial t}(\rho w) + \nabla\cdot(\rho w\vec{V}) = -\frac{\partial P}{\partial z} + \frac{\partial \tau_{xz}}{\partial x} + \frac{\partial \tau_{yz}}{\partial y} + \frac{\partial \tau_{zz}}{\partial z} + \rho g_z. \tag{2.32}$$

By Newton's law of viscosity, the viscous stress components are related to the dynamics viscosity coefficient μ and second viscosity coefficient λ by:

$$\tau_{xx} = 2\mu\frac{\partial u}{\partial x} + \lambda\nabla\cdot\vec{V}\tau_{yy} = 2\mu\frac{\partial v}{\partial y} + \lambda\nabla\cdot\vec{V}, \quad \tau_{zz} = 2\mu\frac{\partial w}{\partial z} + \lambda\nabla\cdot\vec{V}$$

$$\tau_{xy} = \tau_{yx} = \mu\Big(\frac{\partial v}{\partial x} + \frac{\partial u}{\partial y}\Big), \quad \tau_{zx} = \tau_{xz} = \mu\Big(\frac{\partial w}{\partial x} + \frac{\partial u}{\partial z}\Big), \quad \tau_{yz} = \tau_{zy} = \mu\Big(\frac{\partial v}{\partial z} + \frac{\partial w}{\partial y}\Big)$$

Substitute these to equation (2.30), we obtain

$$\frac{\partial}{\partial t}(\rho v)+\nabla\cdot(\rho v\vec{V}) = -\frac{\partial P}{\partial y}+\frac{\partial}{\partial y}\Big(2\mu\frac{\partial v}{\partial y}+\lambda\nabla\cdot\vec{v}\Big)+\frac{\partial}{\partial x}\Big(\mu\Big(\frac{\partial v}{\partial x}+\frac{\partial u}{\partial y}\Big)\Big)+\frac{\partial}{\partial z}\Big(\mu\Big(\frac{\partial v}{\partial z}+\frac{\partial w}{\partial y}\Big)\Big)+\rho g_y \tag{2.33}$$

Similarly equations (2.31) and (2.32) become,

$$\frac{\partial}{\partial t}(\rho u)+\nabla\cdot(\rho u\vec{V}) = -\frac{\partial P}{\partial x}+\frac{\partial}{\partial x}\Big(2\mu\frac{\partial u}{\partial x}+\lambda\nabla\cdot\vec{v}\Big)+\frac{\partial}{\partial y}\Big(\mu\Big(\frac{\partial v}{\partial x}+\frac{\partial u}{\partial y}\Big)\Big)+\frac{\partial}{\partial z}\Big(\mu\Big(\frac{\partial w}{\partial x}+\frac{\partial u}{\partial z}\Big)\Big)+\rho g_x \tag{2.34}$$

and

$$\frac{\partial}{\partial t}(\rho w)+\nabla\cdot(\rho w\vec{V}) = -\frac{\partial P}{\partial z}+\frac{\partial}{\partial x}\Big(\mu\Big(\frac{\partial w}{\partial x}+\frac{\partial u}{\partial z}\Big)\Big)+\frac{\partial}{\partial y}\Big(\mu\Big(\frac{\partial v}{\partial z}+\frac{\partial w}{\partial y}\Big)\Big)+\frac{\partial}{\partial z}\Big(2\mu\frac{\partial w}{\partial z}+\lambda\nabla\cdot\vec{v}\Big)+\rho g_z \tag{2.35}$$

Equations (2.33),(2.34),and (2.35) are complete Navier Stoke equations in conservation form. For compressible flow when $\nabla\cdot\vec{V}=0$ and ρ is constant, then the Navier-Stoke equations for y-component is of the form:

$$\rho\Big(\frac{\partial v}{\partial t}+u\frac{\partial v}{\partial x}+v\frac{\partial v}{\partial y}+w\frac{\partial v}{\partial z}\Big) = -\frac{\partial P}{\partial y}+\mu\Big(\frac{\partial^2 v}{\partial y^2}+\frac{\partial^2 v}{\partial x^2}+\frac{\partial^2 v}{\partial z^2}\Big)+\rho g_y.$$

Similarly for x-component:

$$\rho\Big(\frac{\partial u}{\partial t}+u\frac{\partial u}{\partial x}+v\frac{\partial u}{\partial y}+w\frac{\partial u}{\partial z}\Big) = -\frac{\partial P}{\partial x}+\mu\Big(\frac{\partial^2 u}{\partial y^2}+\frac{\partial^2 u}{\partial x^2}+\frac{\partial^2 u}{\partial z^2}\Big)+\rho g_x,$$

and for z-component:

$$\rho\Big(\frac{\partial w}{\partial t}+u\frac{\partial w}{\partial x}+v\frac{\partial w}{\partial y}+w\frac{\partial w}{\partial z}\Big) = -\frac{\partial P}{\partial z}+\mu\Big(\frac{\partial^2 w}{\partial y^2}+\frac{\partial^2 w}{\partial x^2}+\frac{\partial^2 w}{\partial z^2}\Big)+\rho g_z.$$

With the vectorial form of:

$$\rho\frac{D\vec{V}}{Dt} = -\nabla P+\mu\nabla^2\vec{V}+\rho\vec{g}.$$

2.3 Energy Equation

We require conservation of energy to complete the system of equations. Energy equation is a mathematical statement that is based on the physical law i.e. first law of thermodynamics which states that the sum of the work and heat added to a system will equal the increase of energy. Going by the derivation given by White[122]:

$$\underbrace{dE_t}_{\text{Change of the total energy of the system}} = \underbrace{dQ}_{\text{Change of the heat added}} + \underbrace{dW}_{\text{Change of work done on the system}} \tag{2.36}$$

The quantity E_t consists of internal energy, kinetic and potential energy given by

$$E_t = \rho\left(e + \frac{V^2}{2} - g \cdot r)\right), \tag{2.37}$$

where e is the internal energy, the second term on the right hand side is kinetic energy while the last term is potential energy, r is the displacement of the particle and $V = \frac{dr}{dt}$.

Writing equation (2.36) in terms of time rate of change, it becomes

$$\frac{DE_t}{Dt} = \frac{DQ}{Dt} + \frac{DW}{Dt}. \tag{2.38}$$

Using equation (2.37), then equation (2.38) becomes

$$\rho\left(\frac{De}{Dt} + V\frac{DV}{Dt} - g \cdot V\right) = \frac{DQ}{Dt} + \frac{DW}{Dt}. \tag{2.39}$$

We therefore need to express the Q and W in terms of fluid properties. The heat flow

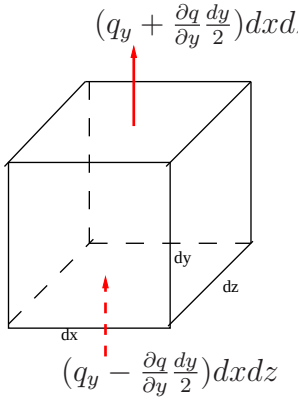

Figure 2.5: y-component of heat flux in and out of control volume

into and out of the control volume is identical to mass flow. From figure (2.5) above, the net heat flow into the control volume in y-component is:

$$\begin{aligned} q_{y_{in}} - q_{y_{out}} &= (q_y - \frac{\partial q}{\partial y}\frac{dy}{2})dxdz - (q_y + \frac{\partial q}{\partial y}\frac{dy}{2})dxdz \\ &= -\frac{\partial q}{\partial y}dydxdz. \end{aligned} \tag{2.40}$$

In the similar manner, we obtain the net heat flow into the control volume in x and z-components. Summing up all the net heat flow into the control volume in y,x and z-components and divide by $dydxdz$ gives the net rate of heat transfer to the fluid per unit volume. i.e.

$$\frac{DQ}{Dt} = -\left(\frac{\partial q}{\partial y} + \frac{\partial q}{\partial x} + \frac{\partial q}{\partial z}\right) = -\nabla q. \tag{2.41}$$

Fourier's Law relates heat flow to the temperature:

$$q = -k\nabla T. \tag{2.42}$$

Therefore, combining equations (2.41) and (2.42) we obtain,

$$\frac{DQ}{Dt} = \nabla \cdot (k\nabla T). \tag{2.43}$$

Work done on the system, by the definition of work done,$work = force \times distance$, hence the rate of work is:

$$\frac{DW}{Dt} = force \times \frac{dr}{dt} = stress \times velocity$$

The net work done on y-component is $-(W_{y_{in}} - W_{y_{out}})$ which is

$$\begin{aligned}
-(W_{y_{in}} - W_{y_{out}}) &= (v\tau_{yy} - \frac{\partial}{\partial y}(v\tau_{yy})\frac{dy}{2})dxdz - \Big((v\tau_{yy} + \frac{\partial}{\partial y}(v\tau_{yy})\frac{dy}{2})dxdz\Big) \\
&+ (v\tau_{xy} - \frac{\partial}{\partial x}(v\tau_{xy})\frac{dx}{2})dydz - \Big((v\tau_{xy} + \frac{\partial}{\partial x}(v\tau_{xy})\frac{dx}{2})dydz\Big) \\
&+ (v\tau_{yz} + \frac{\partial}{\partial z}(v\tau_{yz})\frac{dz}{2})dxdy - \Big((v\tau_{yz} + \frac{\partial}{\partial z}(v\tau_{yz})\frac{dz}{2})dxdy\Big), \\
-(W_{y_{in}} - W_{y_{out}}) &= \Big(\frac{\partial}{\partial y}(v\tau_{yy} + \frac{\partial}{\partial x}(v\tau_{xy} + \frac{\partial}{\partial z}(v\tau_{yz}\Big)dydxdz
\end{aligned} \tag{2.44}$$

Similarly for x-component

$$-(W_{x_{in}} - W_{x_{out}}) = \Big(\frac{\partial}{\partial x}(u\tau_{xx} + \frac{\partial}{\partial y}(u\tau_{xy} + \frac{\partial}{\partial z}(u\tau_{xz}\Big)dydxdz \tag{2.45}$$

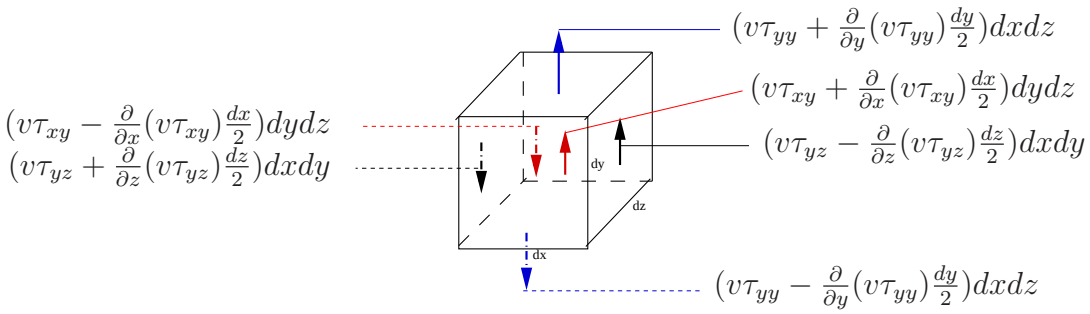

Figure 2.6: y-component of work done in and out of control volume

and for z-component

$$-(W_{zin} - W_{zout}) = \Big(\frac{\partial}{\partial z}(w\tau_{zz} + \frac{\partial}{\partial x}(w\tau_{xz} + \frac{\partial}{\partial y}(w\tau_{yz}\Big)dydxdz. \tag{2.46}$$

Summing equation (2.44), (2.45) and (2.46) divide by $dxdydz$ gives the net rate of work done per unit volume

$$\begin{aligned}\frac{DW}{Dt} = -divW = &\frac{\partial}{\partial x}\Big(u\tau_{xx} + v\tau_{xy} + w\tau_{xz}\Big) \\ &+ \frac{\partial}{\partial y}\Big(u\tau_{xy} + v\tau_{yy} + w\tau_{yz}\Big) \\ &+ \frac{\partial}{\partial z}\Big(u\tau_{xz} + v\tau_{yz} + w\tau_{zz}\Big),\end{aligned} \tag{2.47}$$

which can be written as

$$\frac{DW}{Dt} = \nabla \cdot (V \cdot \tau_{ij}). \tag{2.48}$$

By product rule,

$$\nabla \cdot (V \cdot \tau_{ij}) = V \cdot (\nabla \cdot \tau_{ij}) + \tau_{ij}(\nabla V), \tag{2.49}$$

the first bracket on the right hand side of equation (2.49) related to momentum equation

$$\nabla \cdot \tau_{ij} = \rho\Big(\frac{DV}{Dt} - g\Big). \tag{2.50}$$

Therefore,

$$V \cdot (\nabla \cdot \tau_{ij}) = \rho\Big(V\frac{DV}{Dt} - g \cdot V\Big). \tag{2.51}$$

Combine equation (2.48),(2.49) and (2.51), we obtain:

$$\frac{DW}{Dt} = \rho\Big(V\frac{DV}{Dt} - g \cdot V\Big) + \tau_{ij}(\nabla V). \tag{2.52}$$

Combine equations (2.39) ,(2.43) and (2.52), we obtain:

$$\rho\Big(\frac{De}{Dt}\Big) = \nabla \cdot (k\nabla T) + \tau_{ij}(\nabla V). \tag{2.53}$$

From enthalpy definition, $h = e + \frac{P}{\rho}$ and $\tau_{ij}(\nabla V) = \Phi$, therefore equation (2.53) becomes

$$\rho\frac{Dh}{Dt} = \frac{DP}{Dt} + \underbrace{\nabla \cdot (k\nabla T)}_{\text{heat conduction}} + \underbrace{\Phi}_{\text{viscous dissipation}}, \tag{2.54}$$

where

$$\begin{aligned}\Phi = \mu\Bigg[2\Big(\frac{\partial u}{\partial x}\Big)^2 + 2\Big(\frac{\partial v}{\partial y}\Big)^2 + 2\Big(\frac{\partial w}{\partial z}\Big)^2 + \Big(\frac{\partial v}{\partial x} + \frac{\partial u}{\partial y}\Big)^2 \\ + \Big(\frac{\partial w}{\partial y} + \frac{\partial v}{\partial z}\Big)^2 + \Big(\frac{\partial u}{\partial z} + \frac{\partial w}{\partial x}\Big)^2\Bigg] + \lambda\left(\frac{\partial u}{\partial x} + \frac{\partial y}{\partial y} + \frac{\partial w}{\partial z}\right)^2.\end{aligned} \tag{2.55}$$

Equation (2.54) is called energy equation and it can be written in numerous forms. In this chapter, we considered some of the fundamental governing equations of fluid dynamics which we shall be using in the subsequent chapters.

Chapter 3

Effects of Navier Slip on Entropy Generation in a Porous Channel with Suction/Injection

In this chapter, we investigate the combined effects of suction/injection and asymmetric Navier slips on the entropy generation rate in a steady flow of an incompressible viscous fluid through a porous channel subjected to non-uniform temperature at the walls. The nonlinear model problem is tackled numerically using shooting quadrature. Both the velocity and temperature profiles are obtained and utilized to compute the entropy generation number. The effects of slip parameter, Brinkmann number, the Peclet number and suction/injection Reynolds number on the fluid velocity, temperature profile, skin friction, Nusselt number, entropy generation rate and Bejan number are depicted graphically and discussed quantitatively.

3.1 Introduction

Rapid progress in science and technology has led to the development of an increasing number of flow devices that involve the manipulation of fluid flow in various goeme-

tries. Many textbooks of fluid dynamics fails to mention that the no-slip condition remains an assumption due to unusual agreement with experimental results for a century. Nevertheless, another approach supposed that fluid can slide over a solid surface because the experimental fact was not always accepted in the past. Navier [90] proposed general boundary conditions which include possibility of fluid slip at the solid boundary. He proposed that velocity at a solid surface is proportional to the shear stress at the surface. The phenomenon of slip occurrence has been demonstrated by the recent theoretical and experimental studies, these include; Sahraoui et al [102], Buckingham et al [13], Berh [12], Raoufpanah [96], Chauhan et al [17], Tripathi et al [118], Gupta [42], etc.

Moreover, entropy generation in engineering and industrial flow systems provides insight into the power consumption through thermodynamic losses. Therefore, the entropy minimization provides power optimization for the fluid motion in the porous channel. Efficient energy utilization during the convection in any fluid flow is one of the fundamental problems of the engineering processes to improve the system. Consequently, investigation of entropy generation due to combined effects of wall suction/injection, Navier slip and non-uniform surface temperature become essential. In a pioneering work, Bejan [6] presented the analysis of thermodynamic second-law to inherent irreversibility in heat transfer with respect to thermal design of an engineering system. Thereafter, considerable research studies were carried out to investigate entropy generation such as: Bejan [7], Sahin [105], Sahin et al [104], Makinde et al [60], Makinde [61], Ozalp [92], Erbay et al [40], Vazquez et al [121], Haddad et al [43], e.t.c.

Meanwhile, fluid flow through a porous channel has been studied theoretically and ex-

perimentally by numerous authors due to its wide applications in various fields such as diffusion technology, transpiration cooling, hemodialysis processes, desalination, flow control in nuclear reactors, etc. In a pioneering work, Berman [8] presented an exact solution of the Navier-Stokes equations that describes the steady two-dimensional flow of an incompressible viscous fluid along a channel with parallel rigid porous walls, the flow being driven by uniform suction or injection at the walls. Thereafter, many authors such as Terrill [113, 114], Makinde [62], Robinson [101], Brady [14], Makinde [63], etc., have extended and reconsidered the problem under various physical conditions. To the best of authors knowledge, none of these chapters have addressed combined effects of wall suction/injection and asymmetric Navier slips on steady flow in a porous channel with non uniform walls temperature.

In this chapter, our objective is to investigate the combined effects of wall suction/injection and asymmetric Navier slips on an incompressible viscous flow in a porous channel subjected to non-uniform walls temperature. The work essentially extends the recent work of Ajibade et al [2] to include asymmetric Navier slip and non-uniform wall temperature. The nonlinear model problem is tackled numerically. The chapter is organized as follows: in section 3.2, we define the problem, given the governing equations and present the mathematical formulation. In section 3.3, we derive the entropy generation rate, skin friction, Nusselt number and Bejan number. In section 3.4, we present and discuss the pertinent results graphically and quantitatively. Finally, a concluding remark is given in section 3.5.

3.2 Mathematical Model

We consider steady flow of an incompressible viscous fluid through a uniformly porous channel under the combined action of constant axial pressure gradient, wall suction / injection and asymmetric Navier slip as shown in fig.(3.1) below.

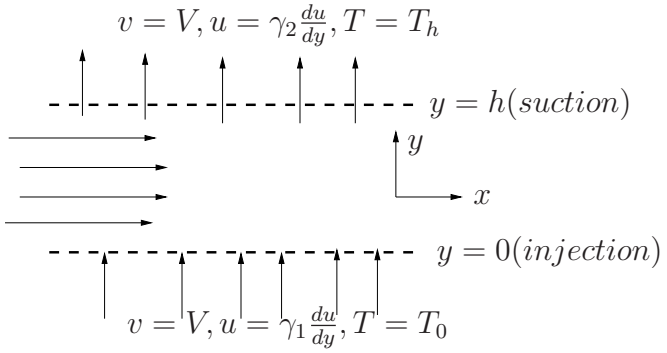

Figure 3.1: Schematic diagram of the problem

The fluid equations for momentum and energy balance governing the problem under consideration can be written as (Ajibade et al[2]):

$$V\frac{du}{dy} = -\frac{1}{\rho}\frac{dP}{dx} + \frac{\mu}{\rho}\frac{d^2u}{dy^2} \tag{3.1}$$

and

$$V\frac{dT}{dy} = \alpha\frac{d^2T}{dy^2} + \frac{\mu}{\rho c_P}\Big(\frac{du}{dy}\Big)^2. \tag{3.2}$$

The boundary conditions are:

$$u(0) = \gamma_1\frac{du(0)}{dy}, \quad T(0) = T_0 \tag{3.3a}$$

and

$$u(h) = \gamma_2\frac{du(h)}{dy}, \quad T(h) = T_h \tag{3.3b}$$

where equations (3.1) and (3.2) are momentum and energy equations respectively, h is the channel width, u is the velocity of the fluid, P is the fluid pressure, V is

the uniform suction/injection at the channel walls, μ is the fluid viscosity, α is the thermal diffusivity, k is the thermal conductivity coefficient, c_P is the specific heat at constant pressure, T is the temperature, γ_1 and γ_2 are slip coefficients. We introduce the following non-dimensional quantities:

$$\theta = \frac{T - T_0}{T_h - T_0}, \quad \alpha = \frac{k}{\rho c_P}, \quad w = \frac{u}{V}, \quad \bar{P} = \frac{hP}{\mu V}, \quad \eta = \frac{y}{h}, \quad X = \frac{x}{h}, \quad G = -\frac{d\bar{P}}{dX}. \tag{3.4}$$

Substituting equation (3.4) into equations (3.1)-(3.3b), we obtain

$$\frac{d^2w}{d\eta_2} - Re\frac{dw}{d\eta} + G = 0 \tag{3.5}$$

and

$$\frac{d^2\theta}{d\eta} - Pe\frac{d\theta}{d\eta} + Br\Big(\frac{dw}{d\eta}\Big)^2 = 0, \tag{3.6}$$

with the boundary conditions

$$w(0) = \beta_1\frac{dw(0)}{d\eta}, \quad \theta(0) = 0 \tag{3.7a}$$

and

$$w(1) = \beta_2\frac{dw(1)}{d\eta}, \quad \theta(1) = 1, \tag{3.7b}$$

where G is the pressure gradient,

$$Re = \frac{Vh\rho}{\mu}(\text{Reynolds number}), \quad Pe = PrRe = \frac{Vh}{\alpha}(\text{Peclet number}),$$

$$Pr = \frac{\mu}{\alpha\rho}(\text{Prandtl number}), \quad Br = \frac{\mu V^2}{\rho c_P\alpha(T_h - T_0)}(\text{Brinkmann number}),$$

$$\beta_1 = \frac{\gamma_1}{h}(\text{lower plate slip parameter}), \quad \beta_2 = \frac{\gamma_2}{h}(\text{upper plate slip parameter}).$$

Moreover, equation (3.5) subjected to boundary conditions in equations (3.7a) and (3.7b) were solved analytically and we obtain

$$w(\eta) = \frac{e^{Re\eta}G(1-\beta_2+\beta_1)}{Re(1-e^{Re}-\beta_1 Re+e^{Re}\beta_2 Re)} + \frac{\eta G}{Re} + \frac{G(\beta_1 Re+Re\beta_1\beta_2 e^{Re}-\beta_1\beta_2 Re-e^{Re}\beta_1+\beta_2-1)}{Re(1-e^{Re}-\beta_1 Re+e^{Re}\beta_2 Re)}. \tag{3.8}$$

The above coupled nonlinear boundary value problem represented by equations (3.5)-(3.6) together with their boundary conditions in equation (3.7a, b) have been solved numerically using the shooting iteration technique together with Runge-Kutta fourth-order integration scheme, Nachtshein and Swigert [88].

3.3 Entropy Generation

Fluid flow and heat transfer processes inside a porous narrow channel are irreversible. The non-equilibrium conditions arise due to the exchange of energy and momentum within the fluid and at porous solid boundaries, thus resulting in entropy generation. Following Bejan [7], the volumetric entropy generation rate is given as :

$$E_G = \frac{k}{T_0^2}\Big(\frac{dT}{dy}\Big)^2 + \frac{\mu}{T_0}\Big(\frac{du}{dy}\Big)^2, \tag{3.9}$$

where the first term on the right side of equation (3.9) is the irreversibility due to heat transfer and the second term is the entropy generation due to viscous dissipation. Using equation (3.4), we express equation (3.9) in dimensionless form as:

$$N_S = \frac{T_0^2 H^2 E_G}{k(T_h-T_0)^2} = \left(\frac{d\theta(\eta)}{d\eta}\right)^2 + \frac{Br}{\Omega}\left(\frac{dw(\eta)}{d\eta}\right)^2, \tag{3.10}$$

where $\Omega = \dfrac{(T_h-T_0)}{T_0}$ is the temperature difference parameter and

$$N_1 = \left(\frac{d\theta(\eta)}{d\eta}\right)^2, \quad N_2 = \frac{Br}{\Omega}\left(\frac{dw(\eta)}{d\eta}\right)^2 \tag{3.11}.$$

The Bejan number is given as:

$$Be = \frac{N_1}{N_S}. \tag{3.12}$$

It is noteworthy that the Bejan number ranges from 0 to 1 and $Be = 0$ is the limit where the irreversibility is dominated by fluid friction effects. $Be = 1$ is the limit where the irreversibility due to heat transfer dominates the flow system by virtue of finite temperature differences. The contribution of both heat transfer and fluid friction to entropy generation are equal when $Be = 1/2$.

3.4 Results and Discussion

In order to validate our results, we have chosen physically meaningful values for the parameters. The Prandtl number was taken in the range of $Pr = 0.71$ to 7.1 which corresponds to Prandtl number in the range of air and that of water. From our model in Fig.(3.1), it is important to note that the fluid suction takes place at the upper wall while the fluid injection occurs at the lower wall simultaneously. In order to validate the accuracy of our numerical procedure, the exact solution obtained in equation (3.8) is compared with the numerical solution obtained using shooting iteration technique together with Runge-Kutta fourth-order integration scheme as illustrated in table 3.1. A perfect agreement is achieved between the numerical and exact solutions.

Fig.(3.2) depicts the effects of increase in Reynolds number (Re). As Re increases, fluid injection into the channel through the lower wall of the channel increases while the rate of fluid suction at the upper wall of the channel increases as well. This leads to a decrease in the fluid velocity at the lower channel wall region and an increase

Table 3.1: Computation showing comparison between the exact and numerical solution of velocity profile for $G = 1$, $Re = \beta_1 = \beta_2 = 0.1$

n	Exact Solution $w(\eta)$	Numerical Solution $w(\eta)$
0	0.03956249	0.03956249
0.1	0.07430662	0.07430662
0.2	0.09934983	0.09934983
0.3	0.11459457	0.11459457
0.4	0.11994234	0.11994234
0.5	0.11529370	0.11529370
0.6	0.10054817	0.10054817
0.7	0.07560428	0.07560428
0.8	0.04035953	0.04035953
0.9	−0.00528959	−0.005289591
1.0	−0.06144767	−0.061447671

in flow reversal (represented by negative velocity) at the upper wall region ($\eta = 1$). Fig.(3.3) shows velocity profile while β_1 is increasing. An increase in slip coefficient

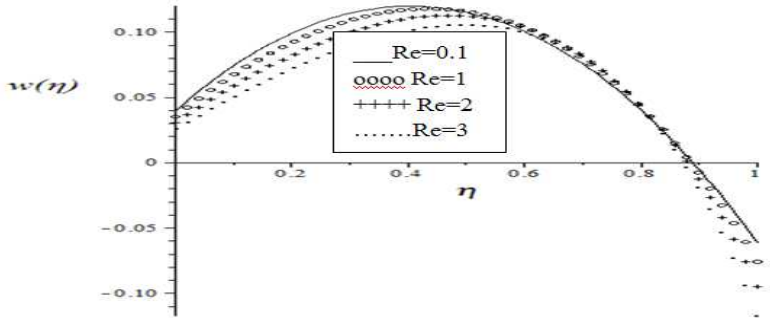

Figure 3.2: Velocity profile, $\beta_1 = \beta_2 = Br = 0.1, G = 1, Pr = 0.71$

β_1 at the lower wall causes an increase in the velocity at the injection wall while the velocity reversal at suction wall increases slightly. In Fig.(3.4) we observed that an increase in the slip coefficient β_2 at the upper wall causes a little decrease in velocity at injection wall while a large decrease in the fluid velocity is noticed with a high rate of flow reversal at the suction wall. Fig.(3.5) depicts the variation in velocity profile

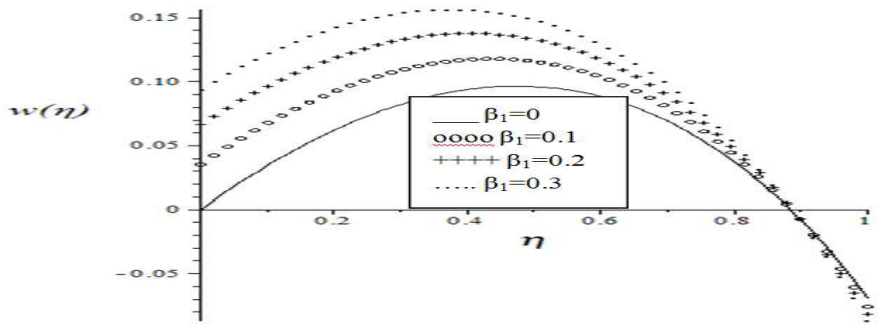

Figure 3.3: Velocity profile, $\beta_2 = Br = 0.1, G = Re = 1, Pr = 0.71$

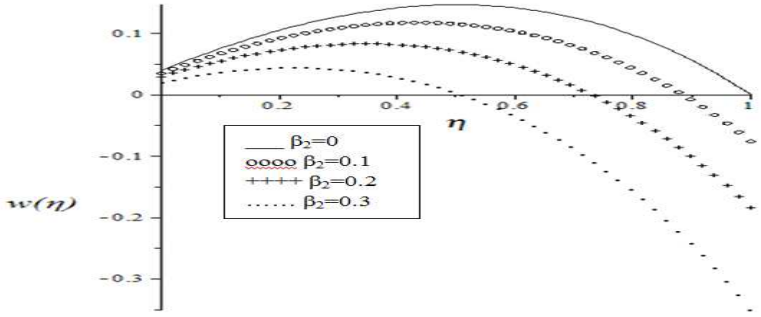

Figure 3.4: Velocity profile, $\beta_1 = Br = 0.1, G = Re = 1, Pr = 0.71$

with increasing values of pressure gradient parameter. As the pressure gradient increases, the velocity at injection wall increases and attains its maximum value along the channel centerline region. A slight increase in the reverse flow appears at suction wall. Fig.(3.6) shows temperature profile when there is increment in Brinkmann (Br) number due to viscous dissipation effects. The fluid temperature increases with an increase Br with minimum value at the injection wall and maximum value at suction wall satisfying the boundary condition. Fig.(3.7) depicts temperature profile when the Prandtl number is increasing from 0.71 (air) to 7.1 (water). Increase in Prandtl number causes a sporadic decrease in temperature at the injection wall region and a slight decrease in temperature at the suction wall region. Similar trend is observed in

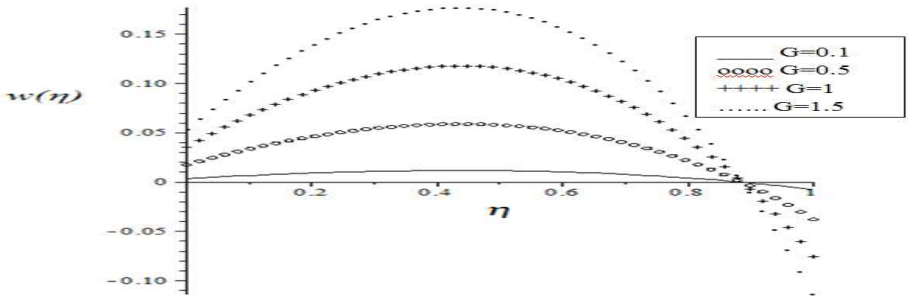

Figure 3.5: Velocity profile, $\beta_1 = \beta_2 = Br = 0.1, Re = 1, Pr = 0.71$

Fig.(3.8) as the Reynolds number increases. A slight decrease in the fluid temperature is noticed with increasing value of Reynolds number.

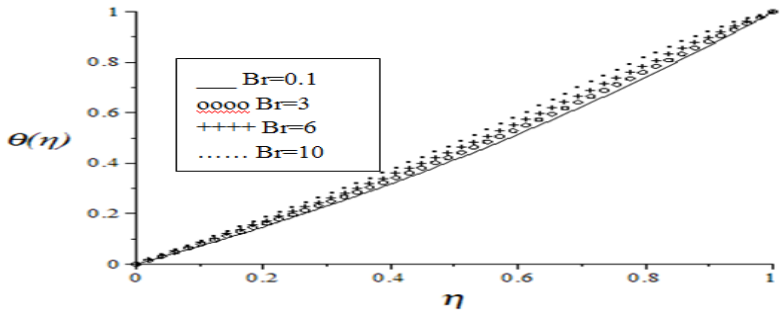

Figure 3.6: Temperature profile, $\beta_1 = \beta_2 = 0.1, G = Re = 1, Pr = 0.71$

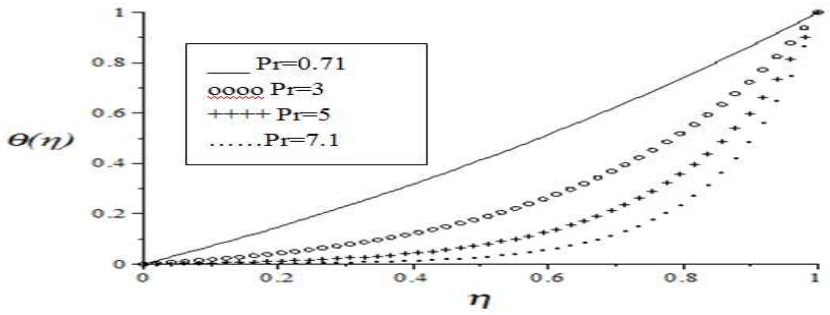

Figure 3.7: Temperature profile, $\beta_1 = \beta_2 = Br = 0.1, G = Re = 1$

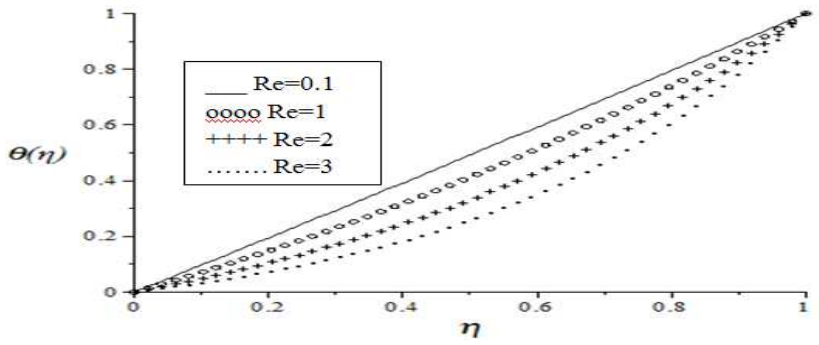

Figure 3.8: Temperature profile, $\beta_1 = \beta_2 = Br = 0.1, G = 1, Pr = 0.71$

Fig.(3.9) illustrates the entropy generation rate when Reynolds number is increasing and other parameters remain constant. The entropy production at the injection walls decreases, however, at suction wall, entropy generation rate increases. Fig.(3.10) depicts entropy generation rate when group parameter $Br\Omega^{-1}$ increases due to a combined decrease in the temperature difference parameter and an increase in the viscous heating. As $Br\Omega^{-1}$ increases, the entropy generation rate at both walls increases but more at suction wall. The entropy generation is lowest within the channel centerline region. In Fig.(3.11), an increase in Prandtl number decreases the rate of entropy production at the injection wall but increase entropy generation rate at the suction wall. Figs.(3.12)-(3.13) depict entropy generation rate when the slip coefficients are increasing while other parameters remain constant. Increase in β_1 and β_2 decrease entropy generation rate at the injection wall and increase entropy generation rate at the suction wall. Fig.(3.14) shows the effect of an increase in pressure gradient parameter (G) on entropy generation rate. As G increases, an increase in entropy production is observed at both walls but the increment in entropy generation is more at suction wall.

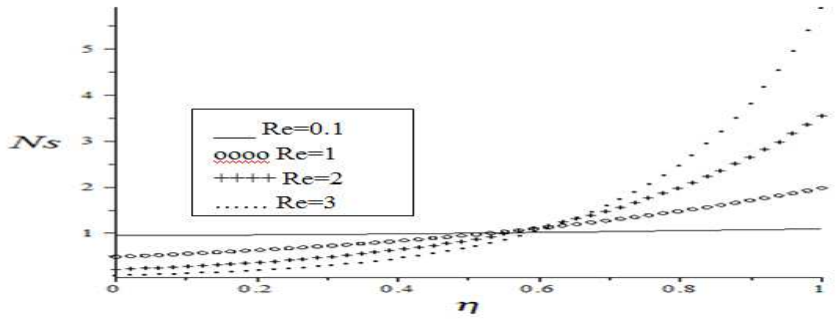

Figure 3.9: Entropy generation rate, $Br\Omega^{-1} = \beta_1 = \beta_2 = 0.1, G = 1, Pr = 0.71$

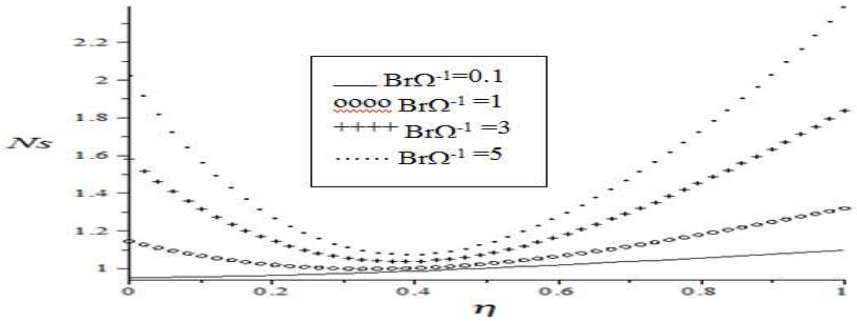

Figure 3.10: Entropy generation rate, $\beta_1 = \beta_2 = Re = 0.1, G = 1, Pr = 0.71$

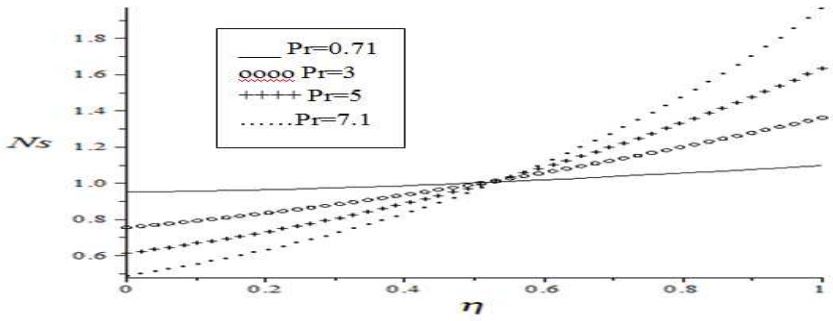

Figure 3.11: Entropy generation rate, $Br\Omega^{-1} = \beta_1 = \beta_2 = Re = 0.1, G = 1$

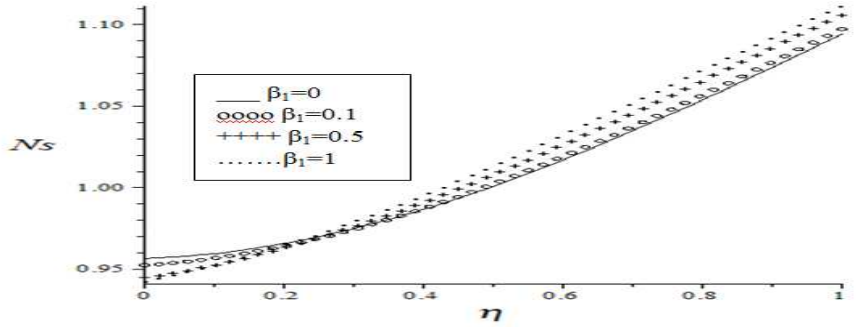

Figure 3.12: Entropy generation rate, $Br\Omega^{-1} = \beta_2 = Re = 0.1, G = 1, Pr = 0.71$

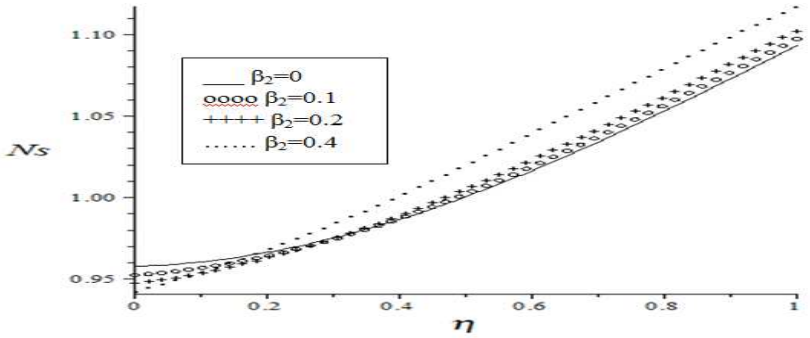

Figure 3.13: Entropy generation rate, $Br\Omega^{-1} = \beta_1 = Re = 0.1, G = 1, Pr = 0.71$

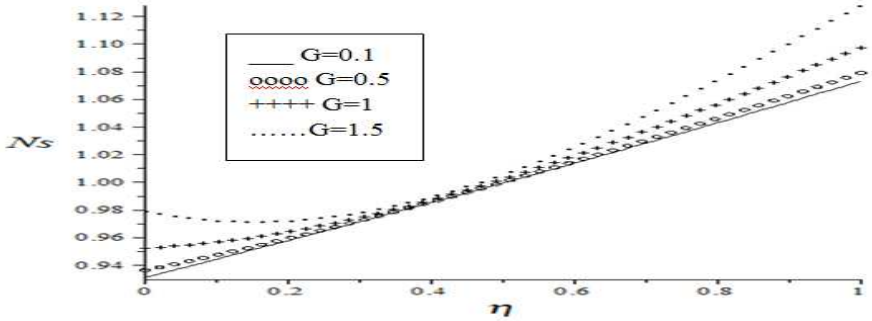

Figure 3.14: Entropy generation rate, $Br\Omega^{-1} = \beta_1 = \beta_2 = Re = 0.1, Pr = 0.71$

Figs.(3.15)-(3.20) illustrate the effects of various thermophysical parameters on the Bejan number. Generally we noticed that heat transfer irreversibility dominates

the flow process within the channel centerline region with Bejan number very close to 1, while the little influence of fluid friction irreversibility can be observed at the channel walls. This perfectly agrees with the observation of Ajibade et al[2]. In Fig.(3.15), we observed that increase in Reynolds number; decreases the Bejan number on injection wall and increases the Bejan number on suction wall. This shows clearly that the irreversibility due to fluid friction tends to dominate the flow system at injection wall while heat transfer irreversibility dominates at the suction wall. Fig.(3.16) depicts the effects of increasing group parameter; the Bejan number at both walls decrease leading to increasing influence of fluid friction irreversibility. Figs.(3.17)-(3.18) demonstrate the effects of asymmetric slip coefficients β_1 and β_2. The Bejan number at injection wall increases while it decreases at the suction wall leading to the increasing influence of heat transfer irreversibility at the lower wall and fluid friction irreversibility at the upper wall. Increase in Prandtl number leads to decrease in Bejan number at injection wall and an increase in Bejan number at the suction wall (see Fig.(3.19)). Consequently, the fluid friction irreversibility tends to dominate the flow system at injection wall while heat transfer irreversibility dominates at the suction wall. Fig.(3.20) shows that an increase in axial pressure gradient causes the influence of fluid friction irreversibility at both walls to increase greatly.

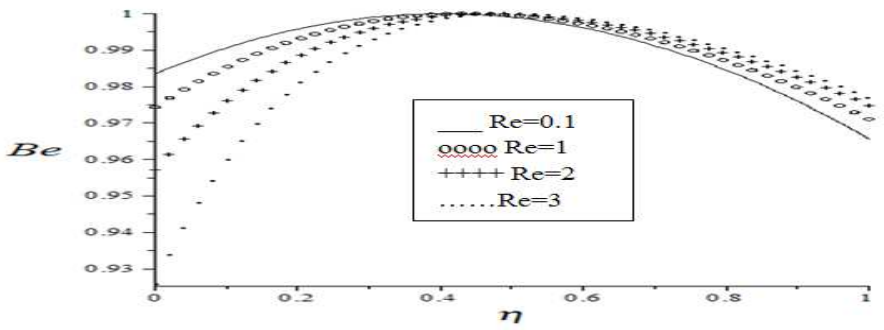

Figure 3.15: Bejan Number, $Br\Omega^{-1} = \beta_1 = \beta_2 = 0.1, G = 1, Pr = 0.71$

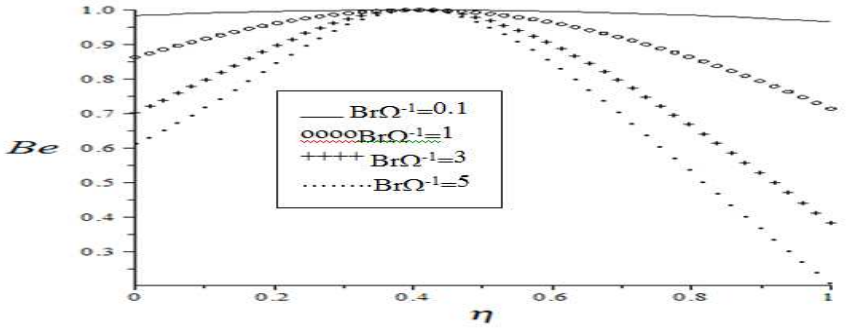

Figure 3.16: Bejan Number, $\beta_1 = \beta_2 = Re = 0.1, G = 1, Pr = 0.71$

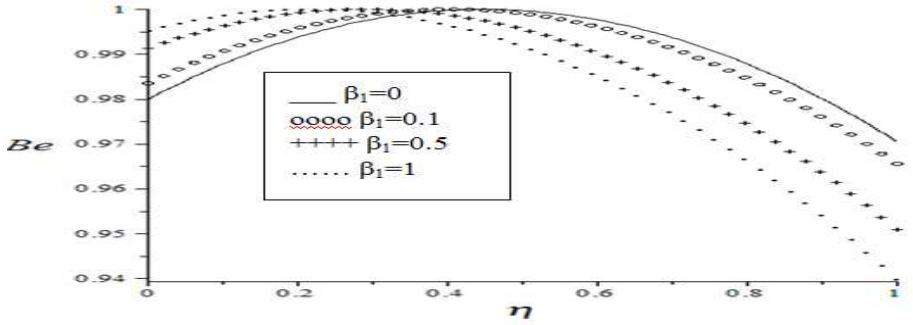

Figure 3.17: Bejan Number, $Br\Omega^{-1} = \beta_2 = Re = 0.1, G = 1, Pr = 0.71$

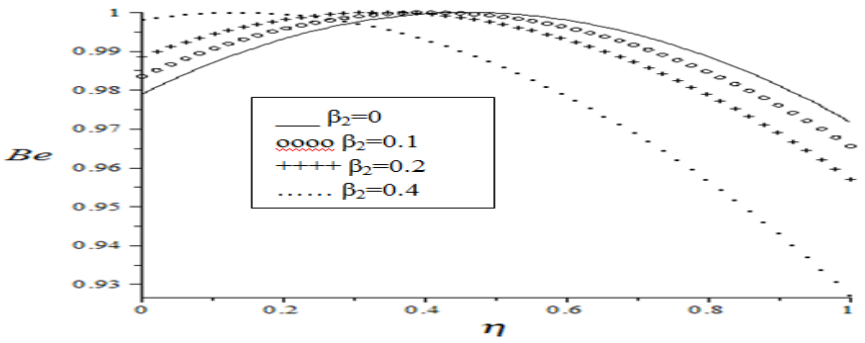

Figure 3.18: Bejan Number, $Br\Omega^{-1} = \beta_1 = Re = 0.1, G = 1, Pr = 0.71$

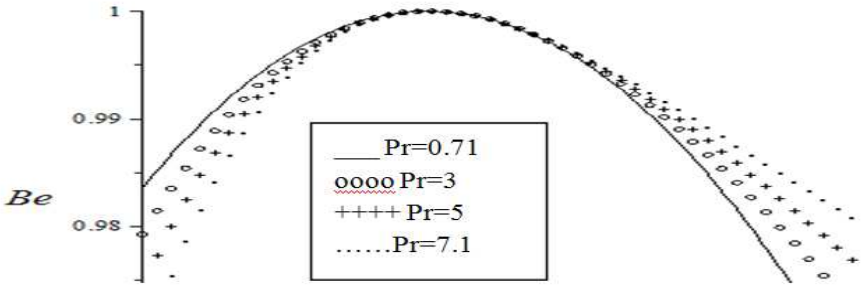

Figure 3.19: Bejan Number $G = 1$,$Br\Omega^{-} = \beta_1 = \beta_2 = Re = 0.1$

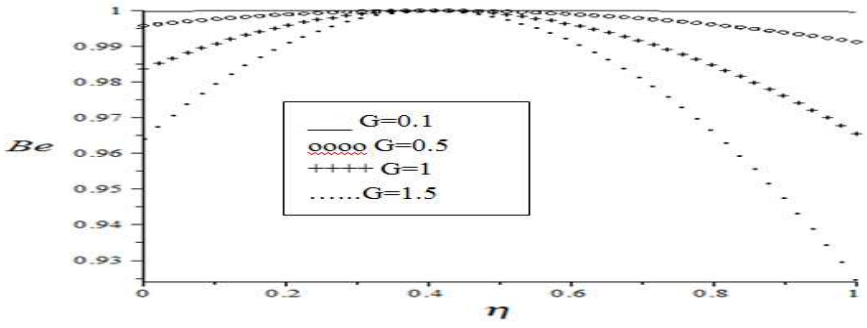

Figure 3.20: Bejan Number $Pr = 0.71$,$Br\Omega^{-} = \beta_1 = \beta_2 = Re = 0.1$

3.5 Conclusion

We analyzed in this chapter, the combined effects of suction/injection and asymmetric Navier slips on the entropy generation rate in a steady flow of an incompressible fluid through a porous channel with non uniform walls temperature, putting into consideration that these will be of help in upgrading the system in terms of energy loss. Our results revealed among others the presence of flow reversal at the channels upper wall due to suction. The heat transfer irreversibility dominates the flow process within the channel centerline region, while the influence of fluid friction irreversibility can be observed at the channel walls. However, as the values of asymmetric slip parameters increase, the dominance effects of heat transfer irreversibility at the lower wall and fluid friction irreversibility at the upper wall increase. Entropy generation minimization has become most important area of research for scientists and engineers in this crucial time. Moreover, with appropriate combination of thermophysical parameter values, entropy minimization can be achieved in a flow process.

Chapter 4

Combined Effect of Buoyancy Force and Navier Slip on Entropy Generation in a Vertical Porous Channel

In this chapter, we investigate the combined effects of buoyancy force and Navier slip on the entropy generation rate in a vertical porous channel with wall suction/injection. The nonlinear model problem is tackled numerically using Runge Kutta - Fehlberg method with shooting technique. Both the velocity and temperature profiles are obtained and utilized to compute the entropy generation number. The effects of slip parameter, Brinkmann number, the Prandtl number and suction/injection Reynolds number on the fluid velocity, temperature profile, Nusselt number, entropy generation rate and Bejan number are depicted graphically and discussed quantitatively.

4.1 Introduction

The study of fluid flow and heat transfer in a porous channel have received considerable attention during the last several decades due to its occurrence in a wide range

of biological and engineering settings such as ground water hydrology, irrigation, and drainage problems and also in absorption and filtration processes in chemical engineering. The scientific treatment of the problem of irrigation, soil erosion and tile drainage are the present development of porous media flow [49,91,122]. Meanwhile, the problem of the slip flow regime is very important in this era of modern science, technology and vast ranging industrialization. In many practical applications, the fluid adjacent to a solid surface no longer takes the velocity of the surface. The fluid at the surface has a finite tangential velocity; it slips along the surface. The flow regime is called the slip flow regime and its effect cannot be neglected. The effects of slip conditions on the hydromagnetic steady flow in a channel with permeable boundaries were discussed by Makinde and Osalusi [64]. Khalid and Vafai [51] obtained the closed form solutions for steady periodic and transient velocity field under slip condition. Watanebe et al [123] studied the effect of Navier Slip on Newtonian fluids at solid boundary. Chen and Tian [21] investigated entropy generation in a micro annulus flow and discussed the influence of velocity slip on entropy generation. Chauhan and Kumar [17] investigated fully developed forced convection in a circular channel filled with a highly porous medium saturated with a rarefied gas and uniform heat flux at the wall in the slipflow region, using the Darcy extended Brinkman-Forchheimer momentum equation and the entropy generation due to heat transfer. Meanwhile, there is continuous transfer of momentum and energy between the fluid and the solid boundaries, causing the fluid to undergo irreversible processes and therefore increase the entropy generation in the system. Since entropy production destroys the available energy in the system, the improvement in the energy utilization during the fluid convection is one of the fundamental problems in engineering processes. The optimal

use of energy can be achieved, if the second law of thermodynamics is taken into consideration. Mahmud and Fraser[57] examined the flow, thermal and entropy generation fields inside a parallel-plate porous channel, when subjected to differentially heated isothermal wall. Chauhan and Olkha [18] investigated the hydrodynamics and heat transfer of the flow of a third-grade fluid incorporating entropy analysis. Chauhan and Kumar [19] analyzed the heat transfer and entropy generation in a situation where the compressible fluid flow is caused by moving an impermeable wall of a composite channel partially filled with a porous medium and a clear fluid. Chauhan and Rastogi [20] considered an unsteady two-dimensional MHD flow and heat transfer through a porous medium adjacent to a non-isothermal stretching sheet. Several researchers have carried out analysis on second law analysis such as [44, 45, 93, 111]. Furthermore, starting from the pioneering work of Bejan [7, 9], several investigations on entropy generation on fluid flow under various physical situations have been studied [22 − 32, 65 − 67]. Chen [31] performed a detailed study on the effects of Reynolds number and Grashof number on entropy generation inside disk driven convectional flow for the first time. Chen et al [32] investigated the effects of Rayleigh number, curvature of annulus and Prandtl number on the flow pattern, temperature distribution and entropy generation for natural convection inside a vertically concentric annular space. It appears that very little or no study has considered the combined effects of buoyancy force and velocity slip on the entropy generation in a porous channel with suction and injection, which is the focus of this chapter. In this chapter, the inherent irreversibility of a porous channel under the influence of velocity slip and buoyancy force is investigated numerically using Runge-Kutta-Fehlberg method with shooting technique. The solution of the resulting momentum and energy balance equations are

reported for representative values of thermo-physical parameters characterizing the fluid convection processes.

4.2 Mathematical Analysis

The steady laminar incompressible viscous boundary layer flow through a vertical porous channel with non-uniform temperature, injection at the left wall and suction at the right wall under the combined effect of buoyancy forces and Navier slip as shown in Fig.(4.1) below are considered.

The density variation due to buoyancy effects is taken into account in the momentum

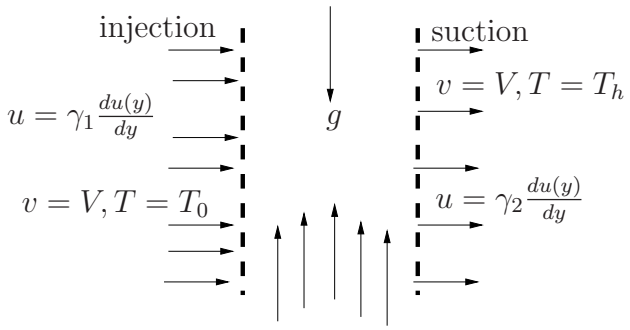

Figure 4.1: Flow configuration and coordinate system

equation using Boussinesq approximation. The momentum and energy equations describing the flow can be written as:

Momentum equation:

$$V\frac{du(y)}{dy} = -\frac{1}{\rho}\frac{dP}{dx} + \frac{\mu}{\rho}\frac{d^2u(y)}{dy^2} + g\beta(T - T_0) \tag{4.1}$$

and Energy equation:

$$V\frac{dT(y)}{dy} = \alpha\frac{d^2T(y)}{dy^2} + \frac{\mu}{\rho c_P}\Big(\frac{du(y)}{dy}\Big)^2, \tag{4.2}$$

with the boundary conditions:

$$v(0) = V, \quad u(0) = \gamma_1 \frac{du(0)}{dy}, \quad T(0) = T_0, \tag{4.3a}$$

$$v(h) = V, \quad u(h) = \gamma_1 \frac{du(h)}{dy}, \quad T(h) = T_h, \tag{4.3b}$$

where is the u velocity of the fluid, P is the fluid pressure, μ is the fluid viscosity, α is the thermal diffusivity,ρ is the fluid density, c_P is the specific heat at constant pressure, T is the temperature, γ_1 and γ_2 are slip coefficients, β is volumetric expansion coefficient and g is acceleration due to gravity. We introduced the following dimensionless quantities:

$$\theta = \frac{T - T_0}{T_h - T_0}, \quad k = -\frac{d\bar{P}}{d\bar{x}}, \quad \bar{x} = \frac{x}{h}, \quad \bar{P} = \frac{Ph}{\mu V}, \quad w = \frac{u}{V}, \quad \eta = \frac{y}{h}. \tag{4.4}$$

Using these dimensionless quantities in equation (4.1) -(4.3b), we obtain,

$$\frac{d^2w(\eta)}{d\eta^2} - Re\frac{dw(\eta)}{d\eta} + K + Gr\theta(\eta) = 0, \tag{4.5}$$

$$\frac{d^2\theta(\eta)}{d\eta^2} - Pe\frac{d\theta(\eta)}{d\eta} + Br\Big(\frac{dw(\eta)}{d\eta})^2 = 0, \tag{4.6}$$

with the boundary conditions

$$w(0) = \beta_1 \frac{dw(0)}{d\eta}, \quad \theta(0) = 0 \tag{4.7a}$$

and

$$w(1) = \beta_1 \frac{dw(1)}{d\eta}, \quad \theta(1) = 1 \tag{4.7b}$$

where

$Re = \dfrac{V\rho h}{\mu}$(Reynolds Number), $\quad Pe = \dfrac{Vh}{\alpha}$(Peclet Number), $\quad \beta_2 = \dfrac{\gamma_1}{h}$(slip parameter),

$K = \dfrac{d\bar{P}}{d\bar{x}}$(Pressure gradient parameter), $\quad Br = \dfrac{V^2\mu}{\rho c_P \alpha(T_h - T_0)}$(Brinkmann Number),

$$Gr = \frac{g\beta h^2(T_h - T_0)}{\mu V}(\text{Grashof Number}), \quad \beta_1 = \frac{\gamma_1}{h}(\text{slip parameter})$$

Equations (4.5)-(4.6) together with boundary conditions (4.7a)-(4.7b) are coupled nonlinear boundary value problems which are solved numerically using Runge-Kutta-Fehlberg method with shooting technique. The numerical solution procedure employed to solve the model boundary valued problem in Equations (4.5)-(4.7b) is based on shooting techniques [66, 88]. It involves, transforming Equations (4.5)-(4.7b) into a set of initial value problems. The transformed initial value problems will contain few unknown initial values that need to be determined. After guessing the unknown initial values, a fourth order Runge-Kutta iteration scheme is employed to integrate the set of initial valued problems until the given boundary conditions are satisfied. The computations are done by a written program which used a symbolic and computational computer language MAPLE. The entire procedure is implemented on MAPLE. The gradient of the velocity at the channel walls referring to skin fiction is equivalent to:

$$S_f = \mu \frac{du}{dy}\Big|_{y=0,h}, \tag{4.8}$$

therefore, the skin-friction coefficient at the wall using dimensionless quantities (4.4) is given by:

$$C_f = \frac{h}{V\mu} = \frac{dw(\eta)}{d\eta}\Big|_{\eta=0,1}. \tag{4.9}$$

The rate of heat transfer at the channels wall in dimensionless form is given by:

$$N_u = -\frac{d\theta(\eta)}{d\eta}\Big|_{\eta=0,1}. \tag{4.10}$$

4.3 Entropy Generation

The convection process along a porous channel is naturally irreversible. Exchange of energy and momentum within the fluid and at the solid boundaries causes non-equilibrium condition, which therefore leads to continuous entropy generation in the porous channel. Bejan [9] gave volumetric rate of entropy generation in a Cartesian coordinates as:

$$E_G = \frac{k}{T_0^2}\left(\left(\frac{dT}{dx}\right)^2 + \left(\frac{dT}{dy}\right)^2\right) + \frac{\mu}{T_0}\left(2\left\{\left(\frac{du}{dx}\right)^2 + \left(\frac{dv}{dy}\right)^2\right\} + \left(\frac{du}{dx} + \frac{dv}{dy}\right)^2\right). \quad (4.11)$$

The velocity and temperature distributions are simplified in many fundamental convection problems by assuming that the flow is fully developed by Fantomo et al[122] as:

$$E_G = \frac{k}{T_0^2}\left(\frac{dT}{dy}\right)^2 + \frac{\mu}{T_0}\left(\frac{du}{dy}\right)^2, \quad (4.12)$$

where the first term on the right hand side of Equation (4.12) is the irreversibility due to heat transfer and the second term is the entropy generation due to viscous dissipation. Introducing the dimensionless quantities defined in equation (4.4) to equation (4.12), we obtain

$$N_S = \frac{T_0^2 h^2 E_G}{k(T_h - T_0)^2} = \left(\frac{d\theta(\eta)}{d\eta}\right)^2 + \frac{Br}{\Omega}\left(\frac{dw(\eta)}{d\eta}\right)^2, \quad (4.13)$$

where $\Omega = (T_h - T_0)/T_0)$ is the temperature difference parameter and:

$$N_1 = \left(\frac{d\theta(\eta)}{d\eta}\right)^2, \quad N_2 = \frac{Br}{\Omega}\left(\frac{dw(\eta)}{d\eta}\right)^2 \quad (4.14)$$

where N_1 represents irreversibility due to heat transfer and N_2 gives entropy generation due to viscous dissipation. In order to have an idea whether the entropy

generation due to viscous dissipation dominates over the irreversibility due to heat transfer or vice versa, the authors defined irreversibility ratio as:

$$\phi = \frac{N_2}{N_1}. \tag{4.15}$$

Entropy generation due to viscous dissipation dominates if $\phi > 0$ and if $0 \leq \phi < 1$, then irreversibility due to heat transfer dominates, but if $\phi = 1$ implies that both of them contribute equally.

The Bejan number (Be) is defined as:

$$Be = \frac{N_1}{N_S} = \frac{1}{1+\phi}, \tag{4.16}$$

where $Be = 1$ is the limit at which heat transfer irreversibility dominates, $Be = 0$ is the limit at which fluid friction irreversibility dominates, and $Be = 1/2$ implies that both of them contribute equally.

4.4 Results and Discussion

The validity of boundary layer approximation for this model channel flow problem can be attributed to the fact that the combined effects of suction and injection on the flow system are more pronounced within the channel walls region [57, 66]. Using appropriate parameters, the detailed discussion and graphical representation of the results of above equations are reported in this section. We refer to vertical lines at $\eta = 0$ as injection wall and at $\eta = 1$ as suction wall in this discussion. Fig.(4.2) depicts the velocity profile while Grashof number (Gr) is increasing and other parameters remain constant.

The buoyancy effect on the flow system is demonstrated by variation in parameter value of Grashof number (Gr). The choice of the values for Gr used in this chapter

is motivated by the increasing effects of buoyancy due to gravity and temperature difference between the channel walls. Increase in Gr, decreased the fluid injection toward the channel from the injection wall and increased the suction fluid rate at the suction wall. Consequently, the velocity increased at the injection wall and decreased at the suction wall. A reversal flow is noticed at the suction wall as Gr is increasing. Towards the centerline of the channel, the flow attains its maximum velocity and it is asymmetric. Fig. (4.3) shows the effect of increasing Reynolds number (Re). As Re is increasing, fluid injection into the channel, as well as the fluid suction rate is increasing. At the injection wall, the velocity decreases and the flow reversal at the suction wall increases.

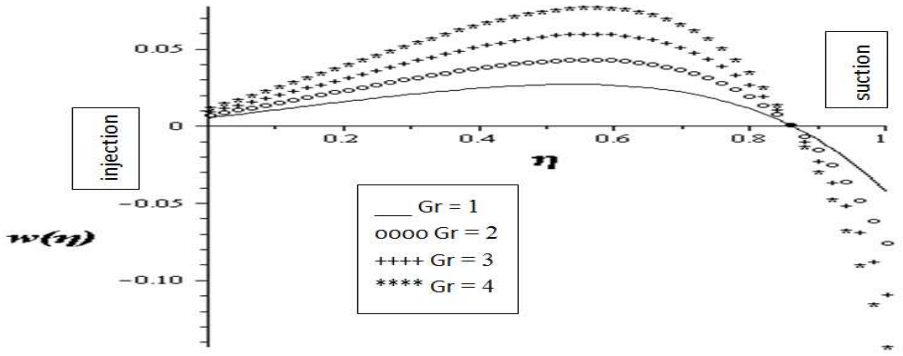

Figure 4.2: velocity Profile,$Re = 2, Br = 1, K = \beta_1 = \beta_2 = 0.1, Pe = 3$

Fig.(4.4) depicts the velocity profile while the pressure gradient (K) is increasing. As the pressure gradient is increasing, there is a little increase in velocity at the injection wall and a reversal flow at the suction wall is noticed. The flow attains its maximum velocity very close to the centerline of the channel. Fig.(4.5) shows the velocity profile as Peclet number (Pe) is increasing. As Pe is increasing, the fluid injection into

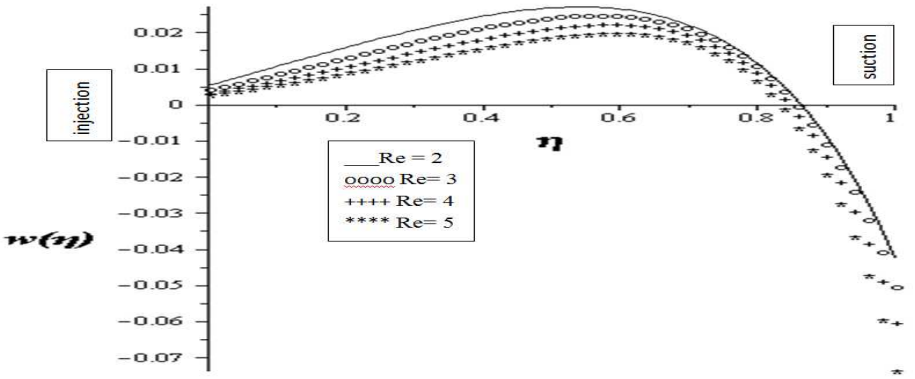

Figure 4.3: velocity Profile,$Gr = Br = 1, K = \beta_1 = \beta_2 = 0.1, Pe = 3$

the channel at the injection wall increases, similarly, there is an increase in the fluid suction rate at the suction wall. The velocity at injection wall decreases a little but at suction wall, the velocity increases. Meanwhile, at the centerline of the channel, the velocity decreases greatly.

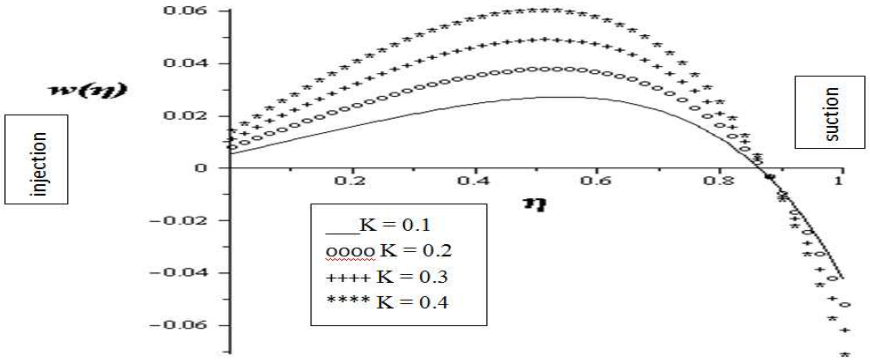

Figure 4.4: velocity Profile,$Re = 2, Br = Gr = 1, \beta_1 = \beta_2 = 0.1, Pe = 3$

Fig.(4.6) shows the velocity profile with increase in slip parameter β_1. As β_1 is increasing, the flow velocity at the injection wall increases and a slight reversal flow effect at the suction wall is noticed. Fig.(4.7) depicts an increase in slip parameter

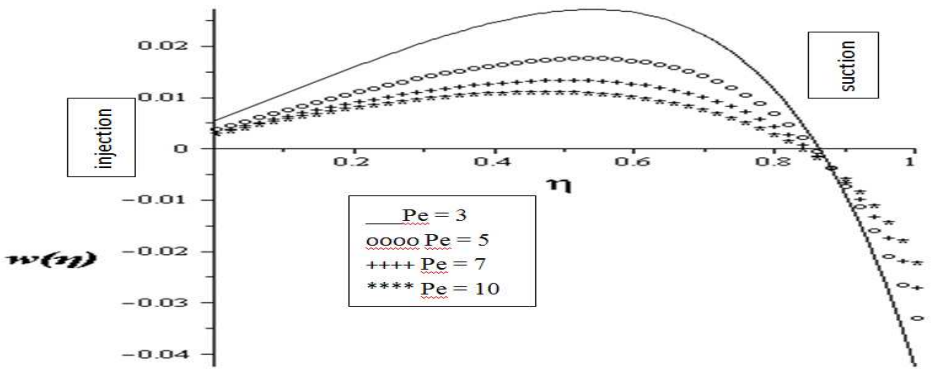

Figure 4.5: velocity Profile,$Gr = Br = 1, K = \beta_1 = \beta_2 = 0.1, Re = 2$

β_2. As β_2 is increasing, the flow velocity at the injection wall decrease slightly but greater decrease in the velocity is noticed at the suction wall.

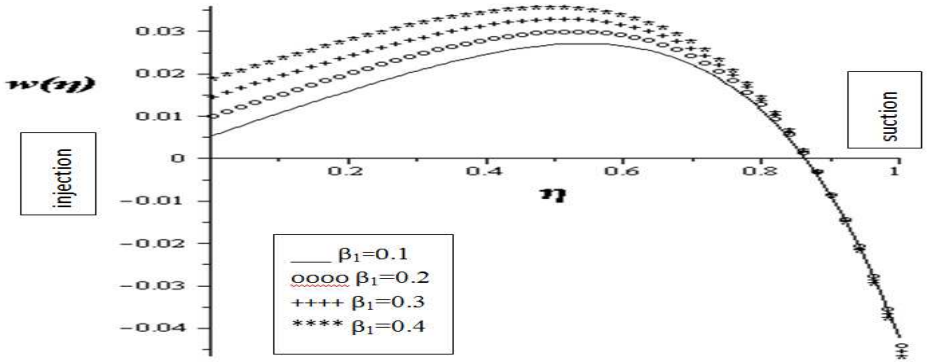

Figure 4.6: velocity Profile,$Re = 2, Br = Gr = 1, K = \beta_2 = 0.1, Pe = 3$

When each of the parameters $(Gr, Re, Br, K, \beta_1, \beta_2)$ varies while others remain constant for the temperature profile, there is no effect on both suction and injection channel walls. Fig.(4.8) depicts the temperature profile as Peclet Number (Pr) is increasing. An increase in the Peclet number leads to a decrease in the temperature at both injection and suction channel walls.

Fig.(4.9) depicts the variation of Peclet number and its effect on entropy generation

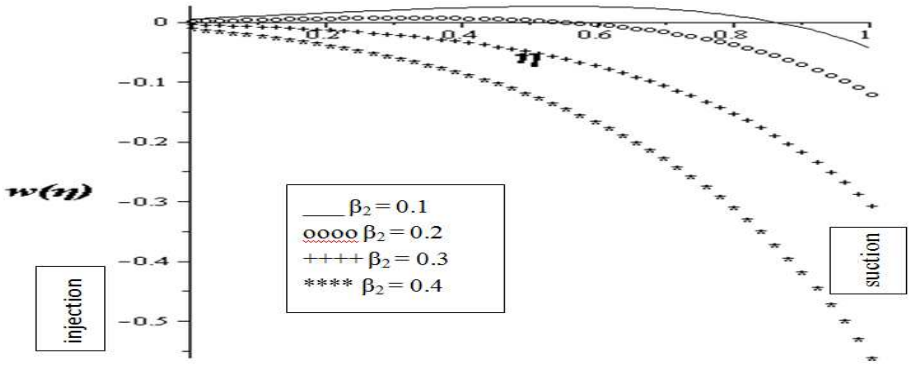

Figure 4.7: velocity Profile,$Gr = Br = 1, K = \beta_1 = K = 0.1, Re = 2$

number. The graph reveals that as the Peclet number is increasing, entropy generation number has no effect on the injection wall but rather on the suction wall, with great increase in entropy generation. This shows that there are restrictive medium leading to high disorder in the fluid particle at the suction wall.

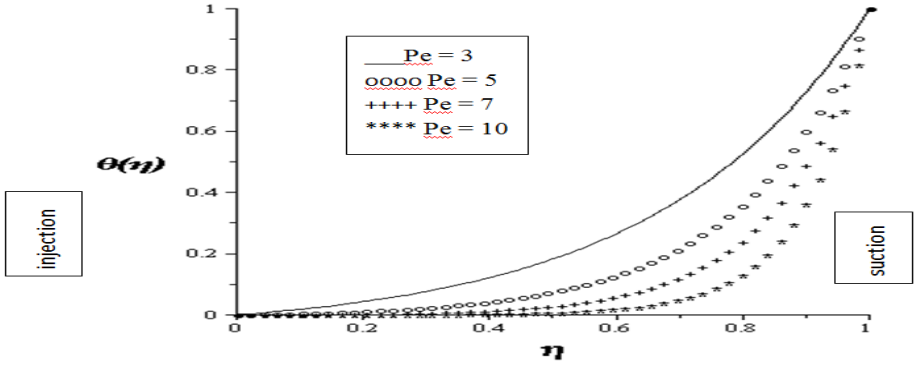

Figure 4.8: Temperature Profile,$Re = 2, Br = Gr = 1, K = \beta_1 = \beta_2 = 0.1$

Figs.(4.10) and (4.11) depict an increase in group parameter $Br\Omega^{-1}$ and Grashof number (Gr) and their effects on entropy generation. As $Br\Omega^{-1}$ and (Gr) are increasing in Figs.(4.10) and (4.11) respectively, a slight increase in entropy generation

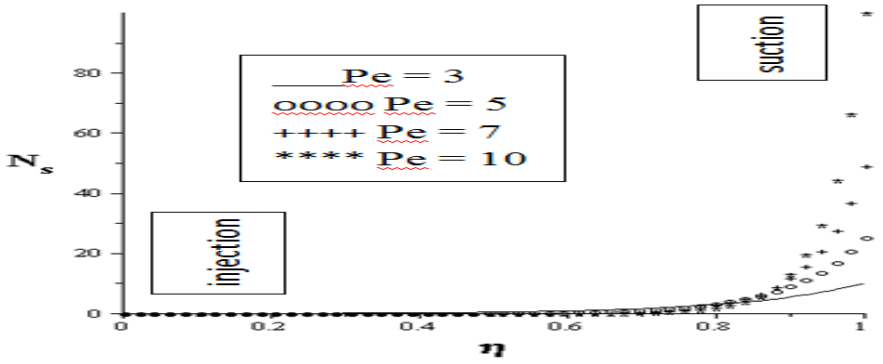

Figure 4.9: Entropy Generation,$Gr = Br = 1, K = \beta_2 = \beta_1 = K = 0.1, Re = 2, \Omega = 1$

on the injection wall and greater increase in entropy generation on the suction wall are noticed. This indicates that, there is little restrictive medium at the injection walls and more restrictive medium at the suction walls. Like Figs.(4.10) and (4.11), Fig.(4.12) holds the same explanation as the pressure gradient parameter K varies. Fig.(4.13) takes into consideration the variation of the asymmetric slip parameter β_1 and its effect on entropy generation. This means that there is less restrictive medium at the injection wall but more restrictive medium at the suction wall. Fig.(4.14) depicts variation in slip parameter β_2 . As β_2 increased, there is an increase in entropy generation on both walls but with a greater increase on the suction wall.

Figs.(4.15)-(4.20) show the effect of Reynolds number, Peclet number, slip parameters, group parameters, pressure gradient and Grashof number on the Bejan number. Fig.(4.15) takes into account the variation of Reynolds number and its effect on the Bejan number. The graph shows that as Reynolds number is increasing, Bejan number on the injection wall is increasing while Bejan number on suction wall is decreasing. Hence, irreversibility due to heat transfer dominates the flow process at the injection wall and irreversibility due to fluid friction dominates at the suction wall. Fig.(4.16)

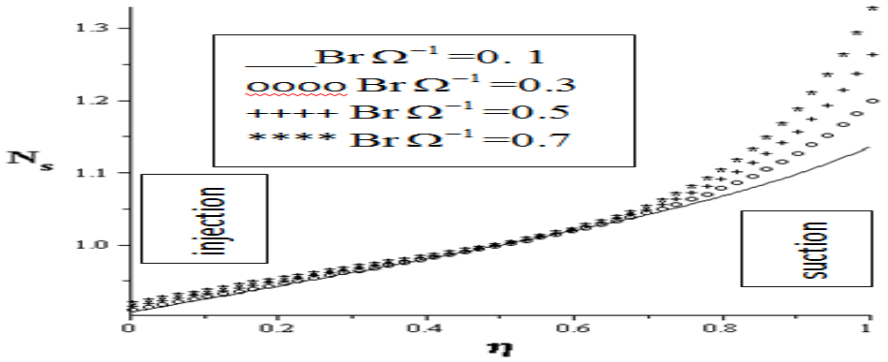

Figure 4.10: Entropy Generation,$Gr = 1, K = \beta_2 = \beta_1 = 0.1, Re = 2, Pe = 0.1$

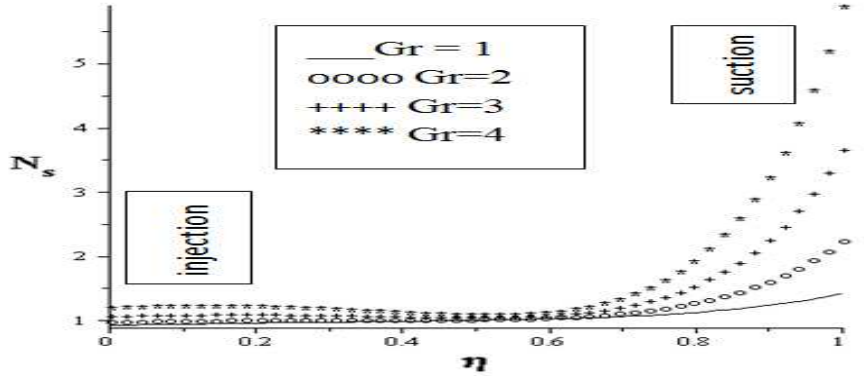

Figure 4.11: Entropy Generation,$Br = 1, K = Pe = \beta_2 = \beta_1 = K = 0.1, Re = 2, \Omega = 1$

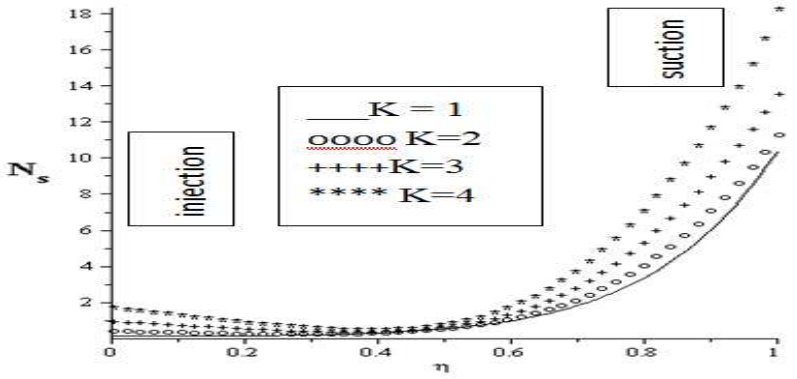

Figure 4.12: Entropy Generation,$Gr = Br = 1, \beta_2 = \beta_1 = 0.1, Re = 2, Pe = 3, \Omega = 1$

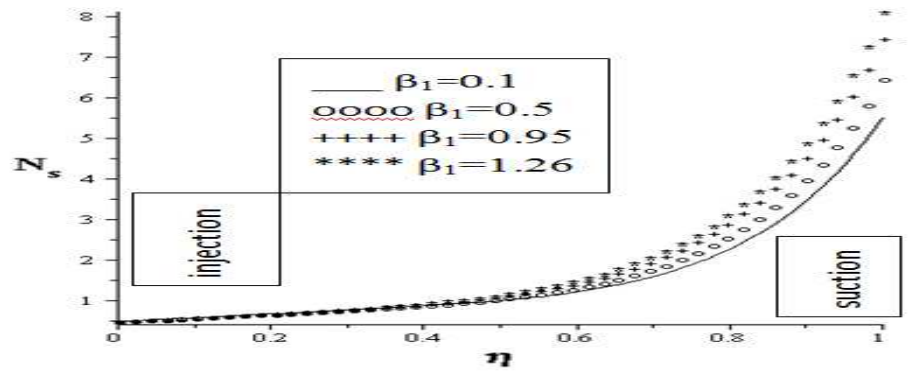

Figure 4.13: Entropy Generation,$Gr = 4, Br = 1, K = \beta_2 = 0.1, Re = 2, Pe = 0.95, \Omega = 1$

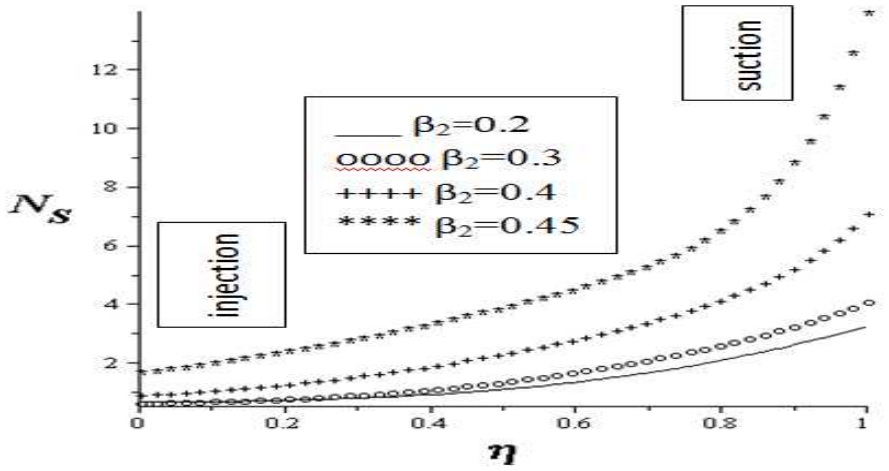

Figure 4.14: Entropy Generation,$Gr = 2, Pe = 3, Br = 1, K = \beta_1 = K = 0.1, Re = 2, \Omega = 1$

considers the variation of the pressure gradient parameter (K) and its effect on Bejan number. As pressure gradient parameter is increasing, a decrease in the Bejan number at both walls is noticed. Hence, irreversibility due to fluid friction dominates at both walls. At the centerline of the channel, both irreversibility due to heat transfer and irreversibility due to fluid friction contribute equally.

Fig.(4.17) looks at increase in Peclet number and its effect on Bejan number. As the

Peclet number is increasing, Bejan number at the injection wall is decreasing and increasing at suction wall. Therefore, irreversibility due to fluid friction dominates the injection channel wall and irreversibility due to heat transfer dominates the flow process at the suction wall, but both of them contributed equally at the centerline of the channel. Fig.(4.18) takes into account the variations of group parameters and its effect on Bejan number. The graph shows that as the group parameter is increasing, at the injection and suction channel walls, Bejan number is decreasing. This implies that irreversibility due to heat transfer decrease at both walls, but at the centerline of the channel both irreversibility due to fluid friction and irreversibility due to heat transfer contributed equally.

Figs.(4.19) and (4.20) show increase in the asymmetric slip coefficients β_1 and β_2

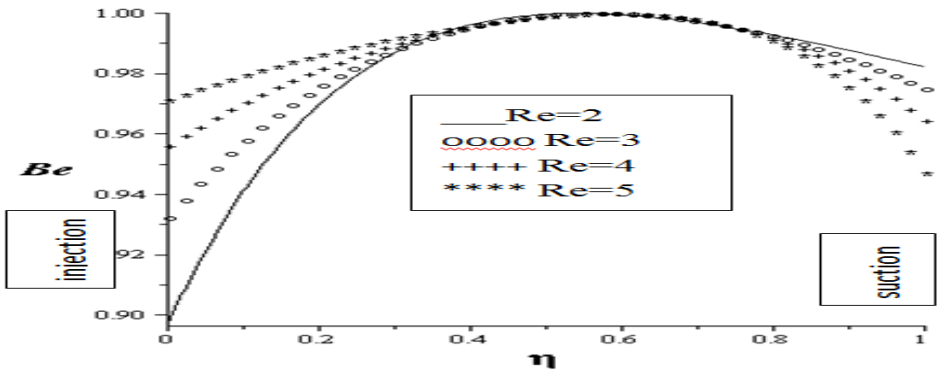

Figure 4.15: Bejan Profile,$Gr = Br\Omega^{-1} = 1, K = \beta_1 = \beta_2 = 0.1, Pe = 3$

with their effects on Bejan number. The graphs show that as asymmetric slip coefficients β_1 and β_2 are increasing; Bejan number is decreasing at injection wall and increasing at suction wall. A flow reversal at suction wall is noticed as well.

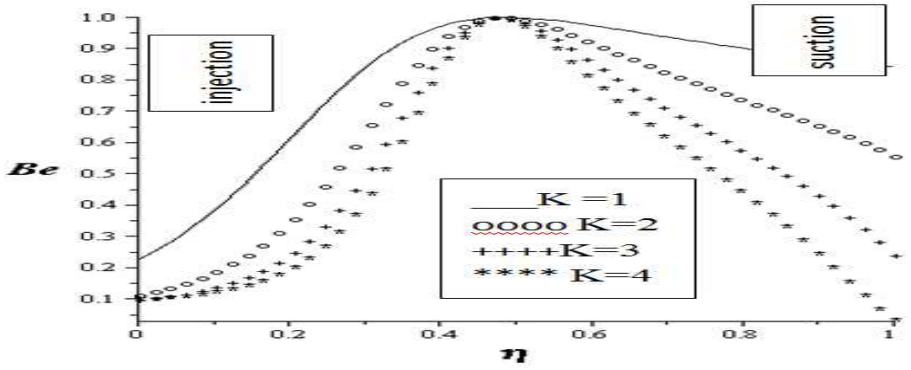

Figure 4.16: Bejan Profile,$Gr = Br\Omega^{-1} = 1, \beta_1 = \beta_2 = 0.1, Re = 2, Pe = 3$

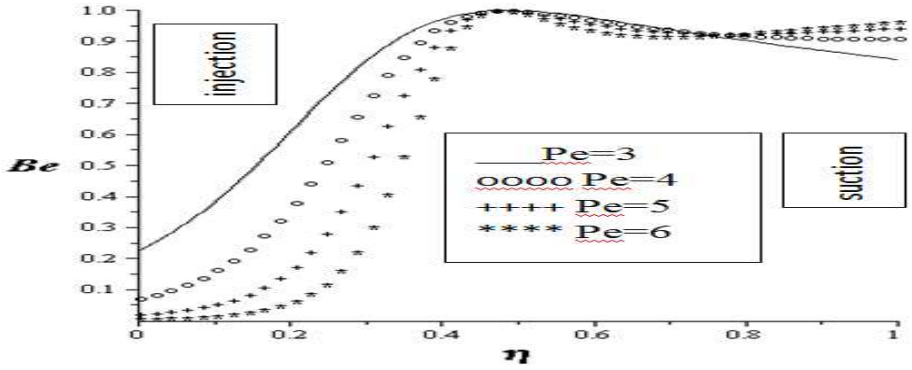

Figure 4.17: Bejan Profile,$Gr = K = Br\Omega^{-1} = 1, \beta_1 = \beta_2 = 0.1, Re = 2$

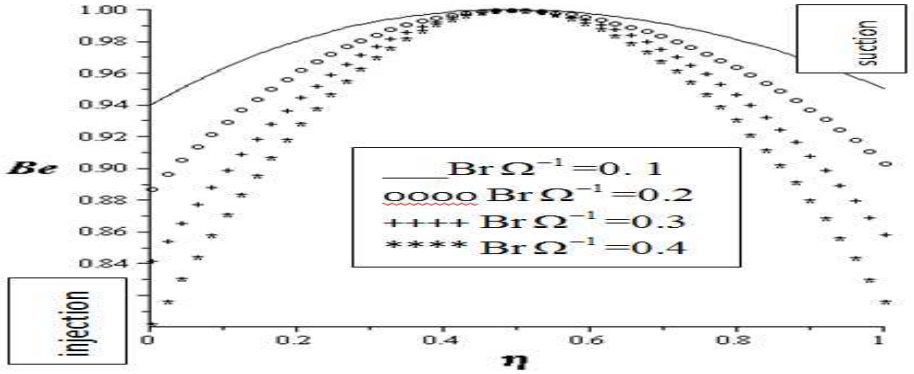

Figure 4.18: Bejan Profile,$Gr = K = 1, \beta_1 = \beta_2 = 0.1, Re = 2, Pe = 1.5$

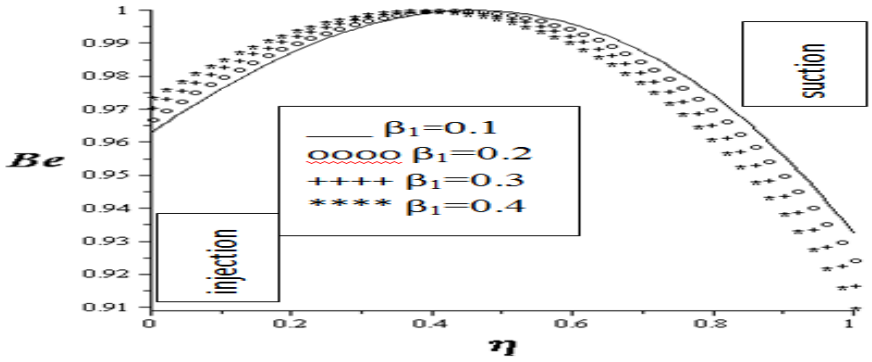

Figure 4.19: Bejan Profile,$Gr = K = Br\Omega^{-1} = 1, \beta_2 = 0.1, Re = 2, Pe = 2$

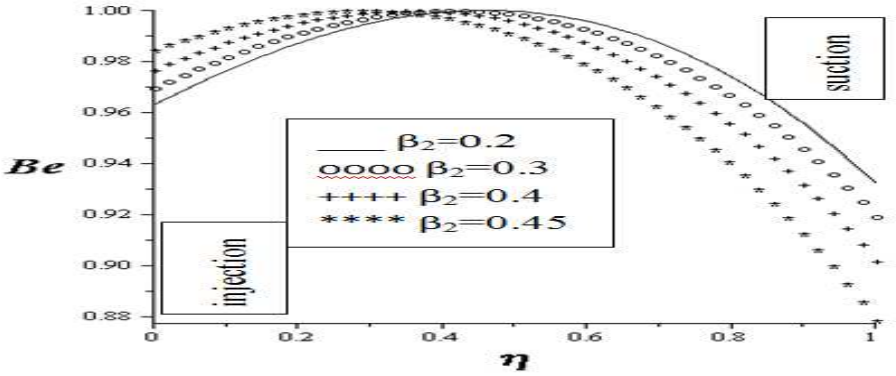

Figure 4.20: Bejan Profile,$Gr = K = 1, Br\Omega^{-1} = \beta_1 = 0.1, Re = 2, Pe = 0.71$

4.5 Conclusions

Combined effect of buoyancy forces and Navier slip on the entropy generation rate in a vertical porous channel with wall suction/injection was investigated. In the course of considering the effect of buoyancy forces (i.e., increases in Grashof number), the we noticed a slight increase in the entropy generation rate at the injection wall and sporadic increase at the suction wall. Furthermore, entropy generation decreased at the injection wall and increased at the suction wall as slip parameter β_1 increased. However, as the slip parameter β_2 increased, the entropy generation rate at both

suction and injection walls increased. Also, increase in both slip parameters β_1 and β_2 resulted in a flow reversal in the Bejan number.

Chapter 5

Entropy analysis of MHD unsteady flow through a porous pipe with buoyancy effects

The chapter focuses on first and second laws analysis for flow and heat transfer inside a uniformly porous vertical pipe. The pipe flow is subjected to constant suction at the wall and is acted upon by a combination of buoyancy forces, a transverse magnetic field and constant pressure gradient. The pipe walls are kept isothermal and the flow of the conducting fluid is assumed to be unsteady with variable viscosity. The non-linear governing equations in cylindrical coordinates are obtained under axisymmetric assumptions and solved numerically using semi-implicit finite difference techniques to obtain expressions for velocity and temperature profiles. The entropy generation number, irreversibility distribution ratio and Bejan number are presented graphically and discussed quantitatively for various values of the embedded parameters.

5.1 Introduction

Investigations of the flow of electrically conducting fluids in a porous geometries is of particular importance due to of its widespread prevalence in a number of engineering and industrial applications such as in geothermal reservoirs, nuclear reactor cooling, Magnetohydrodynamic (MHD) marine propulsion, electronic packages, micro electronic devices, thermal insulation, and petroleum reservoirs. Preliminary experimental evidence suggests promising future applications in the field of metallurgy, in particular in the MHD stirring of molten metal and magnetic-levitation casting. Further applications also arise in the operations of micro-electronic devices. The experimental investigation of modern MHD flow in a laboratory was first carried out by Hartmann and Lazarus [46]. Riley [99] studied buoyancy induced flow and transport in the presence of magnetic field. Chamkha [37] reported the unsteady natural convection in a porous channel in the presence of magnetic field. For a rectangular vertical duct, Hunt [48] and Buhler [15] analyzed the fluid flow problem in magnetic field with or without buoyancy effects. For conducting fluids, Shercliff [109] analyzed the fluid flow characteristics in a pipe under a transverse magnetic field. Alboussiere et al[1] did an asymptotic analysis to study the buoyancy driven convection in a uniform magnetic field. Makinde and Aziz [73] reported the effects of magnetic field and convective heat transfer on mixed convection from a vertical plate embedded in a porous medium. The combined effects of variable viscosity and electrical conductivity on hydromagnetic flow and heat transfer between a fixed plate and moving parallel plate was numerically analyzed by Makinde and Onyejekwe [74]. The investigations in these references are all restricted to first law analysis under the thermodynamics framework.

Meanwhile, the contemporary trend in the field of heat transfer and thermal design is the second law analysis and its design-related concept of entropy generation minimization. The foundation of knowledge of entropy production goes back to Clausius and Kelvins studies on the irreversible aspects of the Second Law of Thermodynamics. Since then the theories based on these foundations have rapidly developed. However, the entropy production resulting from combined effects of velocity and temperature gradients has remained untreated by classical thermodynamics, which has motivated many researchers to conduct analyses of fundamental and applied engineering problems based on second law analysis. Entropy generation is associated with thermodynamic irreversibility, which is common in all types of heat transfer processes. Moreover, in thermodynamical analysis of flow and heat transfer processes, one thing of core interest is to improve the thermal systems to avoid the energy losses and fully utilize the energy resources. Since the pioneering work of Bejan [7, 10], many investigations have been made on entropy generation analysis [54, 60, 69]. Sahin [106] investigated the second law analysis for a viscous fluid in a circular duct with isothermal boundary conditions. Tasnim and Mahmud [112] studied the first and second law characteristics of the flow and the heat transfer inside a vertical channel embedded in a porous medium under the influence of transverse magnetic field. Mahmud and Fraser [58] applied the second law analysis to heat and fluid flow due to forced convection inside a channel. The entropy generation in boundary layer flow was investigated by Arpaci and Selamet [3]. Makinde and Beg [72] studied the effect of magnetic field on entropy generation due to a reactive flow in a channel.

The purpose of this chapter is to analyze the first and second laws of thermodynamics with respect to inherent irreversibility in an unsteady flow of a viscous incompressible conducting fluid through a uniformly porous pipe subjected to constant fluid suction at the isothermal walls and a transversely imposed magnetic field. Expressions for dimensionless velocity, temperature and entropy generation number are presented under axisymmetric conditions. These flow quantities are also presented graphically and discussed quantitatively with respect to the embedded parameters.

The chapter is organized as follows: the mathematical model of the physical problem is described in section 5.2 leading to the relevant (dimensionless) governing equations. We follow this up in section 5.3 with the development of the mathematical tools to be used in analyzing the entropy generation and irreversibility. The numerical method of solution for the nonlinear set of governing partial differential equations is developed in section 5.4 and then employed in section 5.5 to obtain and discuss the relevant graphical results. Concluding remarks follow in section 5.6.

5.2 Mathematical Model

Consider an unsteady flow of an incompressible electrically conducting viscous fluid through a cylindrical pipe under the combined action of constant axial pressure gradient; buoyancy force and uniform suction through pipe wall in the presence of a transversely imposed magnetic field of strength B_0 (see Fig.(5.1)). In addition, there is no applied electric field and all of the Hall effects are neglected. For most industrial applications, the magnetic Reynolds number is assumed to be very small and the induced magnetic field is negligible. The fluid temperature dependent variable

viscosity ($\mu(T)$) is expressed as:

$$\bar{\mu} = \mu_0 e^{-\gamma(T-T_0)}, \tag{5.1}$$

where μ_0 is the initial fluid dynamic viscosity at the temperature T_0 . Then, assum-

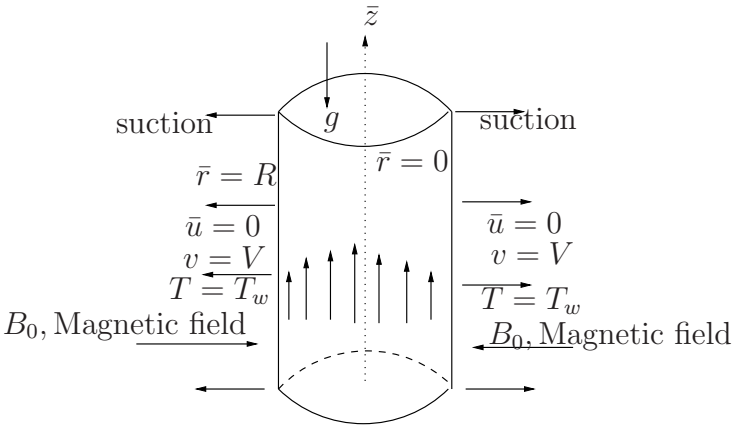

Figure 5.1: Problem's Schematic diagram

ing a Boussinesq incompressible fluid model, the continuity, momentum and energy equations governing the problem are given as [1, 58, 74, 106];

$$\frac{\partial \bar{u}}{\partial \bar{z}} = 0, \tag{5.2}$$

$$\rho\frac{\partial \bar{u}}{\partial \tau} + \rho V\frac{\partial \bar{u}}{\partial \bar{r}} = -\frac{\partial \bar{p}}{\partial \bar{z}} + \frac{1}{\bar{r}}\frac{\partial}{\partial \bar{r}}\Big(\bar{r}\bar{\mu}\frac{\partial \bar{u}}{\partial \bar{r}}\Big) - \sigma B_0^2\bar{u} + \rho g\alpha(T - T_0), \tag{5.3}$$

$$\rho c_p\frac{\partial T}{\partial \tau} + \rho c_p V\frac{\partial T}{\partial \bar{r}} = \frac{k}{\bar{r}}\frac{\partial}{\partial \bar{r}}\Big(\bar{r}\frac{\partial T}{\partial \bar{r}}\Big) + \bar{\mu}\Big(\frac{\partial \bar{u}}{\partial \bar{r}}\Big)^2 + \sigma B_0^2\bar{\mu}^2 \tag{5.4}$$

with the initial and boundary conditions;

$$u(0, \bar{r}) = 0, \quad T(0, \bar{r}) = T_0, \tag{5.5a}$$

$$\bar{u}(\tau, 0) = 0, \quad T(\tau, 0) = T_w, \quad \bar{u}(\tau, R) = 0, \quad T(\tau, R) = T_w \tag{5.5b}$$

where $(\bar{r}, \bar{z})$ are the distance measured in the radial and axial directions respectively, τ is the time,ρ is the fluid density, is the thermal conductivity,α is the volumetric expansion coefficient, g is the gravitational acceleration,σ is the electrical conductivity, T is the fluid temperature,T_w is the channel walls temperature, R is the pipe radius, T_0 is the fluid initial temperature,V is the uniform suction/injection velocity, $\bar{u}$ is the axial velocity, c_p is the specific heat at constant pressure and P is the fluid pressure. We introduce the following non-dimensional quantities into Equations (5.2)-(5.5b);

$$
\begin{aligned}
&r = \frac{\bar{r}}{R}, \quad z = \frac{\bar{z}}{R}, \quad u = \frac{\bar{u}}{V}, \quad v = \frac{\bar{v}}{V}, \quad \mu = \frac{\bar{\mu}}{\mu_0}, \quad \theta = \frac{(T - T_0)}{(T_w - T_0)}, \quad t = \frac{\tau V}{R}, \\
&P = \frac{RP}{\mu_0 V}, \quad Br = \frac{\mu_0 V^2}{k(T_w - T_0)}, \quad Re = \frac{\rho V R}{\mu_0}, \quad \beta = \gamma(T_w - T_0), \\
&A = -\frac{\partial P}{\partial z}, \quad Pr = \frac{\rho c_p V R}{k}, \quad M = \frac{\sigma B_0^2 R^2}{\mu_0}, \quad Gr = \frac{g\alpha(T_w - T_0)\rho R^2}{V\mu_0},
\end{aligned} \tag{5.6}
$$

and obtain;

$$
Re\Big(\frac{\partial u}{\partial t} + \frac{\partial u}{\partial r}\Big) = A + \frac{1}{r}\frac{\partial}{\partial r}\Big(re^{-\beta\theta}\frac{\partial u}{\partial r}\Big) - Mu + Gr\theta, \tag{5.7}
$$

$$
Pr\Big(\frac{\partial \theta}{\partial t} + \frac{\partial \theta}{\partial r}\Big) = \frac{1}{r}\frac{\partial}{\partial r}\Big(r\frac{\partial \theta}{\partial r}\Big) + Bre^{-\beta\theta}\Big(\frac{\partial u}{\partial r}\Big)^2 + BrMu^2 \tag{5.8}
$$

with;

$$
u(0, r) = 0, \quad \theta(0, r) = 0, \tag{5.9a}
$$

$$
u(t, 0) = 0, \quad \theta(t, 0) = 1, \quad u(t, 1) = 0, \quad \theta(t, 1) = 1. \tag{5.9b}
$$

where β is the viscosity variation parameter, Gr is the Grashof number, M is the Magnetic field parameter, Br is the Brinkman number, Re is the suction/injection Reynolds number and Pr is the Prandtl number. Other quantities of interest in this chapter include the wall shear stress ι_w and the heat transfer rate at the channel surface q_w given as

$$
\iota_w = -\bar{\mu}\frac{\partial \bar{u}}{\partial \bar{r}}\Big|_{\bar{r}=R}, \quad q_w = -\frac{\partial T}{\partial \bar{r}}\Big|_{\bar{r}=R} \tag{5.10}
$$

and in dimensionless form, we obtain

$$C_f = \frac{\iota_w R}{\mu_0 V} = -e^{-\beta\theta}\frac{\partial u}{\partial r}\Big|_{r=1}, \quad N_u = \frac{q_w R}{k(T_w - T_0)} = -\frac{\partial \theta}{\partial r}\Big|_{r=1}. \tag{5.11}$$

5.3 Entropy Analysis

Second law analysis in terms of entropy generation rate is a useful tool for predicting the performance of the engineering processes by investigating the irreversibility arising during the processes. According to Woods [126], the local entropy generation rate is defined as:

$$S^m = \frac{k}{T_w^2}\Big(\frac{\partial T}{\partial \bar{r}}\Big) + \frac{\bar{\mu}}{T_w}\Big(\frac{\partial \bar{u}}{\partial \bar{r}}\Big) + \frac{\sigma B_0^2}{T_w}\bar{u}^2. \tag{5.12}$$

The first term in Equation (5.12) is the irreversibility due to heat transfer and the second term is the entropy generation due to viscous dissipation and third term is due to magnetic field. Using Equation (5.6), we express the entropy generation number in dimensionless form as:

$$N_S = \frac{R^2 T_w^2 S^m}{k(T_w - T_0)^2} = \Big(\frac{\partial \theta}{\partial r}\Big)^2 + \frac{Bre^{-\beta\theta}}{\Omega}\Big(\frac{\partial u}{\partial r}\Big)^2 + \frac{MBr}{\Omega}u^2, \tag{5.13}$$

where $\Omega = (T_w - T_0)/T_0$ is the temperature difference parameter. In Equation (5.13), the first term can be assigned as N_1 and the second term due to viscous dissipation as N_2 , i.e.

$$N_1 = \Big(\frac{\partial \theta}{\partial r}\Big)^2, \quad N_2 = \frac{Bre^{-\beta\theta}}{\Omega}\Big(\frac{\partial u}{\partial r}\Big)^2 + \frac{MBr}{\Omega}u^2. \tag{5.14}$$

Following Bejan [10, 11], the irreversibility distribution ratio is defined as $\phi = N_2/N_1$. Heat transfer dominates for $0 \leq \phi < 1$ and fluid friction and magnetic field effects dominate when $\phi > 1$. The contribution of both heat transfer and fluid friction with

magnetic field effects to entropy generation are equal when $\Phi = 1$. Alternatively, the dominant effect of either heat transfer irreversibility or fluid friction with magnetic field irreversibility can be investigated using the Bejan number (Be) defined mathematically as:

$$Be = \frac{N_1}{N_S} = \frac{1}{1+\phi}. \tag{5.15}$$

Clearly, the Bejan number ranges from 0 to 1. $Be = 0$ is the limit where the fluid friction with magnetic field irreversibility dominates and $Be = 1$ corresponds to the limit where the heat transfer irreversibility dominates. The contribution of both heat transfer and fluid friction with magnetic field to entropy generation are equal when $Be = 1/2$. In section 5.4, Equations (5.7)-(5.15) are solved numerically using a semi-implicit finite difference scheme.

5.4 Numerical Procedure

Our numerical algorithm is based on the semi-implicit finite difference scheme and is implemented along the same lines as in, say, $[33-36]$. Implicit terms are taken at the intermediate time level $(N+\xi)$ where $0 \leq \xi \leq 1$. The discretization of the governing equations is based on a linear Cartesian mesh and uniform grid on which finite-differences are taken. We approximate both the second and first spatial derivatives with second-order central differences. The equations corresponding to the first and last grid points are modified to incorporate the boundary conditions. The semi-implicit scheme for the velocity component reads:

$$Re\frac{u_j^{(N+1)} - u_j^{(N)}}{\Delta t} + Mu^{(N+\xi)} - e^{(-\beta\theta_j^{(N)})}u_{rr}^{(N+\xi)} = A + Gr\theta_j^{(N)} + u_r^{(N)}\Big[\mu_r + \frac{\mu}{r_j} - Re\Big]^{(N)}. \tag{5.16}$$

In equation (5.16) it is understood that subscript r denote partial differentiation under the finite difference framework described earlier, the subscript j represents the mesh position and the superscripts denote the time levels such that $\varsigma^{(N+\xi)} = \xi\varsigma^{(N+1)} + (1-\xi)\varsigma^{(N)}$. Since the unsteady problem under investigation is posed as an initial value problem, given a solution at a time level(N), i.e. $[u^{(N)}, \theta^{(N)}]$, the equations for the velocity solution at the subsequent time level $(N+1)$ reduce to:

$$-r_1 u_{j-1}^{(N+1)} + \Big(Re + M\Delta t\xi + 2r_1\Big)u_j^{(N+1)} - r_1 u_{j+1}^{(N+1)} = \text{explicit terms}, \tag{5.17}$$

where the explicit terms contain terms prescribed at the earlier time level (N) and;

$$r_1 = \xi\frac{\Delta t}{\Delta r^2}e^{(-\beta\theta_j^{(N)})}.$$

The solution procedure for $u^{(N+1)}$ thus reduces to inversion of tri-diagonal matrices which is an advantage over a full implicit scheme. The semi-implicit integration scheme for the energy equation is similar to that for the velocity:

$$Pr\frac{\theta_j^{(N+1)} - \theta_j^{(N)}}{\Delta t} - \theta_{rr}^{(N+\xi)} = \theta_r^{(N)}\Big[\frac{1}{r_j} - Pr\Big] + Bre^{(-\beta\theta_j^{(N)})}\Big[u_r^{(N)}\Big]^2 + BrM\Big[u_r^{(N)}\Big]^2. \tag{5.18}$$

The equation for $\theta^{(N+1)}$ thus become:

$$-r\theta_{j-1}^{(N+1)} + (Pr + 2r)\theta_j^{(N+1)} - r\theta_{j+1}^{(N+1)} = \text{explicit terms}, \tag{5.19}$$

where $r = \xi\Delta t/\Delta r^2$. The solution procedure again reduces to inversion of tridiagonal matrices. The schemes (5.17&5.19) were checked for consistency. For $\xi = 1$, these are first-order accurate in time but second order in space. The schemes in Chinyoka [33] have $\xi = 1/2$ which improves the accuracy in time to second order. We use $\xi = 1$ here so that the options of choosing larger time steps is possible.

5.5 Results and Discussion

Unless otherwise stated, we employ the parameter values: $A = 1, \beta = 0.5, M = 0.5, Gr = 0.1, Br = 0.1, Pr = 7.1, Re = 1, \Delta r = 0.02, \Delta t = 0.01, t = 400$

These will be the default values in this work and hence in any graph where any of these parameters is not explicitly mentioned, it will be understood that such parameters take on the default values.

5.5.1 Transient and steady flow profiles

We display the transient solutions in figs.(5.2) and (5.3). Both figures show a transient increase in fluid quantities (velocity and temperature) until a steady state is reached. Fig.(5.3) in particular shows the development of the temperature field from an initial state in which the wall temperature started higher than the bulk fluid temperature.

5.5.1.1 Parameter dependence of solutions

As one way of validating the accuracy of our numerical algorithms, we investigate in this section the response of the velocity and temperature (at steady state) to varying values of the relevant parameters. To ensure that all solutions have indeed reached steady state, we employ a time of $t = 400$ in all graphs under this section. The response of the velocity and temperature to variations in the viscosity parameter β is illustrated in Figs.(5.4) and (5.5) respectively.

An increase in the viscosity parameter corresponds to a decrease in fluid viscosity and hence also reduces the resistance to flow. This in turn leads to increased fluid velocity as shown in Fig.(5.4). The increased fluid velocity in turn increases the magnitude of the sources terms in the energy equation and hence leads to increased fluid

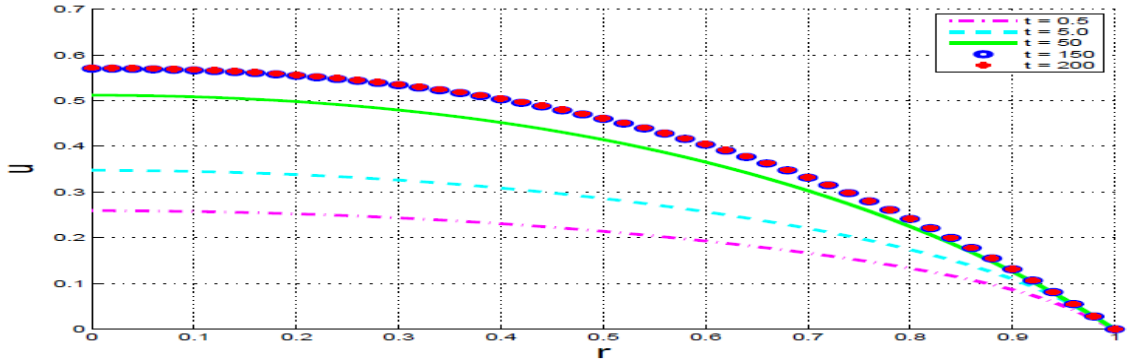

Figure 5.2: Transient and steady state velocity profiles.

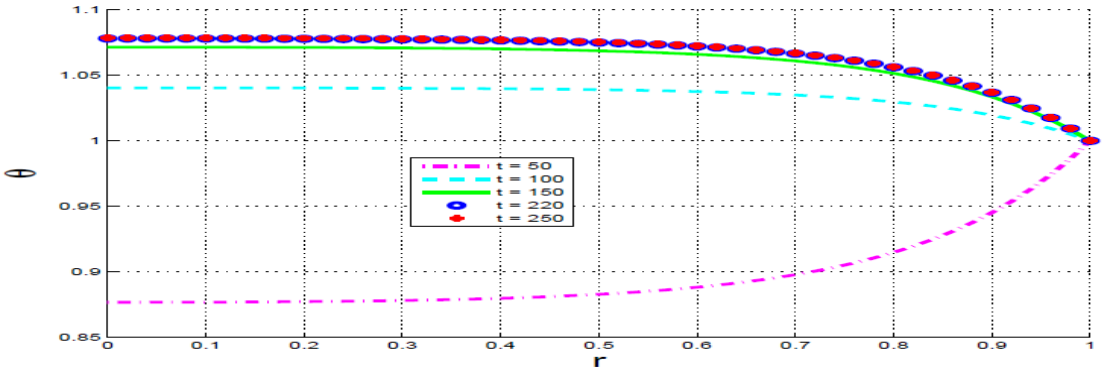

Figure 5.3: Transient and steady state temperature profiles.

temperatures as illustrated in Fig.(5.5).

The response of the velocity and temperature to variations in the Brinkman number (Br) is illustrated in Figs.(5.6) and (5.7) respectively.

The terms linked to the Brinkman number act as strong heat sources in the energy equation. Increases in the Brinkman number hence significantly also increase the fluid temperature shown Fig.(5.7) and hence also increase the fluid velocity, see Fig.(5.6), due to the coupling of the temperature to the velocity through the buoyancy terms.

Figs.(5.8) and (5.9) respectively show the response of the fluid velocity and temperature to variations in the suction Reynolds number. Increases in the suction

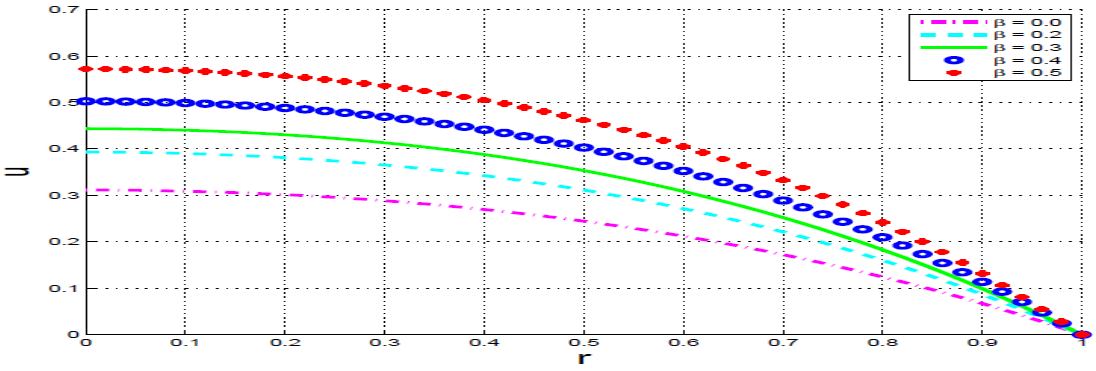

Figure 5.4: Effects of viscosity parameter (β) on steady state velocity.

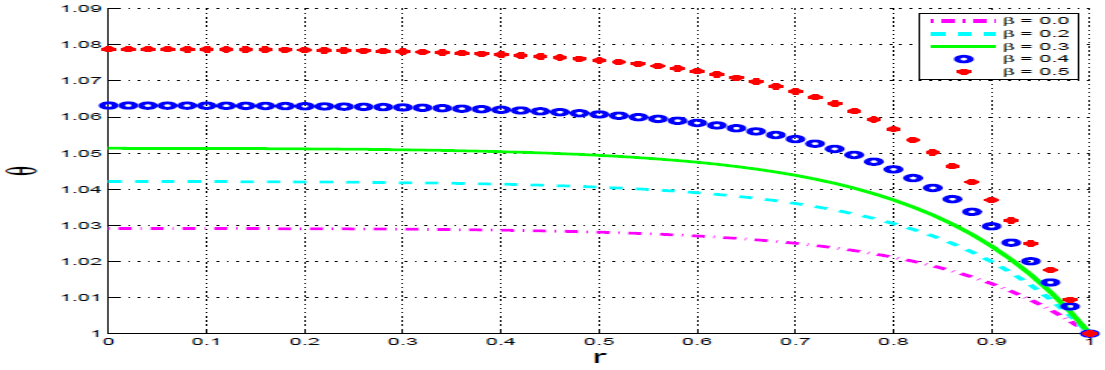

Figure 5.5: Effects of viscosity parameter (β) on steady state temperature.

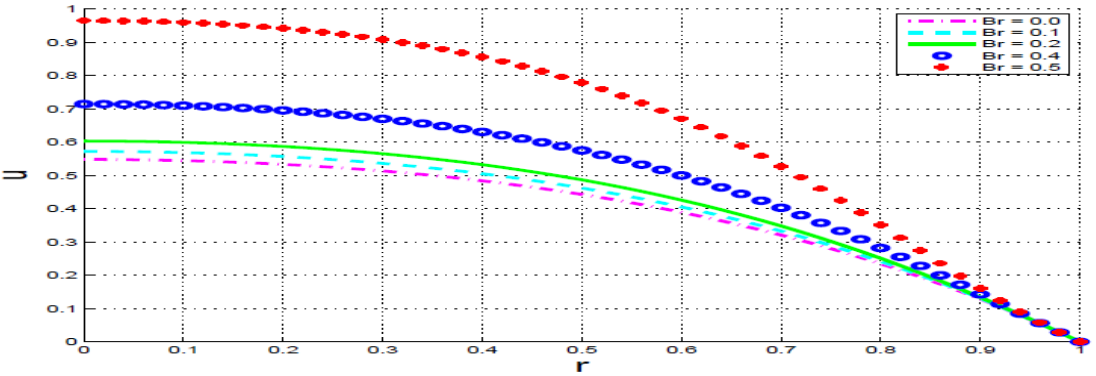

Figure 5.6: Effects of Brinkman number (Br) on steady state velocity.

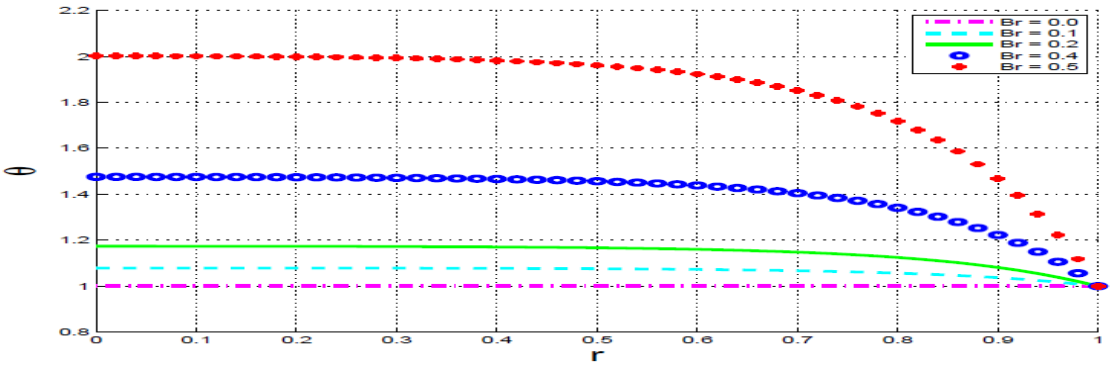

Figure 5.7: Effects of Brinkman number (Br) on steady state temperature.

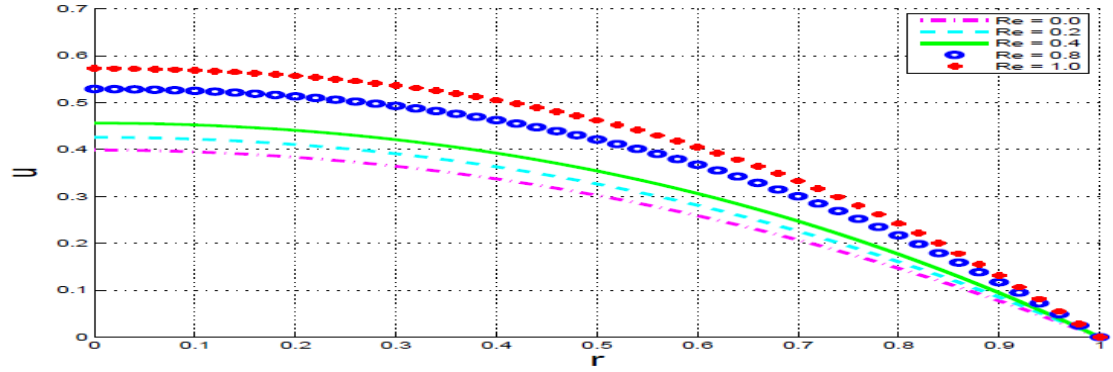

Figure 5.8: Effects of the suction Reynolds number (Re) on steady state velocity.

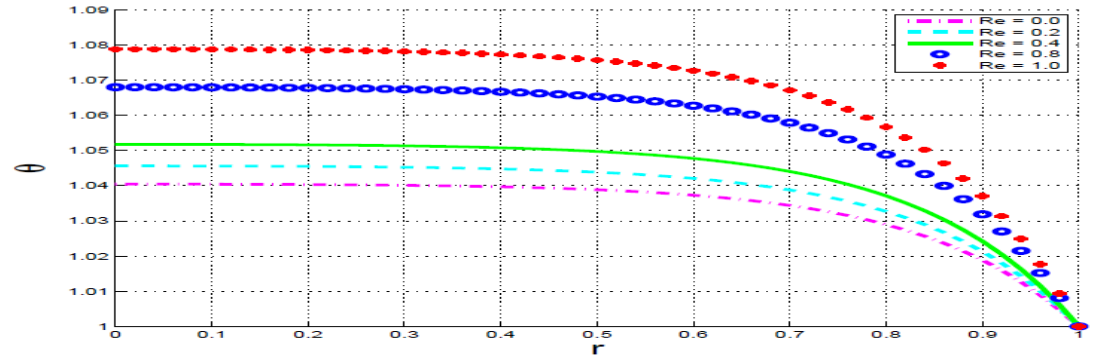

Figure 5.9: Effects of the suction Reynolds number (Re) on steady state temperature.

Reynolds (i.e. the axisymmetric suction strength) increases the velocity of the bulk fluid and hence also the as explained earlier.

The behaviour of the flow quantities in response to increases in the Grashof number is similar to that with respect to the Brinkman number. Both fluid velocity and temperature increase with increasing Gr as illustrated in Figs.(5.10) and (5.11).

An increased magnetic field strength expectedly leads to decreased magnitudes in

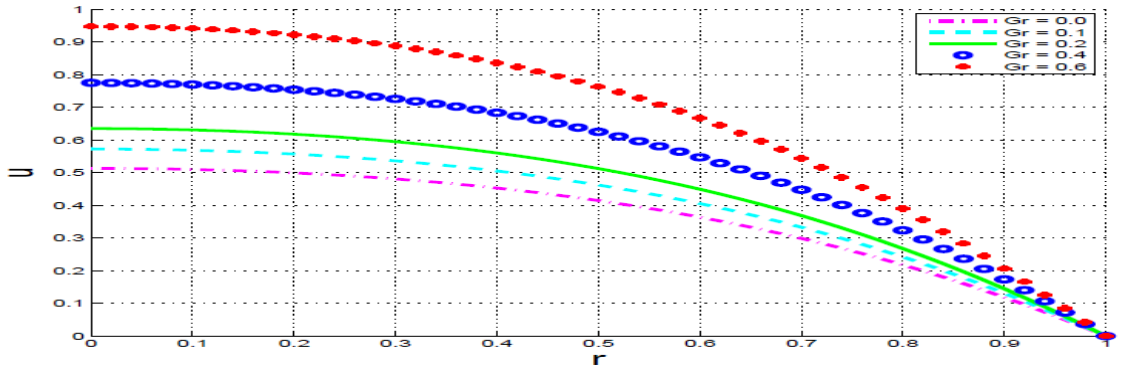

Figure 5.10: Effects of the Grashof number (Gr) on steady state velocity.

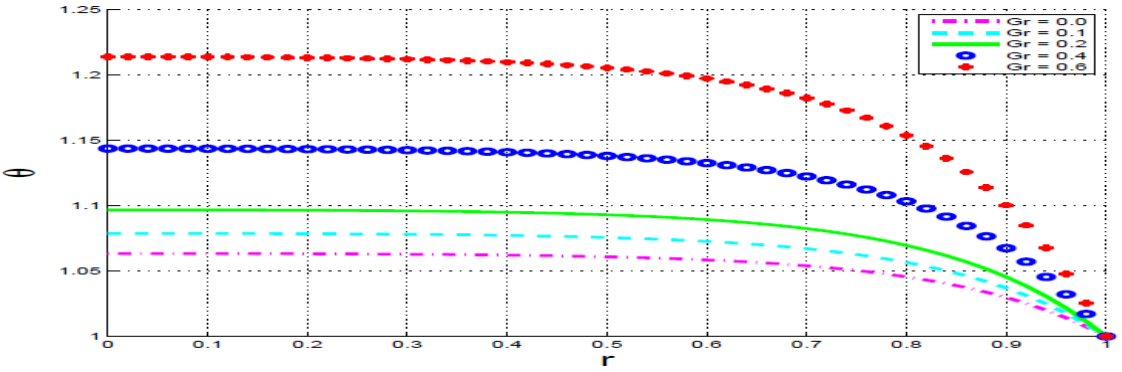

Figure 5.11: Effects of the Grashof number (Gr) on steady state temperature.

fluid velocity due to the increased resistance to flow, see Fig.(5.12). The response of the temperature field however depends on the magnitude of the magnetic field

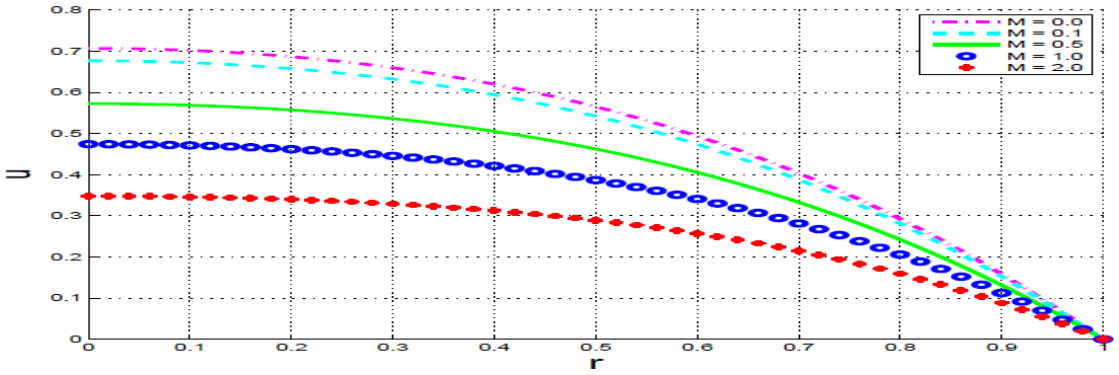

Figure 5.12: Effects of the magnetic field strength (M) on steady state velocity

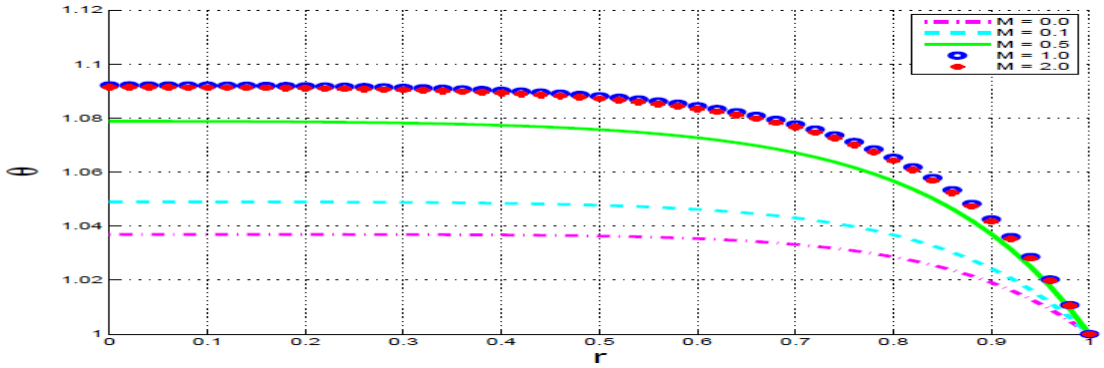

Figure 5.13: Effects of the magnetic field strength (M) on steady state temperature.

strength (M). For low values of M , the magnetic field source terms in the energy equation dominate the effects of the reduced velocity and hence an increase in temperature is noted, Fig.(5.13). For larger values of M the effects of the reduced velocity field dominate leading to corresponding decreases in the temperature field.

5.5.2 Skin friction

The wall shear stress (at the right hand side wall, $r = 1$) dependence on β is illustrated in Fig.(5.14) for varying values of the Brinkman number Br. Similarly, the wall shear stress dependence on Re is illustrated in Fig.(5.15) at different times and

the wall shear stress dependence on M is illustrated in Fig.(5.16) for varying values of the Grashof number.

The results of Figs. (5.14)-(5.16) are consistent with the conclusions of the previous-section, on parameter dependence of solutions. In general, parameters that decrease (increase) the fluid velocity correspondingly decrease (increase) the wall shear stress respectively. This is so, since fluid viscosity at the wall remains constant due to the fixed wall temperatures while the decrease (increase) of the bulk flow velocity correspondingly decreases (respectively increases) velocity gradients at the wall.

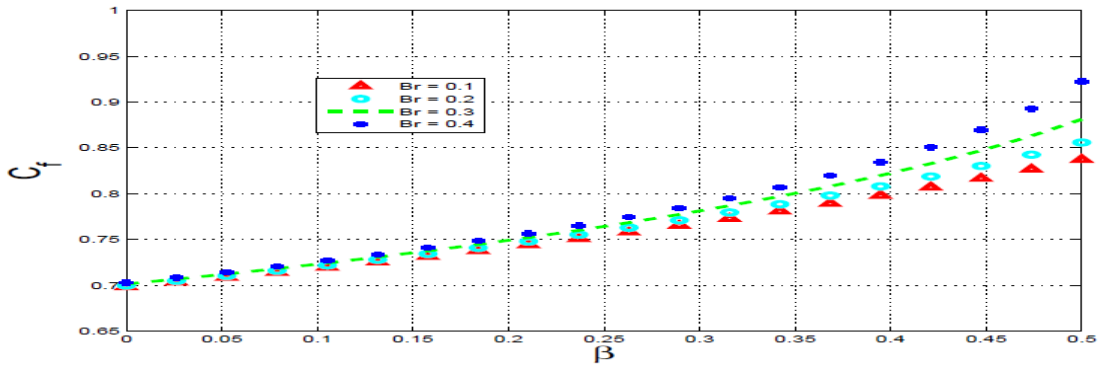

Figure 5.14: Variation of wall shear stress with β and Br.

5.5.3 Wall heat transfer

The wall heat transfer rate dependence on β is illustrated in Fig.(5.17) for varying values of the Brinkman number Br. Similarly, the wall heat transfer rate dependence on Re is illustrated in Fig.(5.18) at different times and the wall heat transfer rate dependence on M is illustrated in Fig.(5.19) for varying values of the Grashof number. As with the wall shear stress, parameters that decrease (increase) the fluid tempera-

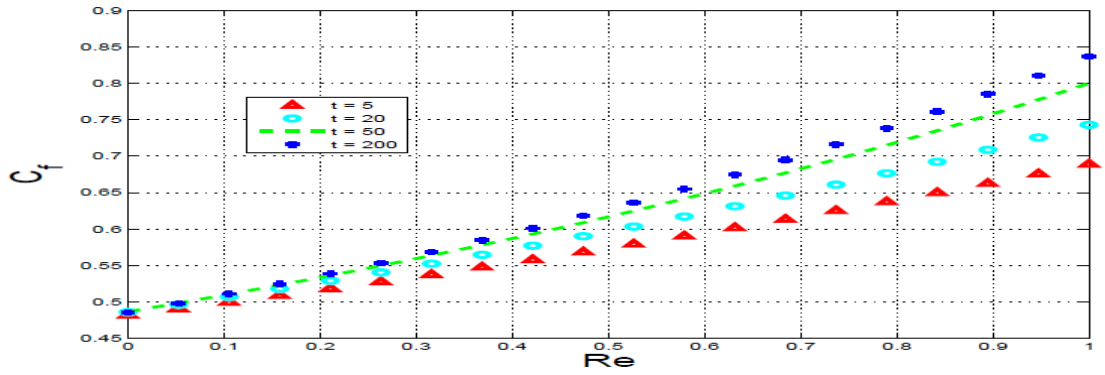

Figure 5.15: Variation of wall shear stress with Re and t.

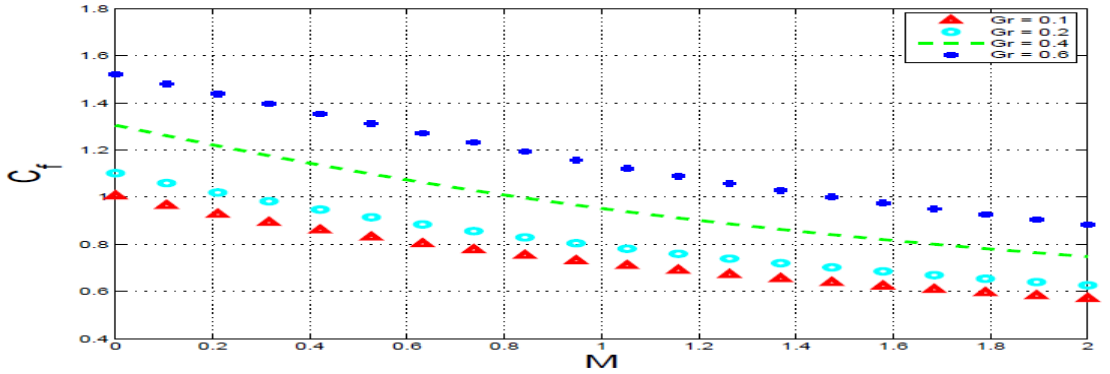

Figure 5.16: Variation of wall shear stress with M and Gr.

ture correspondingly decrease (increase) the wall heat transfer rate respectively. The negative values in Fig.(5.18) simply indicate that we have captured the solution at the early stages of development when the temperature profiles are still convex up! The non-monotonic behaviour of temperature with increases in M (as explained before) is clearly shown in Fig.(5.13).

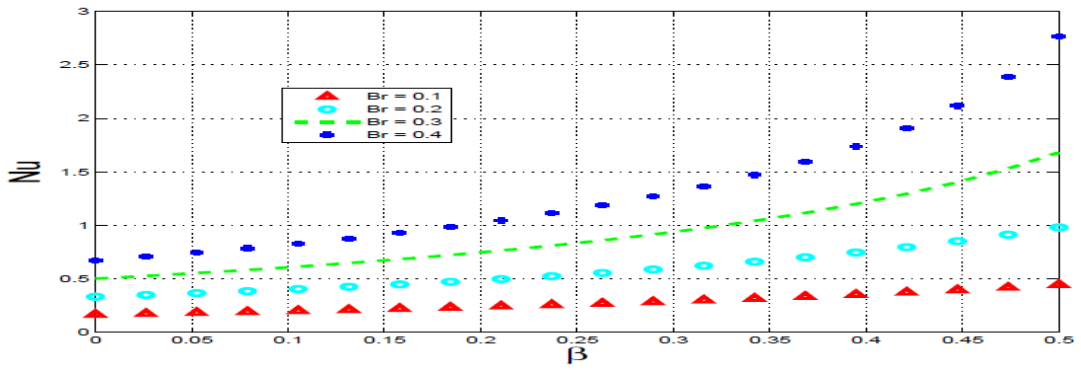

Figure 5.17: Variation of wall heat transfer rate with β and Br.

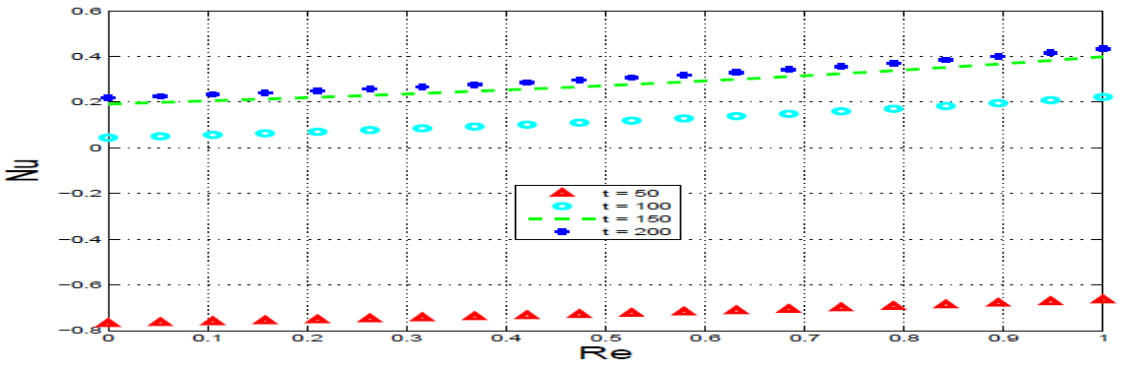

Figure 5.18: Variation of wall heat transfer rate with Re and t.

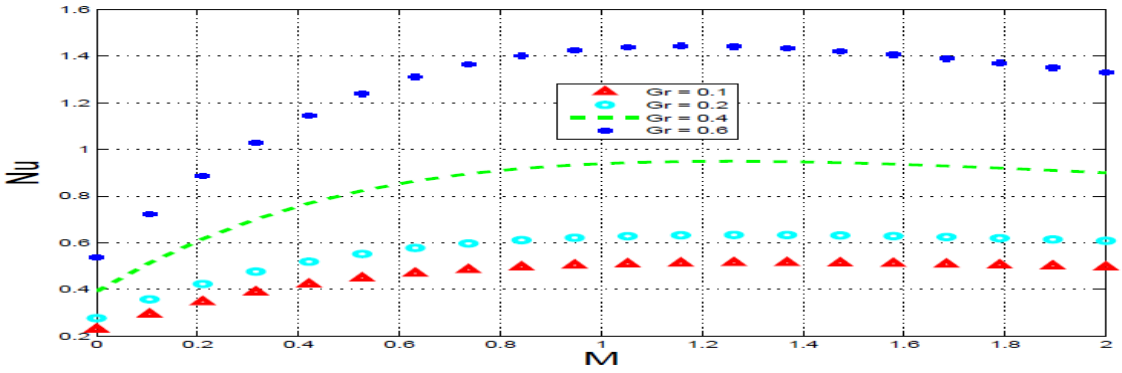

Figure 5.19: Variation of wall heat transfer rate with M and Gr.

5.5.4 Entropy generation

In this section, we plot the entropy generation rate (Ns) across the channel under varying parameter conditions. We use a mesh size of $\Delta y = 0.01$ in all subsequent graphs.

Figs.(5.20)-(5.24) show the expected increase in Ns with corresponding increases in $Br\Omega^{-1}$, β, Gr, Re and t respectively. This follows from the realization that increases in these parameters correspondingly increase the flow quantities and hence also the fluid friction with magnetic field contribution to the entropy generation. In Figs.(5.20)-(5.24), the entropy generation rate is expectedly maximum at the wall where velocity and temperature gradients as well as fluid viscosity are highest and minimum at the channel centerline where the maximum temperature and velocity and hence also zero temperature and velocity gradients are recorded.

The behaviour of the entropy generation rate with increasing magnetic field strength (M) results from the earlier alluded to complex interaction of the effects of M on the flow quantities, see Fig.(5.25).

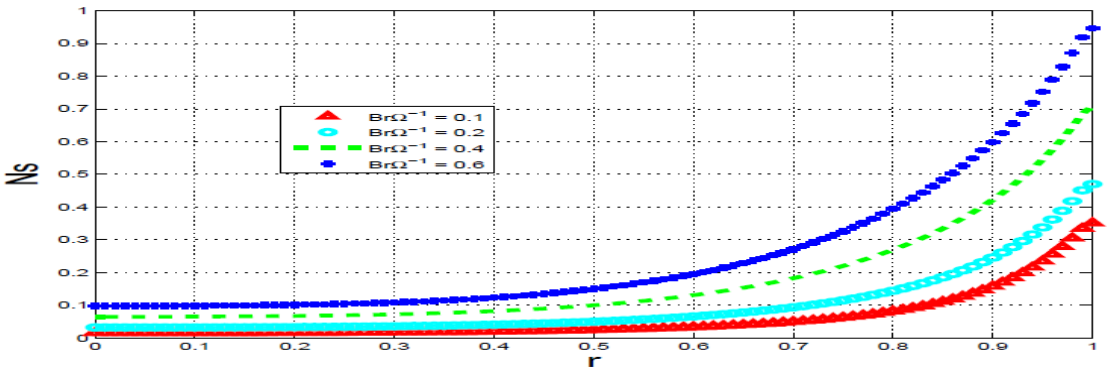

Figure 5.20: Variation of entropy generation rate with r and $Br\Omega^{-1}$

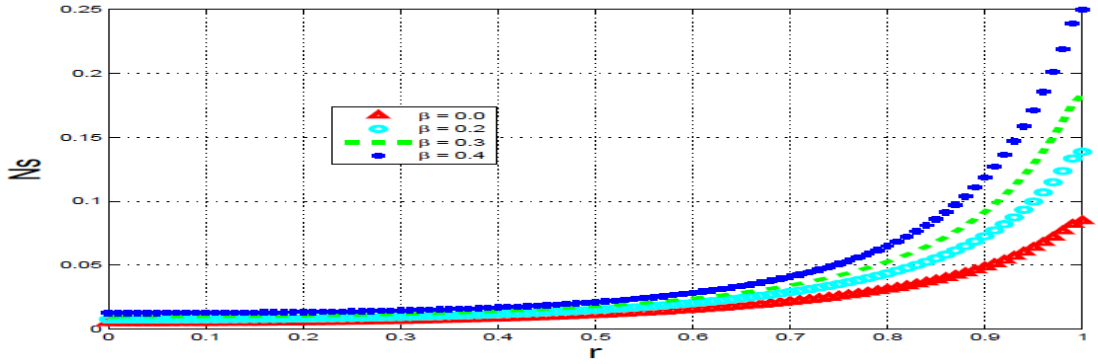

Figure 5.21: Variation of entropy generation rate with r and β.

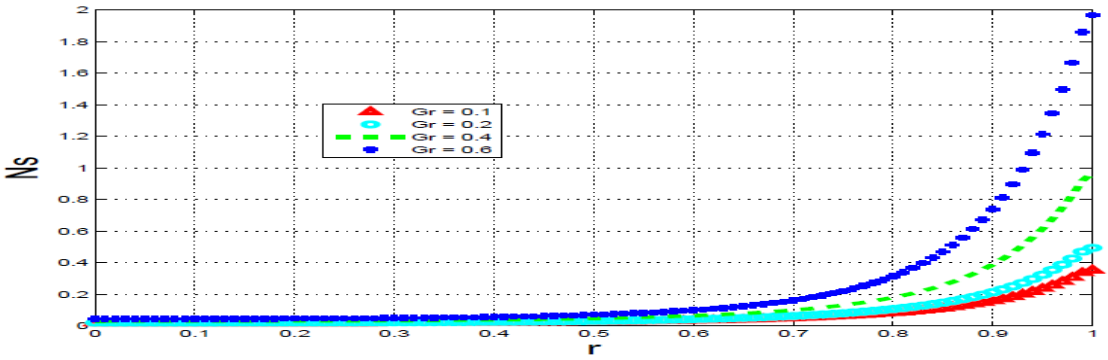

Figure 5.22: Variation of entropy generation rate with r and Gr.

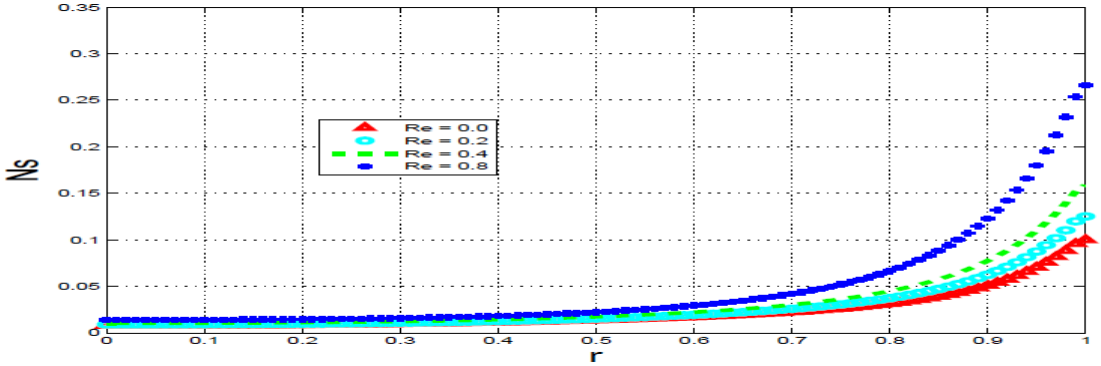

Figure 5.23: Variation of entropy generation rate with r and Re.

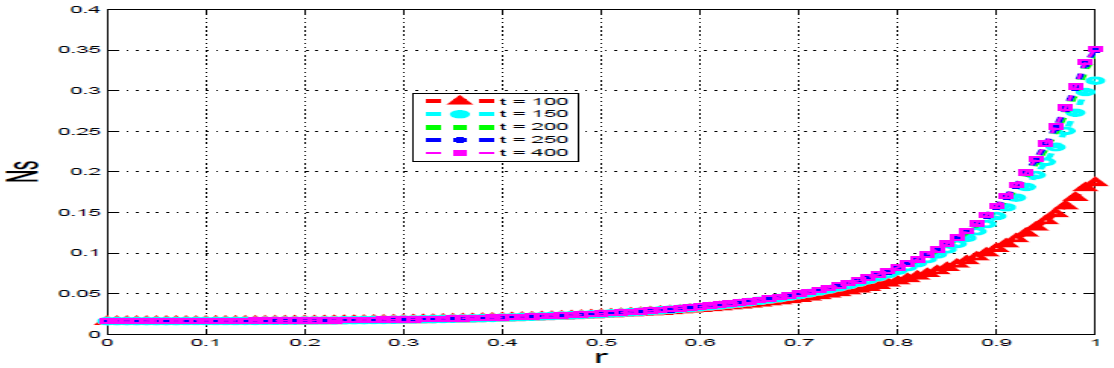

Figure 5.24: Variation of entropy generation rate with r and t.

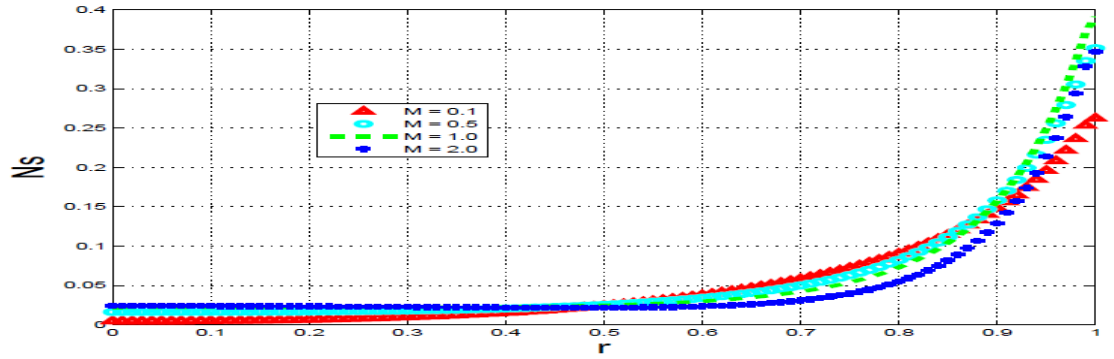

Figure 5.25: Variation of entropy generation rate with r and M .

5.5.5 Bejan number

In this section, we plot the Bejan number (Be) across the channel under varying parameter conditions. The analysis in this section is similar to that for the previous section with Ns now replaced by Be.

Fig.(5.26), shows as expected that higher values of $Br\Omega^{-1}$, which increase the magnitude of fluid friction with magnetic field irreversibility (N_2) but has no effect on the heat transfer irreversibility (N_1), increases the values of Φ leading to lower Bejan numbers.

Figs.(5.27)-(5.31) show that the effects of each of β, Gr, Re, t and M on Be depend on their (individual) competing influence on N_1 and N_2 . In general we notice that these parameters have a higher effect on the heat transfer irreversibility (N_1) than on fluid friction with magnetic field irreversibility (N_2) and hence an increase in any of these parameters gives correspondingly higher Bejan numbers.

Away from the wall (i.e. inside the main flow), the fluid friction with magnetic field irreversibility strongly dominates over heat transfer irreversibility. In the vicinity of the wall, the strength of the fluid parameters will determine which mode of irreversibility dominates over the other.

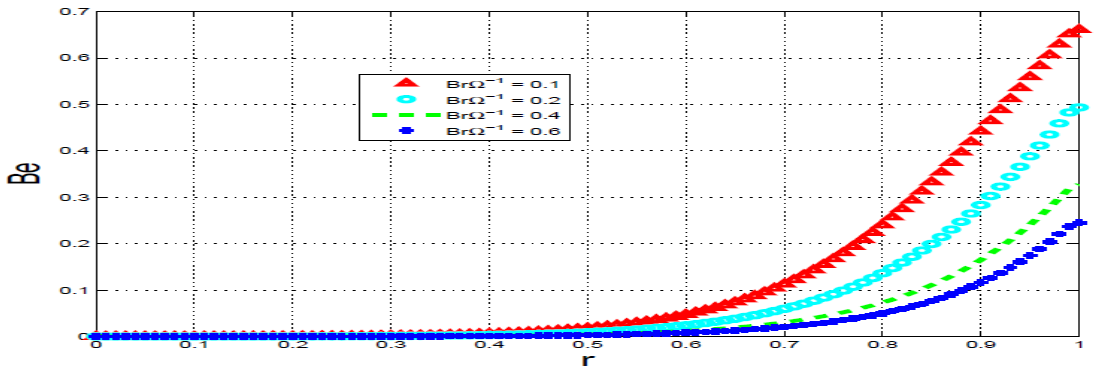

Figure 5.26: Variation of Bejan number with r and $Br\Omega^{-1}$.

5.6 Conclusion

We, computationally, investigate the transient pressure driven pipe flow of a fluid under gravity and axisymmetric conditions in the presence of buoyancy effects and constant suction at the walls. We employ second law analysis to study the irreversibility properties within the flow field. Inside the main pipe flow and away from the wall, the fluid friction with magnetic field irreversibility strongly dominates over

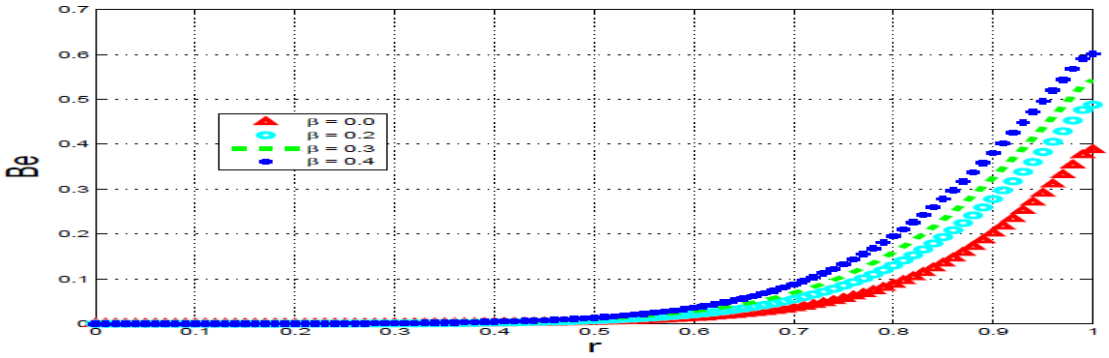

Figure 5.27: Variation of Bejan number with r and β.

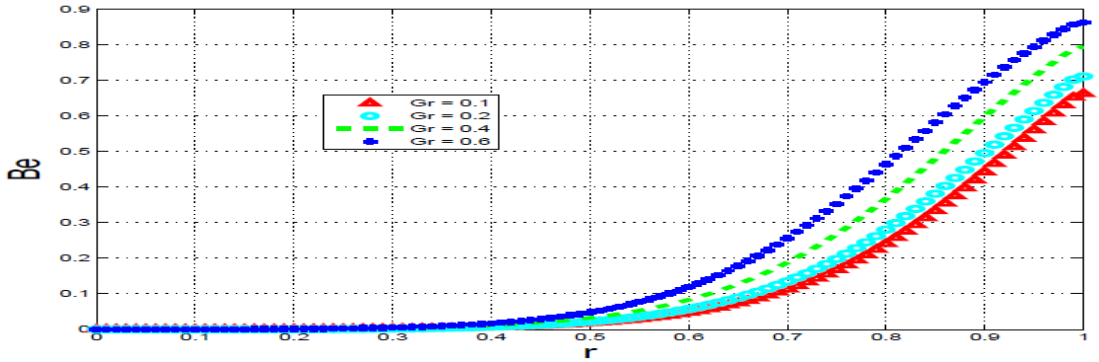

Figure 5.28: Variation of Bejan number with r and Gr.

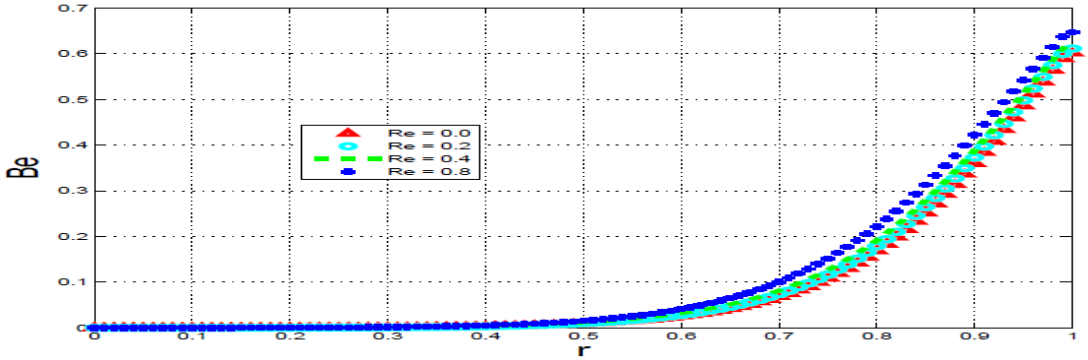

Figure 5.29: Variation of Bejan number with r and Re.

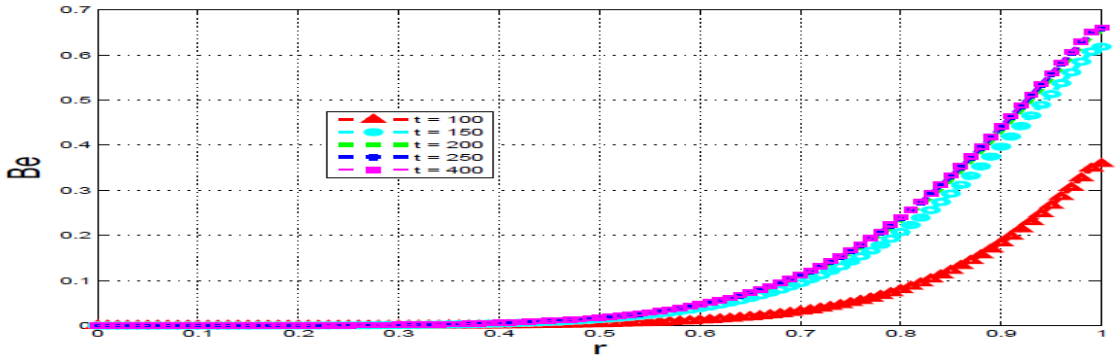

Figure 5.30: Variation of Bejan number with r and t.

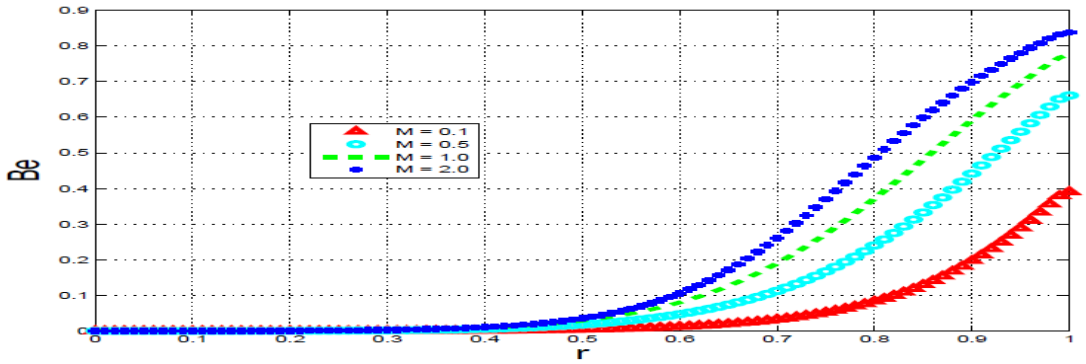

Figure 5.31: Variation of Bejan number with r and M .

heat transfer irreversibility. Close to the wall which is subjected to fluid suction, the strength of the fluid parameters will determine which mode of irreversibility dominates over the other. It is thus possible to choose parameter values so that either heat transfer irreversibility or fluid friction with magnetic field irreversibility dominates in the vicinity of wall.

Chapter 6

Numerical investigation of entropy generation in an unsteady flow through a porous pipe with suction

This chapter investigates the entropy generation rates in an unsteady flow of a variable viscosity incompressible fluid through a porous pipe with uniform suction at the surface. The nonlinear governing equations for momentum and energy balance are derived and solved numerically using a semi-implicit finite difference scheme in order to obtain the fluid velocity and temperature profiles. Numerical results for volumetric entropy generation numbers, irreversibility distribution ratio and the Bejan number are presented graphically and discussed quantitatively for various values of the embedded parameters.

6.1 Introduction

Heat transfer and fluid flow are central to the design and function of a wide spectrum of industrial and engineering systems. In the modern times, the drive has been largely towards the development of industrial and engineering processes that are both cost

effective and environmentally friendly. In this light, the optimization of industrial and engineering systems around issues, say, of minimizing unnecessary energy losses and maximizing performance forms a fundamental area of ongoing importance and research. To this end, the pioneering work of Bejan [7, 9] with respect to entropy generation and minimization deserves special mention. This pioneering work has resulted in a variety of related follow up work by researchers worldwide, see for example the work in [2, 7, 50, 54, 60, 61, 68 − 72, 89, 97, 103, 112]. Each of the cited work looked at either the effect of flow geometry or that of flow properties on entropy generation and a detailed review of the current state of the science in entropy generation is well summarized in recent work [2, 54, 60, 72].

In Ajibade et al [2], it is observed that the literature on suction/injection effects on entropy generation is still quite sparse and thus the investigation in Ajibade et al [2] is dedicated to such suction/injection effects on entropy generation in steady (both Couette and plane Poiseuille) flow. Noting the importance of not only time dependent effects but also of circular pipe geometry in heat transfer and fluid flow systems of industrial and engineering interest, our investigation extends the work in Ajibade et al [2] to the transient regime and relevant cylindrical geometry in which the axi-symmetric assumptions as well as axi-symmetric suction are invoked. In particular most fluid dynamical industrial and engineering designs are such that the flow and heat transfer regimes of interest may take place over short time scales such that observations are recorded before the steady states are achieved, if indeed they are achievable. The work in [33 − 36] for example demonstrate the finite time blow up of solutions for certain reacting flows and hence that steady states may not be achievable for such flows under certain conditions.

In fact, our current chapter together with the work in [33, 34, 36] will no doubt lay the ground work for, among others, future research on the interaction of entropic and energetic effects in the flow of viscoelastic fluids. The current chapter focuses mostly on irreversibility analysis due to entropy generation but, among other work, the investigations in [33, 34, 36] have analyzed reversibility effects due to the energy elastic properties of viscoelastic fluids. The comparative results of Chinyoka [34] in particular demonstrate that entropic heat generation is minimized for viscoelastic fluids via the said energy elastic properties. Similarly, the results of Chinyoka [36] demonstrate the effects of suction/injection on heat transfer characteristics of reacting shear-banded viscoelastic flows.

The objectives of this investigation is to examine the entropy generation rates in an unsteady flow of a variable viscosity incompressible fluid through a porous pipe with uniform suction at the surface. The chapter is organized as follows: the mathematical model of the physical problem is described in section 6.2 leading to the relevant (dimensionless) governing equations. We follow this up in section 6.3 with the development of the mathematical tools to be used in analyzing the entropy generation and irreversibility. The numerical method of solution for the nonlinear set of governing partial differential equations is developed in section 6.4 and then employed in section 6.5 to obtain and discuss the relevant graphical results. Concluding remarks follow in section 6.6.

6.2 Mathematical Model

The configuration of the problem studied in this chapter is depicted in Fig.(6.1) which is an infinite porous cylinder of radius a. The flow is considered to be unsteady in

the $\bar{z}$-direction under the action of uniform suction/injection through pipe walls. The fluid is incompressible and the temperature (T) dependent viscosity ($\bar{\mu}(T)$) can be expressed as:

$$\bar{\mu} = \mu_0 e^{-\gamma(T-T_0)}, \tag{6.1}$$

where μ_0 is the initial fluid dynamic viscosity at the initial temperature T_0 and γ is a viscosity variation parameter which depends on the particular fluid.

Let $(\bar{u}, \bar{v})$ represents velocity in $(\bar{z}, \bar{r})$ direction respectively, τ represent the time, ρ

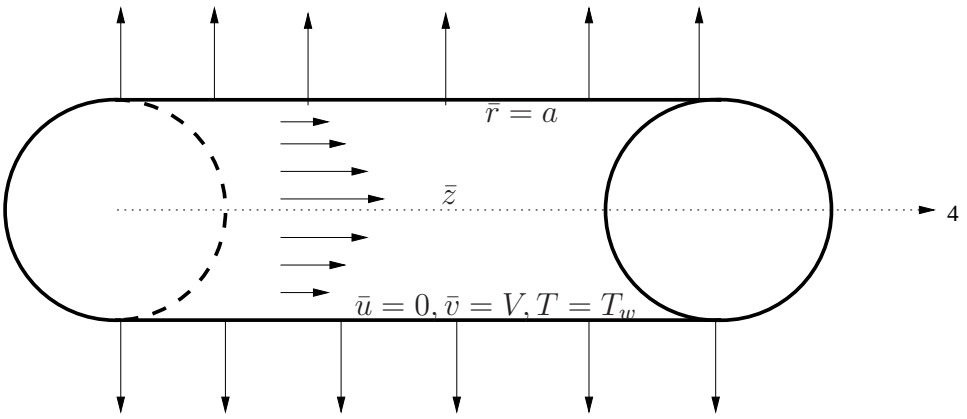

Figure 6.1: Schematic diagram

the fluid density, κ the thermal conductivity, T the fluid temperature, T_w the pipe wall temperature, a the pipe radius, T_0 the fluid initial temperature, V the uniform suction/injection velocity, c_p the specific heat at constant pressure and P the fluid pressure. Under these conditions the continuity, momentum and energy equations governing the problem may be written as in $[54, 60, 61, 69 - 71]$

$$\frac{\partial \bar{u}}{\partial \bar{z}} = 0, \tag{6.2}$$

$$\rho \frac{\partial \bar{u}}{\partial \tau} + \rho V \frac{\partial \bar{u}}{\partial \bar{r}} = -\frac{\partial \bar{P}}{\partial \bar{z}} + \frac{1}{\bar{r}} \frac{\partial}{\partial \bar{r}} \Big(\bar{r} \bar{\mu} \frac{\partial \bar{u}}{\partial \bar{r}} \Big), \tag{6.3}$$

$$\rho c_P \frac{\partial T}{\partial \tau} + \rho c_P V \frac{\partial T}{\partial \bar{r}} = \frac{\kappa}{\bar{r}} \frac{\partial}{\partial \bar{r}} \Big(\bar{r} \frac{\partial T}{\partial \bar{r}} \Big) + \bar{\mu} \Big(\frac{\partial \bar{u}}{\partial \bar{r}} \Big)^2. \tag{6.4}$$

The initial and boundary conditions are given as:

$$\bar{u}(0, \bar{r}) = 0, \quad T(0, \bar{r}) = T_0, \tag{6.5a}$$

$$\frac{\partial \bar{u}}{\partial \bar{r}}(\tau, 0) = 0, \quad \frac{\partial T}{\partial \bar{r}}(\tau, 0) = 0, \quad \bar{u}(\tau, a) = 0, \quad T(\tau, a) = T_w. \tag{6.5b}$$

We introduce the following non-dimensional quantities into Equations (6.2)-(6.5b);

$$r = \frac{\bar{r}}{H}, \quad z = \frac{\bar{z}}{H}, \quad u = \frac{\bar{u}}{V}, \quad \mu = \frac{\bar{\mu}}{\mu_0}, \quad Br = \frac{\mu_0 V^2}{\kappa(T_w - T_0)}, \quad \theta = \frac{(T - T_0)}{(T_w - T_0)}, \quad t = \frac{\tau V}{a},$$
$$p = \frac{a\bar{P}}{\mu_0 V}, \quad v = \frac{\bar{v}}{V}, \quad Re = \frac{\rho V a}{\mu_0}, \quad \beta = \gamma(T_w - T_0), \quad Pr = \frac{\rho c_p V a}{\kappa}. \tag{6.6}$$

We further assume that the flow is driven by a constant and adverse pressure gradient:

$$G = -\frac{\partial p}{\partial z},$$

and obtain the dimensionless governing equations as:

$$Re \Big(\frac{\partial u}{\partial t} + \frac{\partial u}{\partial r} \Big) = G + \frac{1}{r} \frac{\partial}{\partial r} \Big(r e^{-\beta\theta} \frac{\partial u}{\partial r} \Big) \tag{6.7}$$

$$Pr \Big(\frac{\partial \theta}{\partial t} + \frac{\partial \theta}{\partial r} \Big) = \frac{1}{r} \frac{\partial}{\partial r} \Big(r \frac{\partial \theta}{\partial r} \Big) + Br e^{-\beta\theta} \Big(\frac{\partial u}{\partial r} \Big)^2 \tag{6.8}$$

with the corresponding initial and boundary conditions;

$$u(0, r) = 0, \quad \theta(0, r) = 0, \tag{6.9a}$$

$$\frac{\partial u}{\partial r}(t, 0) = 0, \quad \frac{\partial \theta}{\partial r}(t, 0) = 0, \quad u(t, 1) = 0, \quad \theta(t, 1) = 0, \quad \text{for} \quad t > 0 \tag{6.9b}$$

where β is the viscosity variation parameter, Br is the Brinkman number, Re is the suction/injection Reynolds number and Pr is the Prandtl number. Other quantities

of interest in this study include the wall shear stress ι_w and the heat transfer rate at the pipe surface q_w given as:

$$\iota_w = -\bar{\mu}\frac{\partial \bar{u}}{\partial \bar{r}}\Big|_{\bar{r}=a}, \quad q_w = -\frac{\partial T}{\partial \bar{r}}\Big|_{\bar{r}=a}. \tag{6.10}$$

The dimensionless wall shear stress C_f and dimensionless heat transfer rate N_u are defined as;

$$C_f = \frac{\iota_w a}{\mu_0 V} = -e^{-\beta\theta}\frac{\partial u}{\partial r}\Big|_{r=1}, \quad N_u = \frac{q_w a}{\kappa(T_w - T_0)} = -\frac{\partial \theta}{\partial r}\Big|_{r=1}. \tag{6.11}$$

6.3 Irreversibility Analysis

Entropy generation related to the unsteady flow and heat transfer in a porous pipe with suction/injection is considered. In engineering design problems, the determination of the entropy generation rate in the system is extremely important in order to optimize energy in the system for efficient operation of the system. The general equation for the entropy generation per unit volume is given by [7, 9, 89];

$$S^m = \frac{\kappa}{T_w^2}(\nabla T)^2 + \frac{\bar{\mu}}{T_w}\Psi. \tag{6.12}$$

The first term in Equation (6.12) is the irreversibility due to heat transfer and the second term is the entropy generation due to viscous dissipation. Using Equation (6.6), we express the entropy generation number in dimensionless form as,

$$N_S = \frac{a^2 T_w^2 S^m}{\kappa(T_w - T_0)^2} = \Big(\frac{\partial \theta}{\partial r}\Big)^2 + \frac{Bre^{-\beta\theta}}{\Omega}\Big(\frac{\partial u}{\partial r}\Big)^2, \tag{6.13}$$

where $\Omega = (T_w T_0)/T_0$ is the temperature difference parameter. In Equation (6.13), the first term can be assigned as N_1 and the second term due to viscous dissipation as N_2 , i.e.

$$N_1 = \Big(\frac{\partial \theta}{\partial r}\Big)^2, \quad N_2 = \frac{Bre^{-\beta\theta}}{\Omega}\Big(\frac{\partial u}{\partial r}\Big)^2. \tag{6.14}$$

Following Bejan [9], the irreversibility distribution ratio is defined as $\phi = N_2/N_1$. Heat transfer dominates for $0 \leq \phi < 1$ and fluid friction dominates when $\phi > 1$. The contribution of both heat transfer and fluid friction to entropy generation are equal when $\phi = 1$. Alternatively, the dominant effect of either heat transfer irreversibility or fluid friction irreversibility can be investigated using the Bejan number (Be) define mathematically as

$$Be = \frac{N_1}{N_S} = \frac{1}{1+\phi}. \tag{6.15}$$

Clearly, the Bejan number ranges from 0 to 1. $Be = 0$ is the limit where the fluid friction irreversibility dominates and $Be = 1$ corresponds to the limit where the heat transfer irreversibility dominates. The contribution of both heat transfer and fluid friction to entropy generation are equal when $Be = 1/2$.

In section 6.4, Equations (6.7)-(6.15) are solved numerically using a semi-implicit finite difference scheme.

6.4 Numerical Procedure

Our numerical algorithm is based on the semi-implicit finite difference scheme and is implemented along the same lines as in, say, [33−36]. In this section, it will be understood that subscript r denotes partial differentiation under the given finite difference framework, the subscript j will represent the mesh position and the superscripts N and $N+1$ will denote current and future time levels.

Implicit terms are taken at the intermediate time level $(N+\xi)$ where $0 \leq \xi \leq 1$ and, for example,

$$\theta^{(N+\xi)} = \xi\theta^{(N+1)} + (1-\xi)\theta^{(N)}.$$

The discretization of the governing equations is based on a linear Cartesian mesh and uniform grid on which finite-differences are taken. We approximate both the second and first spatial derivatives with second-order central differences, for example,

$$\theta_r = \frac{\theta_{j+1} - \theta_{j-1}}{2\Delta r}, \theta_{rr} = \frac{\theta_{j+1} - 2\theta_j + \theta_{j-1}}{\Delta r^2}.$$

The time derivatives are approximated via first-order forward difference formulas, for example,

$$\frac{\partial \theta}{\partial t} = \frac{\theta^{(N+1)} - \theta^{(N)}}{\Delta t}.$$

As with standard finite difference methods, the equations corresponding to the first and last grid points are modified to incorporate the boundary conditions. The semi-implicit scheme for the velocity component reads:

$$Re\frac{\partial u_j}{\partial t} + Reu_r^{(N)} = G + e^{(-\beta\theta_j^{(N)})}u_{rr}^{(N+\xi)} + e^{(-\beta\theta_j^{(N)})}\theta_j^{(N)}u_r^{(N)} + \frac{1}{r}e^{(-\beta\theta_j^{(N)})}u_r^{(N)}. \quad (6.16)$$

Since the unsteady problem under investigation is posed as an initial value problem, given a solution at a time level (N), i.e. $[u^{(N)}, \theta^{(N)}]$, the objective is to obtain the velocity and temperature fields at the subsequent time level $(N+1)$. By replacing the continuous partial derivatives in Equation (6.16) with the relevant finite difference formulas given earlier, the equation for the velocity filed reduces to the following linear system of algebraic equations:

$$-r_1 u_{j-1}^{(N+1)} + (Re + 2r_1)u_j^{(N+1)} - r_1 u_{j+1}^{(N+1)} = \text{explicit terms}, \quad (6.17)$$

where the explicit terms contain terms prescribed at the earlier time level (N) and;

$$r_1 = \xi\frac{\Delta t}{\Delta r^2}e^{(-\beta\theta_j^{(N)})}.$$

The solution procedure for $u^{(N+1)}$ thus reduces to inversion of tri-diagonal matrices which is an advantage over a full implicit scheme. The semi-implicit integration scheme for the energy equation is similar to that for the velocity:

$$Pr\frac{\partial\theta_j}{\partial t} + Pr\theta_r^{(N)} = \theta_{rr}^{(N+\xi)} + \frac{1}{r}\theta_r^{(N)} + Bre^{(-\beta\theta^{(N)})_j}(u_r^{(N)})^2. \tag{6.18}$$

On replacing the continuous partial derivatives in Equation (6.18) with the relevant finite difference formulas given earlier, the equation for $\theta(N+1)$ thus reduces to the following linear system of algebraic equations:

$$-r\theta_{j-1}^{(N+1)} + (Pr+2r)\theta_j^{(N+1)} - r\theta_{j+1}^{(N+1)} = \text{explicit terms}, \tag{6.19}$$

where $r = \xi\Delta t/\Delta r^2$. The solution procedure again reduces to inversion of tri-diagonal matrices. The schemes (6.17) and (6.19) were checked for consistency. For$\xi = 1$, these are first-order accurate in time but second order in space. The schemes in [33] have $\xi = 1/2$ which improves the accuracy in time to second order. We use $\xi = 1$ here so that we are free to choose larger time steps.

6.5 Results and Discussion

Unless otherwise stated, we employ the parameter values: $G = 1$, $\beta = 0.5$, $Br = 1$, $Pr = 7.1$, $Re = 1$, $\Delta r = 0.01$, $\Delta t = 0.5$ and $t = 500$.

These will be the default values in this work and hence in any graph where any of these parameters is not explicitly mentioned, it will be understood that such parameters take on the default values.

6.5.1 Transient and steady flow profiles

We display the transient solutions in Figs.(6.2) and (6.3). Both figures show a transient increase in fluid quantities (velocity and temperature) until a steady state is reached.

We draw attention to the apparent change in concavity of the steady state velocity profiles close to the pipe wall, see Fig.(6.2). This change in concavity is due to the suction at the wall and will lead to some counter intuitive effects on the wall shear stress as will be demonstrated later.

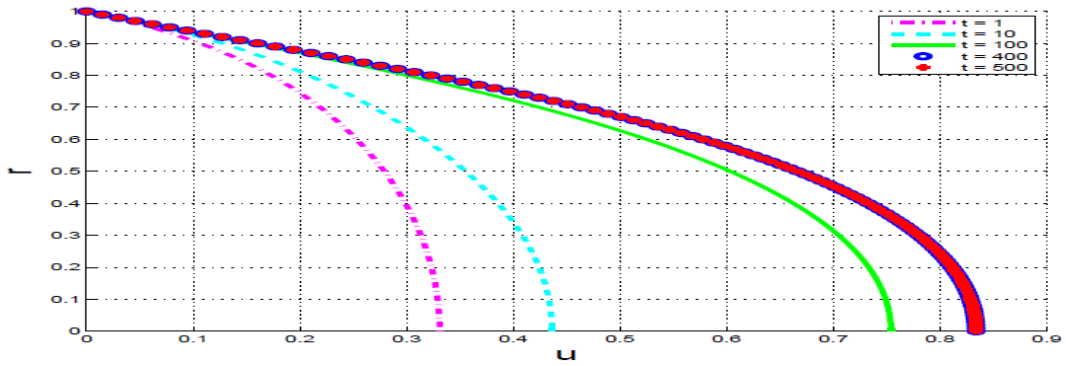

Figure 6.2: Transient and steady state velocity profiles.

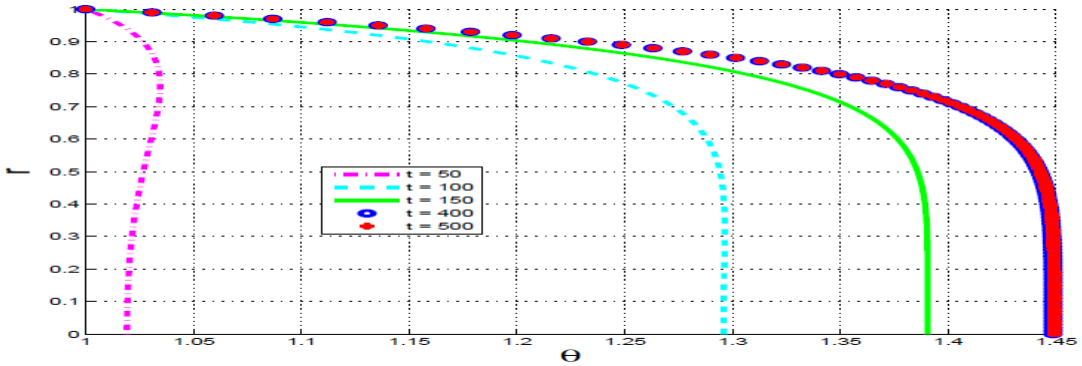

Figure 6.3: Transient and steady state temperature profiles.

6.5.1.1 Parameter dependence of solutions

In this section, we investigate the response of the velocity and temperature (at steady state) to varying values of the embedded parameters. The response of the velocity and temperature to variations in the viscosity parameter β is illustrated in Figs.(6.4) and (6.5) respectively.

An increase in the viscosity parameter corresponds to a decrease in fluid viscosity and hence a reduce resistance to flow. This in turn leads to increased fluid velocity within the bulk flow as illustrated in Fig.(6.4). The increased fluid velocity in turn increases the magnitude of the viscous heating sources terms in the energy equations and hence leads to increased fluid temperatures as illustrated in Fig. 6.5.

The response of the velocity and temperature to variations in the Brinkman number (Br) is illustrated in Figs.(6.6) and (6.7) respectively. As previously explained,

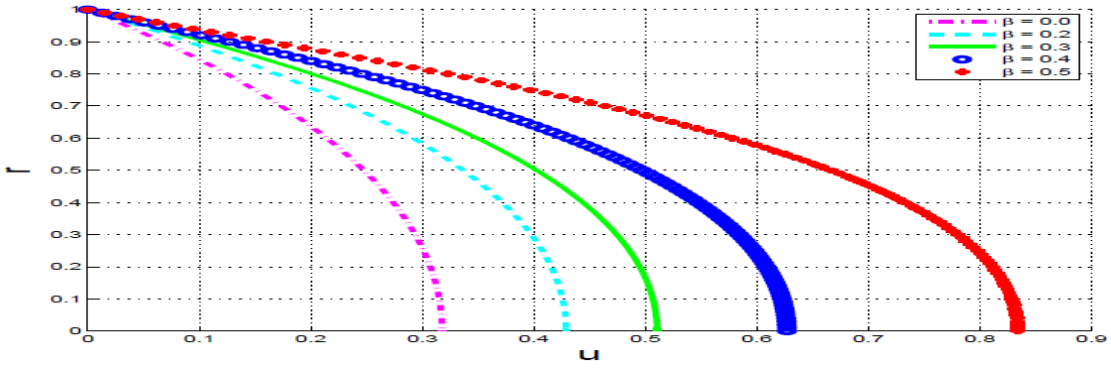

Figure 6.4: Effects of viscosity parameter (β) on steady state velocity.

the increased strength of the viscous heating source terms (due to increases in the Brinkman number) is directly responsible for the significant increase in fluid temperature shown Fig.(6.7). The temperature is coupled to the velocity through the temperature dependent viscosity. The fluid viscosity decreases significantly in re-

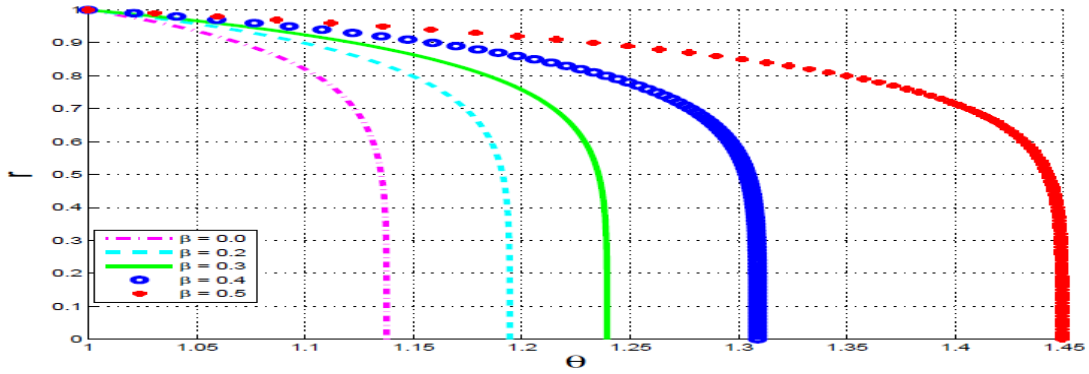

Figure 6.5: Effects of viscosity parameter (β) on steady state temperature.

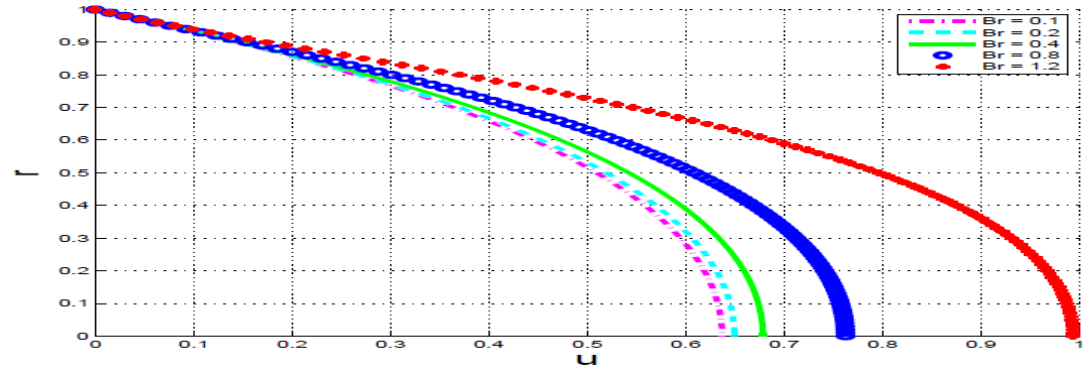

Figure 6.6: Effects of Brinkman number (Br) on steady state velocity.

sponse to the large increases in fluid temperature (due to increases in the Brinkman number). The decreased viscosity is ultimately responsible for the increased fluid velocity with increased Brinkman number shown in Fig.(6.6).

The suction Reynolds number primarily represents the strength of the suction through the walls but may also be thought of as a measure of the friction between the fluid molecules. Thus $Re = 0$ may represent, not only, the case of (steady) Hagen-Poiseuille flow in a pipe with impermeable walls but may also indicate a densely packed fluid in which viscosity between fluid particles is very high. Similarly, $Re > 0$ would represent

flow with uniform suction and hence a loosely packed fluid with diminished viscosity between fluid particles. Figs.(6.8) and (6.9) respectively show the response of the fluid velocity and temperature to variations in the suction Reynolds number. The reduced viscosity between fluid molecules with increased Re leads to corresponding increases in the fluid velocity as shown in Fig.(6.8). As explained before, the nature of the coupling of the velocity to the source terms in the energy equation leads to corresponding increases in fluid temperature with increased suction Reynolds numbers (i.e. with increased fluid velocity strength) as shown in Fig.(6.9).

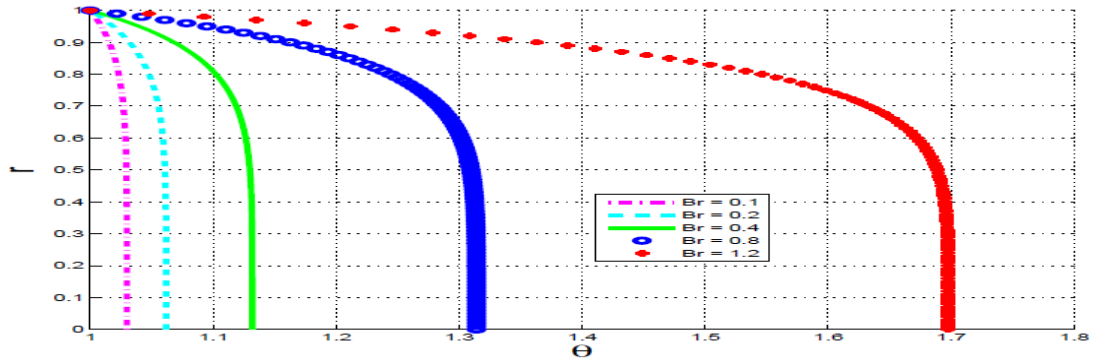

Figure 6.7: Effects of Brinkman number (Br) on steady state temperature.

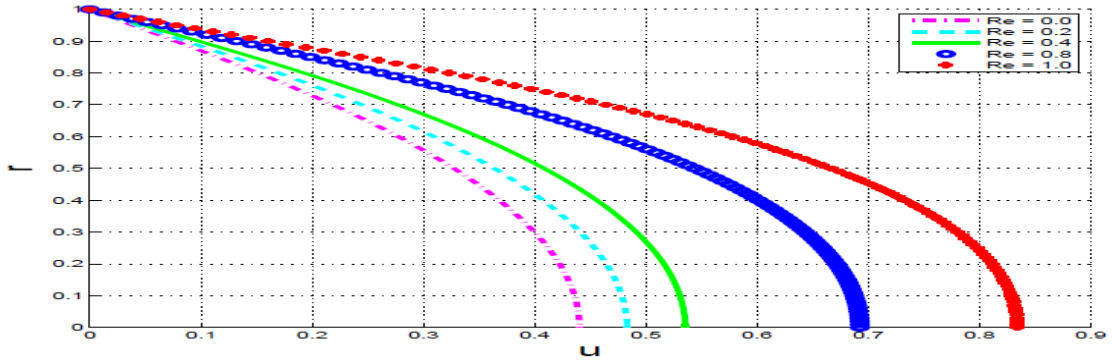

Figure 6.8: Effects of the suction Reynolds number (Re) on steady state velocity.

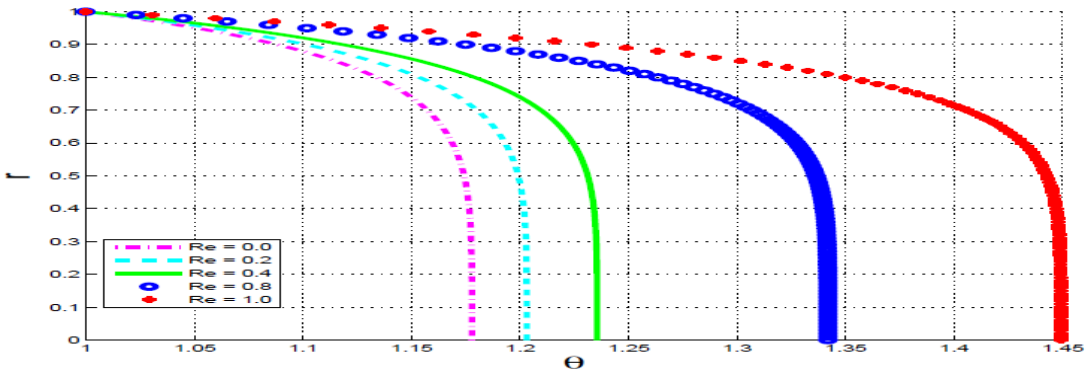

Figure 6.9: Effects of the suction Reynolds number (Re) on steady state temperature.

6.5.2 Skin friction

The wall shear stress dependence on β is illustrated in Fig.(6.10) for varying values of the Brinkman number Br. Similarly, the wall shear stress dependence on Re is illustrated in Fig.(6.11) at different times.

Keeping in mind the results of the previous section, on parameter dependence of solutions, the results shown in Figs.(6.10) and (6.11) may at first glance seem counter intuitive. In particular, we would expect that parameters that decrease (increase) the fluid velocity correspondingly decrease (increase) the wall shear stress respectively. However, this will usually hold if the velocity profiles have uniform concavities in which case the decrease (increase) of the bulk flow velocity would correspondingly decrease (respectively increase) velocity gradients at the wall. The change in concavity of the velocity profiles close to the wall thus explains the decrease in wall shear stress with increases in either Br or time shown in Figs. (6.10) and (6.11).

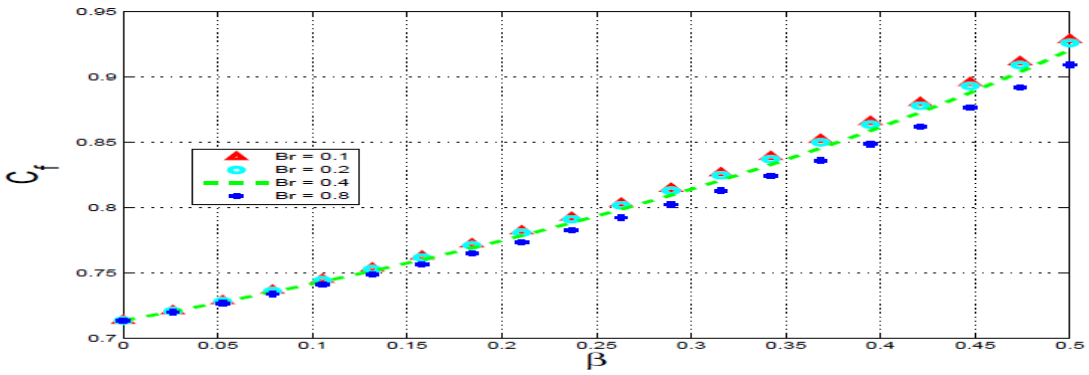

Figure 6.10: Variation of wall shear stress with β and Br.

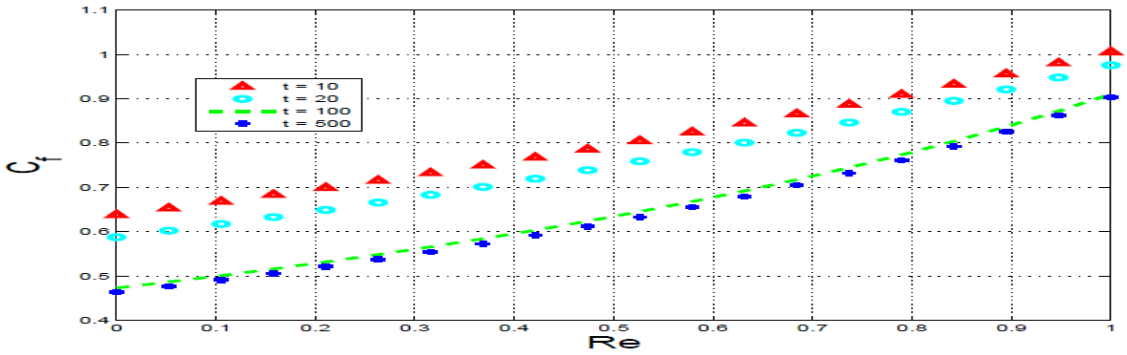

Figure 6.11: Variation of wall shear stress with Re and t.

6.5.3 Wall heat transfer

The wall heat transfer rate dependence on β is illustrated in Fig.(6.12) for varying values of the Brinkman number Br. Similarly, the wall heat transfer rate dependence on Re is illustrated in Fig.(6.13) at different times. As expected, parameters that decrease (increase) the bulk fluid temperature correspondingly decrease (increase) the wall heat transfer rate respectively. The negative values in Fig. 13 at the earlier times simply indicate that we have captured the developing temperature profiles close to the initial stages when the maximum temperature still obtains at the walls.

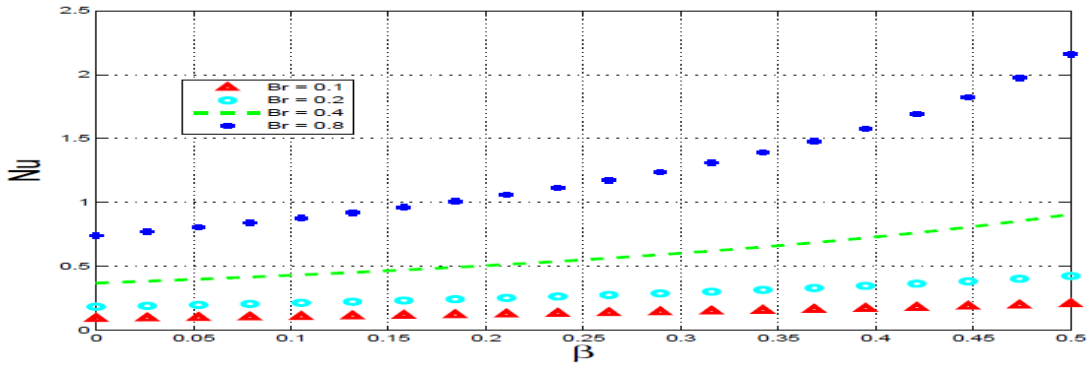

Figure 6.12: Variation of wall heat transfer rate with β and Br.

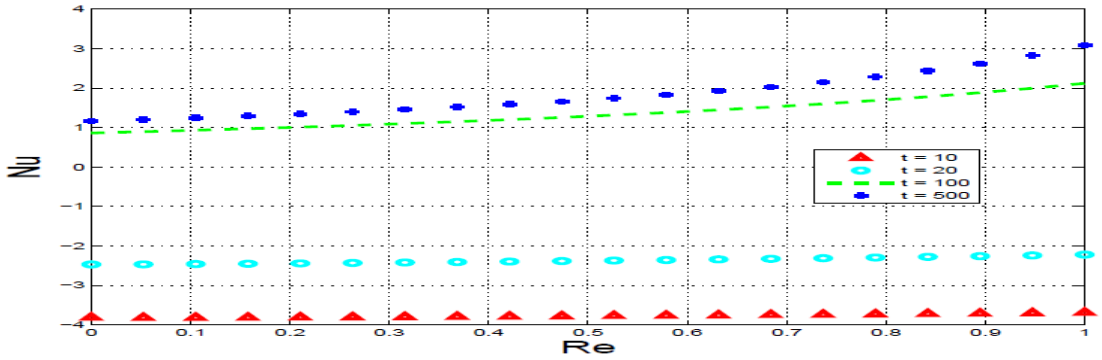

Figure 6.13: Variation of wall heat transfer rate with Re and t.

6.5.4 Entropy generation

In this section, we plot the entropy generation rate (N_s) across the pipe under varying parameter conditions. Figs. 6.14 show the expected increase in Ns with corresponding increases in $Br\Omega^{-1}$. This follows from the realization that increases in $Br\Omega^{-1}$ correspondingly increase the fluid friction contribution to the entropy generation. Similarly Figs. (6.15) and (6.16) show that at higher β or Re values, the increased fluid velocity (see Figs. (6.4) and (6.8)) and hence increased velocity gradients (see Figs.6.10 and 6.11) each leads to overall increases in the magnitudes of N_2 and hence the observed

increase in entropy generation rates. In Figs. (6.14), (6.15) and (6.16), the entropy generation rate is expectedly maximum at the walls where velocity and temperature gradients as well as fluid viscosity are highest and minimum at the centerline where these quantities are at their minimum. As soon as a time, t_{min} , is reached at which

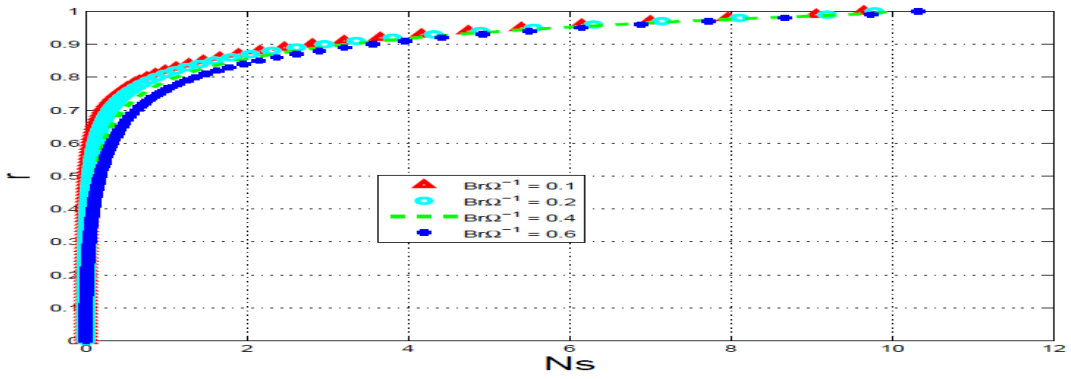

Figure 6.14: Variation of entropy generation rate with r and $Br\Omega^{-1}$.

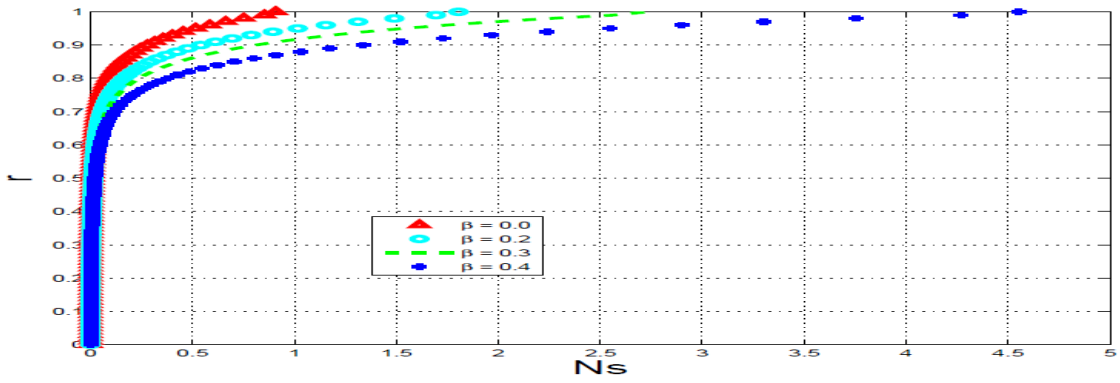

Figure 6.15: Variation of entropy generation rate with r and β.

the temperature gradient at the wall becomes negative, the entropy generation rate N_S will increase with increasing time as shown in Fig.(6.17). As with Figs.(6.14), (6.15) and (6.16), this is due to the significantly increased temperature gradients as time increases beyond t_{min}, see Fig.(6.13). In Fig.(6.17), we have included a time

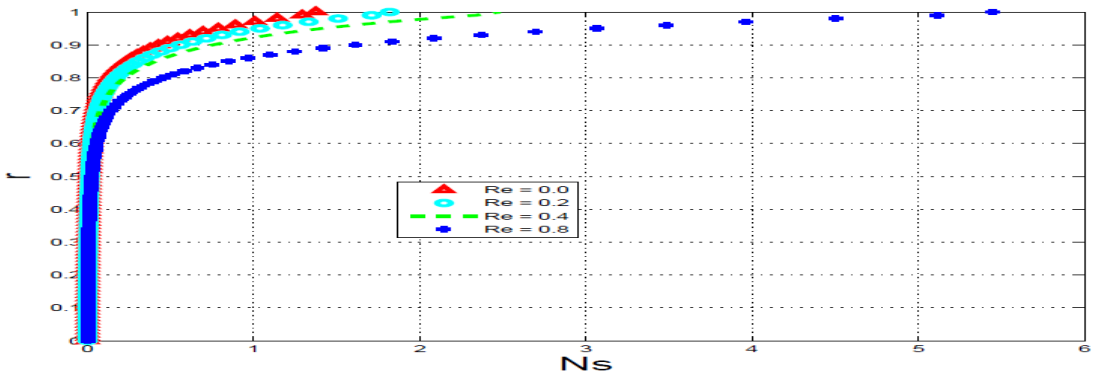

Figure 6.16: Variation of entropy generation rate with r and Re.

$t = 10 < t_{min}$ which is close to the initial condition and hence at which time we have very large temperature gradients and hence the correspondingly large values of the entropy generation rates.

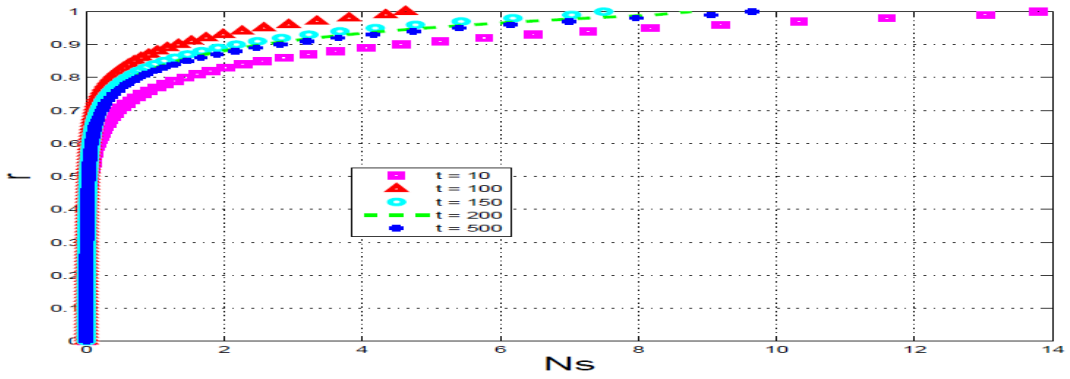

Figure 6.17: Variation of entropy generation rate with r and t.

6.5.5 Bejan number

In this section, we plot the Bejan number (Be) across the pipe under varying parameter conditions. The analysis in this section is similar to that for the previous section with N_S now replaced by Be.

Fig. (6.18), shows as expected that higher values of $Br\Omega^{-1}$, which increase the

magnitude of fluid friction irreversibility (N_2) but has no effect on the heat transfer irreversibility (N_1), increases the values of ϕ leading to lower Bejan numbers. Similar conclusions are inferred from Fig. (6.19) in which the increase in β reduces the magnitude of N_2 (with N_1 unaffected) and hence also of ϕ thus giving correspondingly higher Bejan numbers.

As with Fig. (6.19), a decrease in ϕ with either an increase in Re or an increase in

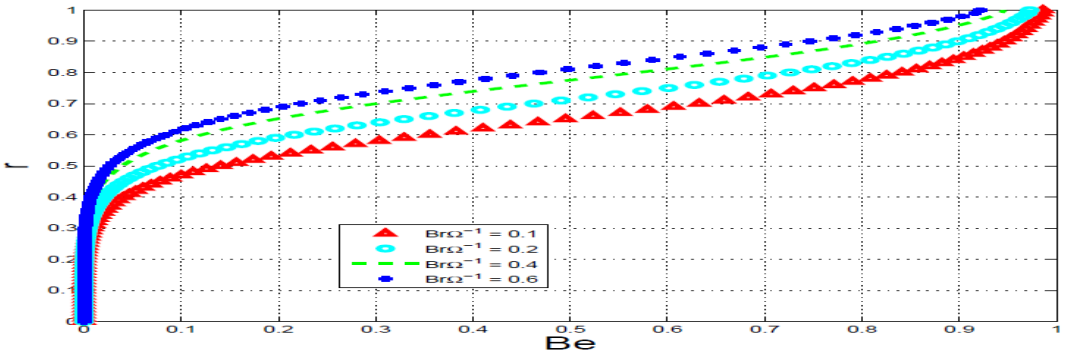

Figure 6.18: Variation of Bejan number with r and $Br\Omega^{-1}$.

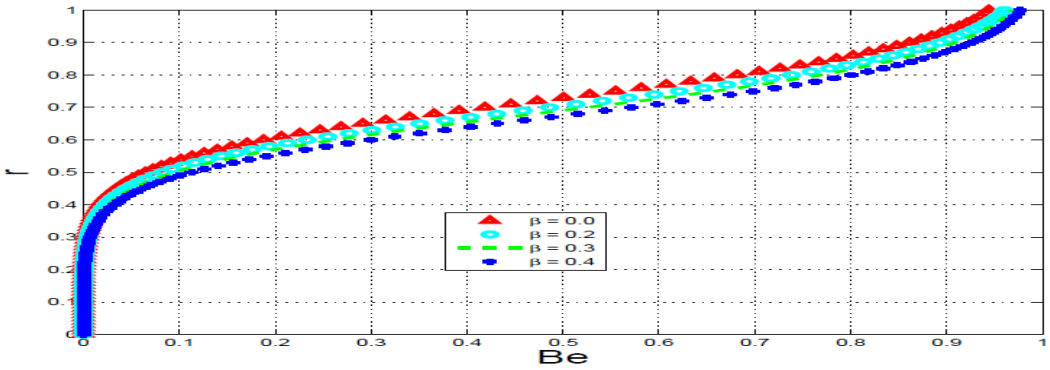

Figure 6.19: Variation of Bejan number with r and β.

time (beyond t_{min}) is illustrated in Figs.(6.20) and (6.21). This increase in ϕ is due to the much larger increases in temperature (and temperature gradients) as compared

to the velocity (and velocity gradients) as either Re or t increases. The result, as shown in Figs. (6.20) and (6.21), is thus an increase in the Bejan number as either Re or t increases.

Figs.(6.18)- (6.21) all indicate that fluid friction irreversibility dominates close to the pipe centerline. The temperature profiles exhibit are quite blunt around the centerline and hence there exists a significant radius around the centerline where the temperature gradients are zero or very nearly so. This is in contrast to the much sharper velocity fronts and hence the significantly larger velocity gradients around the same regions and hence the dominance of N_2 over N_1 . Figs.(6.18)-(6.21) also all indicate that heat transfer irreversibility dominates in the vicinity of the walls. This is due to the significantly larger temperature gradients (as compared to the velocity gradients) close to the walls. Inside the main flow, Figs. (6.18)-(6.21) show an interplay of both modes of irreversibility and also that fluid parameters may be chosen so as to enhance (or reduce) the dominance of any of the two forms of irreversibility.

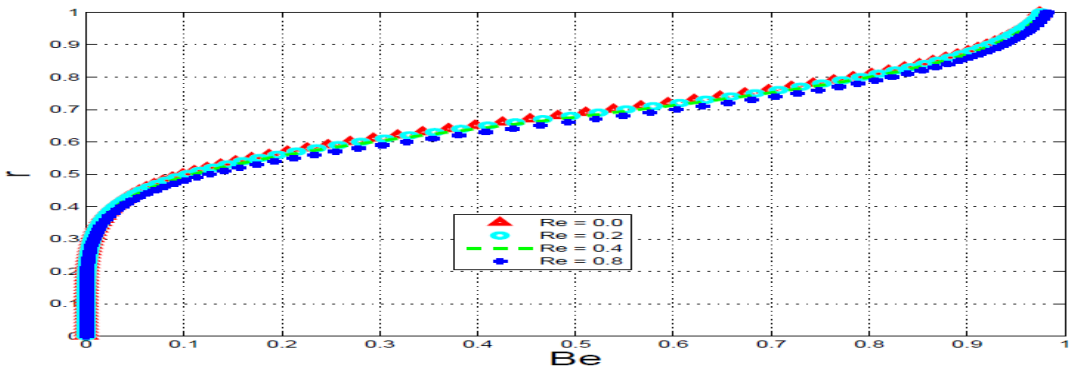

Figure 6.20: Variation of Bejan number with r and Re.

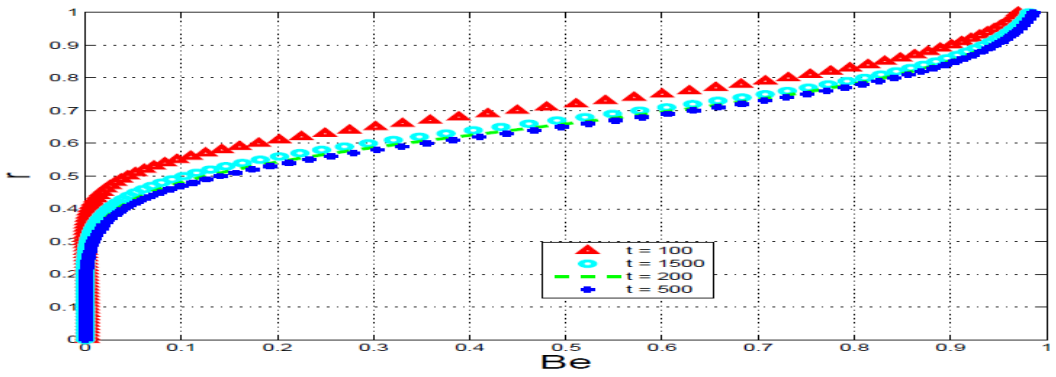

Figure 6.21: Variation of Bejan number with r and t.

6.6 Conclusion

We, numerically, investigate the transient pressure driven pipe flow of a fluid in the presence of uniform suction at the walls and employ second law analysis to study the irreversibility properties within the flow field. The suction at the walls lead to velocity profiles of non-uniform concavity in the wall region. In the regions of maximum velocity, heat transfer irreversibility dominates and fluid friction irreversibility is relatively insignificant. Fluid friction irreversibility dominates close to the pipe centerline and heat transfer irreversibility dominates in the vicinity of the walls. Away from the pipe walls (and inside the main flow) fluid parameters may be chosen so as to enhance (or reduce) the dominance of either heat transfer or fluid friction irreversibility. In particular, the following parameters can (depending on their magnitude) enhance or reduce the dominance of either heat transfer or fluid friction irreversibility, these are the (i) Brinkman number, Br, (ii) viscosity variation parameter, β, (iii) Reynolds number, Re and the (iv) time, t.

Chapter 7

CONCLUDING REMARKS

In this thesis, we considered the theoretical analysis of laminar flow, thermal stability and entropy generation in a porous channel and porous pipe. we investigated in chapter 3 the combined effects of suction/injection and asymmetric Navier slip on the entropy generation rate in a steady flow of an incompresible viscous fluid through a porous channel subjected to a non-uniform temperature at the walls. We solved the problems using both numerical and analytical methods. The velocity results were compared as shown in table 3.1 . The effect of some of the parameter were tested and our results revealed flow reversal at the channel upper wall as a result of suction. Heat transfer irreversibility dominated the centreline of the flow channel and fluid friction irreversibility were observed at the channel walls. Heat transfer irreversibility dominated lower wall and fluid friction irreversibility dominated upper wall as the values of asymmetric slip parameters were increased.

In chapter 4, combined effect of buoyancy force and Navier slip on entropy generation in a vertical porous channel with suction/injection walls was carried out. We solved numerically using Runge-Kutta-Ferhlberg method with shooting technique. Velocity and temperature profile were obtained which we used to compute entropy generation

and Bejan number. Our results revealed that bouyancy force had effect on entropy generation rates at both walls but the increase were more pronounced at suction wall than injection wall. We also observed opposite effect on the entropy generation rate on the walls as slip parameter β_1 increases but same effect on entropy generation rate as β_2 increases or decreases.

In chapter 5, we carried out entropy analysis of MHD unsteady flow through a porous pipe with buoyancy effects. We analysed the first and second law of thermodynamic with respect to inherent irreversibility in an unsteady flow of a viscous in compressible conducting fluid through a uniformly porous pipe subjected to constant fluid suction at the isothermal walls and transverse imposed magnetic field. Under axisymmetric assumption, we obtained in cylindrical coordinate the nonlinear governing equations and solve numerically using semi-implicit finite difference technique to obtain solution for fluid velocity and temperature profile. Our results reveal that inside the cyclidrical pipe flow and away from the suction wall, magnetic fields irreversibility with fluid friction strongly dominates over heat transfer irreversibility. Also increase in viscosity parameter reduces resistance to fluid flow and increase fluid velocity. Furthermore, increase in Buoyancy effect (Gr) and heat sources (Br), increase both velocity and temperature profiles of the fluid.

In chapter 6, we investigated numerically the entropy generation rate in an unsteady flow of a variable voscosity incompressible fluid through a porous pipe with uniform suction at the surface. The nonlinear equations were solved numerically using semi-implicit finite difference sheme to obtain fluid velocity and temperature profile. We used these to compute the entropy generation and Bejan number. Our results reveal that at maximum velocity, heat transfer irreversibility dominates and fluid friction

irreversibility is relatively insignificant. Close to the pipe centreline, fluid friction irreeversibility dominates and heat transfer irreversibility dominates in the vicinity of the walls.

7.1 Further work

For future work, one can look at the interaction of entropic and energetic effects on the flow of viscoelastic fluid.

Appendix

Articles already published or submitted for publication

(1) **A. S. Eegunjobi, O. D. Makinde: Combined Effect of Buoyancy Force and Navier Slip on Entropy Generation in a Vertical Porous Channel. *Entropy*, 14, 1028-1044, (2012) (Published)**

(2) **A. S. Eegunjobi, O. D. Makinde: Effects of Navier Slip on Entropy Generation in a Porous Channel with Suction/Injection. *Journal of Thermal Science and Technology*,Vol. 7, No. 4, 522-535, (2012). (Published)**

(3) **O. D. Makinde, T. Chinyoka, A. S. Eegunjobi: Numerical investigation of entropy generation in an unsteady flow through a porous pipe with suction. *International Journal of Exergy*- Accepted and in press 2012.**

(4) **T. Chinyoka, O. D. Makinde, A. S. Eegunjobi: Entropy analysis of MHD unsteady flow through a porous pipe with buoyancy effects. *Journal of porous media*-Submitted 2012.**

Bibliography

[1] T. Alboussiere, J. P. Garandet, R. Moreau: Buoyancy-driven convection with a uniform magnetic field, Part 1: Asymptotic analysis. *J. Fluid Mech*, Vol.253, 545-563, (1983).

[2] A. O. Ajibade, B. K. Jha, A. Omame: Entropy Generation under the effect of suction/injection. *Applied Mathematical Modelling*, 35, 4630-4046, (2011)

[3] V. S. Arpaci, A. Selamet, S. H. Kao: *Introduction to heat transfer*. Prentice-Hall, New York, (2000).

[4] M. M. Awartani, M. H. Hamdan: Fully developed flow through a porous channel bounded by flat plates. *Applied Mathematics and Computation*, 169, 749757,(2005).

[5] O. Aydin, W. J. Yang: Natural convection in enclosures with localized heating from below and symmetrical cooling from sides. *International Journal of Numerical Methods for Heat and Fluid Flow*, 10, pp. 519529, (2000).

[6] A. Bejan: Second-Law analysis in heat transfer and thermal design. *Adv. Heat Transfer*, Vol.15, pp1-58, (1982).

[7] A. Bejan: *Entropy generation minimization*. CRC Press: New York, NY, USA, (1996).

[8] A. S. Berman: Laminar flow in channels with porous walls. *J. Appl. Phys*, 24, 1232-1235, (1953).

[9] A. Bejan: *Convection Heat Transfer*. John Wiley and Sons, New York, NY, USA, (1984).

[10] A. Bejan: A study of entropy generation in fundamental convective heat transfer. *J. Heat Transfer*, Vol. 101, 718-725, (1979).

[11] A. Bejan: *Entropy Generation Through Heat and Fluid Flow*. (Canada: Wiley) chapter 5, p98, (1994).

[12] M. Berh: On the Application of Slip Boundary Condition on Curve Boundaries. *Int.J. for Numerical Methods in fluid*, 45, 43-51, (2004).

[13] R. Buckingham, M. Shearer, A. Bertozzi: Thin Film Travelling Waves and the Navier Slip Condition. SIAM *J. Appl Maths*, vol 63, No2 pp722-744, (2003).

[14] J. F. Brady: Flow development in a porous channel and tube. *Phys. Fluids*, 27, 1061-1067, (1984).

[15] L. Buhler: Laminar buoyant magnetohydrodynamic flow in a vertical rectangular ducts. *Phys. Fluids*, Vol. 10, 223-236, (1998).

[16] N. M. Bujurke, V. S. Madalli, B. G. Mulimani: Long series analysis of laminar flow through parallel and uniformly porous walls of different permeability. *Comput. Methods Appl. Mech. Engrg.*, 160, 39-56, (1998).

[17] D. S. Chauhan, V. Kumar: Effect of Slip condition on forced convection and entropy generation in a circular channel occupied by highly porous medium: Darcy extended Brinkmann-Forchheimer model. *Turkish J. Eng. Env. Sci.*, 33, 91-104, (2009).

[18] D. S. Chauhan, A. Olkha: Entropy generation and heat transfer effects on non-Newtonian fluid flow in annular pipe with natural permeable boundaries. *Int. J. Energ. Tech.*, 3, 1-19, (2011).

[19] D. S. Chauhan, V. Kumar: Heat transfer and entropy generation during compressible fluid flow in a channel partially filled with porous medium. *Int. J. Energ. Tech.*, 3, 1-10, (2011).

[20] D. S.Chauhan, P. Rastogi: Heat transfer and entropy generation in MHD flow through a porous medium past a stretching sheet. *Int. J. Energ. Tech.*, 3, 1-13, (2011).

[21] S. Chen, Z. Tian: Entropy generation analysis of thermal micro-Couette flows in slip regime. *Int. J. Therm. Sci.*, 49, 2211-2221, (2010).

[22] S. Chen, J. Tolke, M. Krafczyk: Numerical investigation of double-diffusive (natural) convection in vertical annuluses with opposing temperature and concentration gradients.*Int. J. Heat Fluid Flow*, 31, 217-226, (2010).

[23] S. Chen, R. Du: Entropy generation of turbulent double-diffusive natural convection in a rectangle cavity. *Energy*, 36, 1721-1734, (2011).

[24] S. Chen: Entropy generation of double-diffusive convection in the presence of rotation. *Appl. Math. Comput.*, 217, 8575-8597, (2011).

[25] S. Chen, J. Li, H. Han, Z. Liu, Z. Zheng: Effects of hydrogen addition on entropy generation in ultra-lean counter-flow methane-air premixed combustion. *Int. J. Hydrogen Energ.*, 35, 3891-3902, (2010).

[26] S. Chen, J. Mi, H. Liu, C. Zheng: First and second thermodynamic-law analyses of hydrogen-air counter-flow diffusion combustion in various combustion modes. *Int. J. Hydrogen Energ.*, 37, 5234-5245, (2012).

[27] S. Chen, C. Zheng: Entropy generation in impinging flow confined by planar opposing jets. *Int. J. Therm. Sci.*, 49, 20672075, (2010).

[28] S. Chen, Z. Liu, J. Liu, J. Li, L. Wang, C. Zhen: Analysis of entropy generation in hydrogenenriched ultra-lean counter-flow methane-air non-premixed combustion. *Int. J. Hydrogen Energ.*, 35, 12491-12501, (2010).

[29] S. Chen, H. Han, Z. Liu, J. Li, C. Zheng: Analysis of entropy generation in non-premixed hydrogen versus heated air counter-flow combustion. *Int. J. Hydrogen Energ.*, 35, 4736-4746, (2010).

[30] S. Chen: Analysis of entropy generation in counter-flow premixed hydrogen-air combustion. *Int. J. Hydrogen Energ.*, 35, 1401-1411, (2010).

[31] S. Chen: Entropy generation inside disk driven rotating convectional flow. *Int. J. Therm. Sci.*,50, 626-638, (2011).

[32] S. Chen, Z. Liu, S. Bao, C. Zheng: Natural convection and entropy generation in a vertically concentric. *Int. J. Therm. Sci.*, 49, 2439-2452, (2010).

[33] T. Chinyoka: Computational dynamics of a thermally decomposable viscoelastic lubricant under shear. Transactions of ASME, *J. Fluids Engineering*, Vol. 130(12), 121201(7pages), (2008).

[34] T. Chinyoka: Poiseuille flow of reactive Phan-Thien-Tanner liquids in 1D channel flow. Transactions of ASME, *J. Heat Transfer*, Vol. 132(11), 111701(7pages), (2010).

[35] T. Chinyoka, O. D. Makinde: Computational dynamics of unsteady flow of a variable viscosity reactive fluid in a porous pipe. *Mechanics Research Communications*, Vol. 37, 347-353, (2010).

[36] T. Chinyoka: Suction-injection control of shear banding in non-isothermal and exothermic channel flow of Johnson-Segalman liquids. Transactions of ASME, *J. Fluids Engineering*, Vol. 133(7), 071205(12pages), (2011).

[37] A. J. Chamkha: Unsteady hydromagnetic natural convection in a fluid-saturated porous medium channel. *Adv. Filtration Separation Technol.*, 10 369-375, (1996).

[38] T. C. Chawla, S. H. Chan: Combined radiation and convection in thermally developing Poiseuille flow with scarttering. *J. Heat Transfer*, 102, 297-302, (1980).

[39] B. Calgagni, F. Marsili, M. Paroncini: Natural convective heat transfer in square enclosures heated from below. *Applied Thermal Engineering*, 25, pp. 2522-2531, (2005).

[40] L. B. Erbay, M. S. Ercan, B. Sulus, M. M. Yalcin: Entropy Generation during Fluid Flow between two Parallel plates with moving Bottom plate. *Entropy*, 5, 506-516, (2003).

[41] Fethi Kamisli: Laminar flow of a non-Newtonian fluid in channels with wall suction or injection. *International Journal of Engineering Science*, 44, 650-661, (2006).

[42] M. Gupta: Effect of wall Slip on the Flow in a flat Die for Sheet Extrusion. ANTEC pp1191-1196, (2011).

[43] O. Haddad, M. Abuzaid, M. Al-Nimir: Entropy generation due to Laminar Incompressible forced convection flow through parallel-plates micro channel. *Entropy*, 6(5), 413-426, (2004).

[44] K. Hooman: Entropy-energy analysis of forced convection in a porous-saturated circular tube considering temperature-dependent viscosity effects. *Int. J. Exergy*, 3, 436-451,(2006).

[45] K. Hooman, H. Gurgenci, A. A. Merrikh: Heat transfer and entropy generation optimization of forced convection in a porous-saturated duct of rectangular cross-section. *Int. J. Heat Mass Tran.*, 50, 2051-2059, (2007).

[46] J. Hartmann, F. Lazarus: Hg-Dynamics II, Theory of laminar flow of electrically conductive Liquids in a Homogeneous Magnetic Field. *K.Dan. Vidensk. Selsk. Mat. Fys. Medd.* Vol. 15(7), 1-45, (1937).

[47] M. A. Hossain, M. Kutubuddin, I. Pop: Radiation-conduction interaction on mixed convection past a horizontal circular cylinder. *Int. J. Heat Mass transfer*, 35, pp. 307-314, (1999).

[48] J. C. R. Hunt: Magnetohydrodynamic flow in a rectangular duct. *J. Fluid Mech.*, Vol. 21, 577-590, (1965).

[49] D. B. Ingham, I. Pop: *Transport Phenomena in Porous Media*. Pergamon: Oxford, UK, (2002).

[50] G. Ibanez, S. Cuevas, M. Lopez de Haro: Minimization of entropy generation by asymmetric convective cooling, *Int. J. Heat Mass Transfer*, Vol. 46, 1321-1328, (2003).

[51] A. R. A. Khaled, K. Vafai: The effect of the slip condition on stokes and couette flows due to an oscillatory wall: Exact solutions. *Int. J. Non. Lin. Mech.*, 39, 795-809, (2004).

[52] G. Jocelyne, D. John, M. Noel: Laminar Flow in Channel with Porous walls. *The Chemical Engineering Journal*, 42, 193-204, (1989).

[53] M. Kaviany: Laminar flow through a porous channel bounded by isothermal parallel plates. *Int.J. Heat Mass Transfer*, Vol 28, No 4 851-858, (1985).

[54] N. S. Kobo, O. D. Makinde: Second law analysis for a variable viscosity reactive Couette flow under Arrhenius kinetics. *Mathematical Problems in Engineering*, 278104(pp1-15), (2010).

[55] O. Laurent, S. Philippe, Q. Michel: Laminar flow in channels with wall suction or injection: a new model to study muti-channel fitration systems. *Chemical Engrg. Sci.*, 59, 1034-1051, (2004).

[56] J. J. Jou, K. Y. Kung, C. H. Hsu: Thermal stability of horizontal superposed porous and fluid layers in a rotating system. *Int. J. Heat Mass Transfer*, Vol.39, No 9, 1847-1857, (1996).

[57] S. Mahmud, R. A. Fraser: Flow, thermal and entropy generation characteristic inside a porous channel with viscous dissipation. *Int. J. Therm. Sci.*, 44, 21-32, (2005).

[58] S. Mahmud, R. A. Fraser: Thermodynamic analysis of flow and heat transfer inside channel with two parallel plates. *Energy*, Vol. 2, 140-146, (2002).

[59] S. Mahmud, R. A. Fraser: Free Convection and Irreversibility Analysis inside a Circular Porous Enclosure. *Entropy*, 5, 358-365, (2003).

[60] O. D. Makinde, A. Aziz: Second law analysis for a variable viscosity plane Poiseuille flow with asymmetric convective cooling. *Computers and Mathematics with Applications*, Vol 60, pp3012-3019, (2010).

[61] O. D. Makinde: Thermodynamic second law analysis for a gravity driven variable viscosity liquid film along an inclined heated plate with convective cooling. *Journal of Mechanical Science and Technology*, Vol. 24 (4), pp899-908, (2010).

[62] O. D. Makinde: Extending the utility of perturbation series in problems of laminar flow in a porous pipe and diverging channel. *J. Austral. Math. Soc. Ser B*, 40,1-11, (1998).

[63] O. D. Makinde: On MHD mixed convection with Soret and Dufour effects past a vertical plate embedded in a porous medium. *Latin American Applied Research*, 41, 63-68, (2011).

[64] 0. D. Makinde, E. Osalusi : MHD steady flow in a channel with slip at the permeable boundaries. *Rom. J. Phys.*, 51, 319-328, (2006).

[65] O. D. Makinde, E. Osalusi: Second law analysis of laminar flow in a channel filled with saturated porous media. *Entropy*, 7, 148-160, (2005).

[66] O. D. Makinde: Second law analysis for variable viscosity hydromagnetic boundary layer flow with thermal radiation and Newtonian heating. *Entropy*, 13, 1446-1464,(2011).

[67] S. Mahmud, S. H. Tasnim, H. A. A. Mamun: Thermodynamics analysis of mixed convection in a channel with transverse hydromagnetic effect. *Int. J Therm. Sci.*, 42, 731-740, (2003).

[68] O. D. Makinde: Irreversibility analysis for gravity driven non-Newtonian liquid film along an inclined isothermal plate. *Physica Scripta*, Vol. 74 , 642-645, (2006).

[69] O. D. Makinde: Irreversibility analysis of variable viscosity channel flow with convective cooling at the walls. *Canadian Journal of Physics*, Vol. 86(2), 383-389, (2008).

[70] O. D. Makinde: Entropy-generation analysis for variable-viscosity channel flow with non-uniform wall temperature. *Applied Energy*, Vol. 85, 384-393, (2008).

[71] O. D. Makinde, M. Maserumule: Inherent irreversibility and thermal stability for steady flow of variable viscosity liquid film in a cylindrical pipe with convective cooling at the surface, *Int. J. Num. Methods for Heat and Fluid Flow*, vol. 20, No. 1, 5-16, (2010).

[72] O. D. Makinde, O. Anwar Beg: On inherent irreversibility in a reactive hydromagnetic channel flow. *Journal of Thermal Science*, Vol.19, No.1, 72-79, (2010).

[73] O. D. Makinde, A. Aziz: MHD mixed convection from a vertical plate embedded in a porous medium with a convective boundary condition. *International Journal of Thermal Science*, Vol. 49, 1813-1820, (2010).

[74] O. D. Makinde, O. O. Onyejekwe: A numerical study of MHD generalized Couette flow and heat transfer with variable viscosity and electrical conductivity. *Journal of Magnetism and Magnetic Materials*, Vol. 323, (2011)

[75] O. D. Makinde: Computer extension and bifurcation study by analytic continuation of porous tube flow. *Jour. Math. Phys. Sci.*, Vol. 30, 1-24, (1996).

[76] O. D. Makinde: Extending the utility of perturbation series to problems of laminar flow in a porous and a diverging tube. *Jour. Australian Math. Soc. Series B*, Vol. 41, 118-128, (1999).

[77] O. D. Makinde: Laminar flow in a channel of varying width with permeable boundaries. *Rom. Jour. Phys.*, 40, Nos. 4-5, 403, (1995).

[78] O. D. Makinde: Unsteady incompressible flow in a porous channel. *Proc. Rom. Appl. Indust. Math. Oradea*, 47-58, (1994).

[79] O. D. Makinde, P. Sibanda, E. M. Lungu: On suction driven flow in a channel filled with porous media. *Jour. Inst. Math. Comp. Sci.*, Vol. 10, No. 1, 23-28, (1999).

[80] O.D. Makinde: Thermal stability of a reactive viscous flow through a porous-saturated channel with convective boundary conditions. *Applied Thremal Engineering*, Vol.29, Issue 8-9, 1773-1777, (2009).

[81] O. D. Makinde: Heat and mass transfer in a pipe with moving surface: Effects of viscosity variation and energy dissipation. *Quaestiones Mathematicae*, Vol. 24, 97-108, (2001).

[82] O. D. Makinde: Hermite-Pade approach to thermal radiation effect on inherent irreversibility in a variable viscosity channel flow. *Computers and Mathematics with Applications*, 58(11-12), 2330-2338, (2009).

[83] O. D. Makinde, E. Osalusi: Entropy generation in a liquid film falling along an inclined porous heated plate. *Mechanics Research Communications*, 33, 692698, (2006).

[84] O. D. Makinde, R. L. Maserumule: Thermal criticality and entropy analysis for variable viscosity Couette flow. *Physica Scripta*, Vol. 78, 015402 (6pp), (2008).

[85] J. M. McDonough: *Lectures in Elementary Fluid Dynamics*. University of Kentucky, Lexington, KY 40506-0503, (2009).

[86] S. H. Munson-McGee: An approximate analytical solution for the fluid dynamics of laminar flow in a porous tube. *Journal of Membrane Science*, 197, 223-230, (2002).

[87] Y. Moussy, A. D. Snider: Laminar flow over pipes with injection and suction through the porous wall at low Reynolds number. *Journal of Membrane Science*, 327, 104-107, (2009)

[88] P. R. Nachtshein, P. Swigert: *Satisfaction of the Asymptotic Boundary Conditions in Numerical Solution of the System of Nonlinear Equation of Boundary Layer Type.*NASA TND-3004.NASA: Washington, DC, USA, (1965).

[89] U. Narusawa: The second law analysis of mixed convection in rectangular ducts. *Heat and Mass Transfer*, Vol. 37, 197-203, (2001).

[90] Navier. CLMH: M emoire sur les lois du mouvement des fluides. *Mem. Acad. R. Sci. Paris*, 6, 389-416, (1823).

[91] D. A. Nield, A. Bejan: *Convection in Porous Media.* 3rd ed.; Springer: New York, NY, USA, (2006).

[92] A. A. Ozalp: Combined effects of pipe Diameters Reynlods number and wall heat flux and on flow, heat Transfer and Second law characteristics of laminar-Transitional micro-pipe flows. *Entropy*, 12, 445-472, (2010).

[93] I. Ozkol, G. Komurgoz, A. Arikoglu: Entropy generation in the laminar natural convection from a constant temperature vertical plate in an infinite fluid. Proc. IME *J. Power. Energ.*, 221,609-616, (2007).

[94] G. Raithby: Laminar heat transfer in the thermal entrance region of circular tubes and two-dimensional rectangular ducts with wall suction and injection. *Int. J. Heat and Mass Transfer*, 14, 223-243, (1971).

[95] M. M. Rashidi, S. M. Sadri: Solution of the Laminar Viscous Flow in a Semi-Porous Channel in the Presence of a Uniform Magnetic Field by Using the Differential Transform Method. *Int. J. Contemp. Math. Sciences*, Vol. 5, no. 15, 711-720, (2010).

[96] A. Raoufpanah: Effects of Slip Condition on the characteristics of flow in ice melting process. *Int. J. of Engineering*, Vol.18, No.3, 1-9, (2005).

[97] R. S. Reddy Gorla, L. W. Byrd, D. M. Pratt: Second law analysis for microscale flow and heat transfer. *Applied Thermal Engineering*, Vol. 27, 1414-1423, (2007).

[98] M. G. Reddy, N. B. Reddy, B. R. Reddy: Unsteady MHD convective heat and mass transfer flow past a semi-infinite vertical porous plate with variable viscosity and thermal conductivity. *Int. J. Appl. Math and mech.*, 5(6), pp. 1-14, (2009).

[99] N. Riley: Magnetohydrodynamics free convection. *J. Fluid Mech.*, Vol.18, 577-586, (1964).

[100] N. Rott: Themoacoustics. *Adv. Appl. Mech.*, 20, 135-175, (1980).

[101] W. A. Robinson: The existence of multiple solution for the laminar flow in uniform porous channel with suction at both wall. *J. Engrg. Math*, 10, 23-40, (1976).

[102] M. Sahraoui, M. Kaviany: Slip and no-slip temperature boundary conditions at the interface of porous, plane media: Convection. *Int. J. Heat Transfer*, Vol.37, No6, pp 1029-1044, (1994)

[103] A. Z. Sahin: Effect of variable viscosity on the entropy generation and pumping power in a laminar fluid flow through a duct subjected to constant heat flux. *Heat Mass Transfer*, Vol. 35, 499-506, (1999).

[104] A. Z. Sahin, R. Ben-Mansom: Entropy generation in laminar fluid flow through a circular pipe. *Entropy*, 5, 404-416, (2003)

[105] A. Z. Sahin: Entropy generation in turbulent liquid flow through a smooth duct subjected to constant wall temperature. *Int. J. Heat and Mass Transfer*, 43, 1469-1478, (2000).

[106] A. Z. Sahin: A second law comparison for optimum shape of duct subjected to constant wall temperature and laminar flow. *Heat Mass Transfer*, Vol.33, 425-430, (1998).

[107] G. W. Swift: *Themoacoustics: A unifying perspective for some engines and refrigerators*. ASA Publication, New York, (2002).

[108] J. R. Sellar: Laminar flow in channel with porous wall at high suction Reynolds number. *J. Appl. Phys*, 26, 489-490, (1955).

[109] J. A. Shercliff: Steady motion of conducting fluids in pipes under transverse magnetic fields. *Proc. Cambridge Philos. Soc.* , Vol. 49, 136-144, (1953).

[110] F. M. Skalak, C. Wang: On the Nonunique solution of laminar flow through a porous tube or channel. Siam *J.Appl, Math*, Vol 34, No 3, 535-544, (1978).

[111] S. H. Tasnim, S. Mahmud, M. A. H. Mamun: Entropy generation in a porous channel with hydromagnetic effects. *Exergy*, 2, 300-308, (2002).

[112] S. H. Tasnim, S. Mahmud: Entropy generation in a vertical concentric channel with temperature dependent viscosity. *Int. Comm. Heat Mass Transfer*, Vol. 29, No. 7, 907-918, (2002).

[113] R. M. Terrill: Laminar flow in a uniformly porous channel. *Aeronaut. Q.*, 15, 299-310, (1964).

[114] R. M. Terrill: Laminar flow in a uniformly porous channel with large injection. *Aeronaut. Q.*, (1965).

[115] R. M. Terril: Laminar flow through a channel with uniformly porous wall of different permeability. *Appl. Scint. Res. Sec. A* , 15, 440-468, (1965).

[116] R. M. Terril: Laminar flow with large injection through parallel and uniformly porous walls of different permeability. *Quart. J. Mech. Appl.Math*, 21, 413-432, (1968).

[117] R. M. Terril: Heat Transfer in laminar flow between parallel porous plates. *Int. J. Heat Mass Transfer*, Vol.8, 1491-1497, (1965).

[118] D. Tripathi, P. K. Gupta, S. Das: Influence of slip condition on peristaltic transport of a viscoelastic fluid with fractional Burgens model. *Thermal Science*, Vol.15, No.2, 501-515, (2011).

[119] S. Tsangaris, D. Kondaxakis, N. W. Vlachakis: Exact solution for flow in a porous pipe with unsteady wall suction and/or injection. *Communications in Nonlinear Science and Numerical Simulation*, 12, 1181-1189, (2007).

[120] K. Vafai, C. L Tien: Boundary and inertial effects on flow and heat transfer in porous media. *Int. J. Heat Mass Transfer*, 24, 195-203, (1981).

[121] F. Vazquez, M. A. Olivare-Robles, S. Medina: Size effects on the entropy production in oscillation flow between parallel plates. *Entropy*, 13, 542-553, (2011).

[122] B. Fantomo, M. Godet, J. Frene: Studies of Engine Bearings and Lubrication. *(Society of Automotive Engineer Special Publication 539)*, 23-32, (1983).

[123] S. Vladimir, K. Darko: Mathematical modeling of changing of dynamic viscosity, as a function of temperature and pressure, of mineral oils for hydraulic systems. FACTAS Universitatis, *Mechanical Engineering series*, 4 (1), 27-34, (2006).

[124] J. F. Douglas, J. M. Gasiorek, J. A. Swaffield: *Fluids Mechanics*. Addison Wesley Longman Ltd., Harlow, (1995).

[125] W. M. Kays, M. E. Crawford: *Convective heat and mass transfer*. Mcgraw-Hill, Inc., (1993).

[126] L. C. Woods: *Thermodynamics of fluid systems*. Oxford University Press, Oxford, (1975).

[127] S. W. Yuan, A. B. Finkelstein: Laminar pipe flow injection and suction through a porous wall. *Trans. ASME* ,78, 719-724, (1956).

[128] F. M. White: *Viscous fluid flow*, 3rd Edition. McGraw-Hill, Inc., (2006).